
HEATSTORE

UTES and its integration in the heating system - Defining optimal design and operational strategies for the demonstration cases

Prepared by: Koen Allaerts, VITO
Fleury De Oliveira, UNIGE
Pierre Hollmuller, UNIGE
Luca Guglielmetti, UNIGE
Loïc Quiquerez, SIG
Charles Maragna, BRGM
Charlotte Rey, Storengy
Geoffroy Gauthier, PE
Rob Kleinlugtenbelt, IF Technology
Ryvo Octaviano, TNO
Martijn Clarijs, TNO

Checked by: Fleury De Oliveira, UNIGE
Koen Allaerts, VITO

Approved by: Holger Cremer, TNO

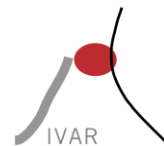
Please cite this report as: Allaerts, K. (ed.) 2021: UTES and its integration in the heating system -Defining optimal design and operational strategies for the demonstration cases, GEO THERMICA – ERA NET Cofund Geothermal. 96 pp.

This report represents HEATSTORE project deliverable number D3.3

TNO innovation
for life



storengy



KWR



u^b



delta h
Ingenieurgesellschaft



HEATSTORE (170153-4401) is one of nine projects under the GEO THERMICA – ERA NET Cofund aimed at accelerating the uptake of geothermal energy by 1) advancing and integrating different types of underground thermal energy storage (UTES) in the energy system, 2) providing a means to maximise geothermal heat production and optimise the business case of geothermal heat production doublets, 3) addressing technical, economic, environmental, regulatory and policy aspects that are necessary to support efficient and cost-effective deployment of UTES technologies in Europe.

This project has been subsidized through the ERANET cofund GEO THERMICA (Project n. 731117), from the European Commission, RVO (the Netherlands), DETEC (Switzerland), FZJ-PtJ (Germany), ADEME (France), EUDP (Denmark), Rannis (Iceland), VEA (Belgium), FRCT (Portugal), and MINECO (Spain).



About HEATSTORE

High Temperature Underground Thermal Energy Storage

The heating and cooling sector is vitally important for the transition to a low-carbon and sustainable energy system. Heating and cooling is responsible for half of all consumed final energy in Europe. The vast majority – 85% - of the demand is fulfilled by fossil fuels, most notably natural gas. Low carbon heat sources (e.g. geothermal, biomass, solar and waste-heat) need to be deployed and heat storage plays a pivotal role in this development. Storage provides the flexibility to manage the variations in supply and demand of heat at different scales, but especially the seasonal dips and peaks in heat demand. Underground Thermal Energy Storage (UTES) technologies need to be further developed and need to become an integral component in the future energy system infrastructure to meet variations in both the availability and demand of energy.

The main objectives of the HEATSTORE project are to lower the cost, reduce risks, improve the performance of high temperature (~25°C to ~90°C) underground thermal energy storage (HT-UTES) technologies and to optimize heat network demand side management (DSM). This is primarily achieved by 6 new demonstration pilots and 8 case studies of existing systems with distinct configurations of heat sources, heat storage and heat utilization. This will advance the commercial viability of HT-UTES technologies and, through an optimized balance between supply, transport, storage and demand, enable that geothermal energy production can reach its maximum deployment potential in the European energy transition.

Furthermore, HEATSTORE also learns from existing UTES facilities and geothermal pilot sites from which the design, operating and monitoring information will be made available to the project by consortium partners.

HEATSTORE is one of nine projects under the GEOTHERMICA – ERA NET Cofund and has the objective of accelerating the uptake of geothermal energy by 1) advancing and integrating different types of underground thermal energy storage (UTES) in the energy system, 2) providing a means to maximize geothermal heat production and optimize the business case of geothermal heat production doublets, 3) addressing technical, economic, environmental, regulatory and policy aspects that are necessary to support efficient and cost-effective deployment of UTES technologies in Europe. The three-year project will stimulate a fast-track market uptake in Europe, promoting development from demonstration phase to commercial deployment within 2 to 5 years, and provide an outlook for utilization potential towards 2030 and 2050.

The 23 contributing partners from 9 countries in HEATSTORE have complementary expertise and roles. The consortium is composed of a mix of scientific research institutes and private companies. The industrial participation is considered a very strong and relevant advantage which is instrumental for success. The combination of leading European research institutes together with small, medium and large industrial enterprises, will ensure that the tested technologies can be brought to market and valorised by the relevant stakeholders.

Document Change Record

This section shows the historical versions, with a short description of the updates.

Version	Short description of change
2021.02.26	Draft structure
2021.05.12	Draft document
2021.05.18	First review round
2021.06.03	Second review round
2021.06.23	Final document
2021.10.31	Final revised document

Table of Content

About HEATSTORE	3
1 Introduction.....	7
2 System simulations for optimizing thermal energy systems with UTES.....	8
2.1 Methods and modelling approaches used at the demo sites	8
2.2 Research questions	8
2.3 Background on the simulation tools and software	9
2.3.1 Overview	9
2.3.2 Application level	10
3 System simulations with HT-BTES (France)	12
3.1 Introduction & base-case definition.....	12
3.2 System modelling.....	12
3.2.1 Building	12
3.2.2 Distribution to the building	14
3.2.3 Borehole Thermal Energy Storage (BTES)	14
3.2.4 Solar panels and solar tank	15
3.2.5 Heat Pump	15
3.2.6 Miscellaneous hydraulic components.....	16
3.3 Control strategy.....	17
3.4 Simulation results.....	20
3.5 Analysis of sensitivity towards the design parameters	21
3.6 Conclusion	24
4 System simulations and smart control on a district heating network with HT-ATES (The Netherlands).....	25
4.1 Introduction	25
4.2 HT-ATES modelling with HST.....	25
4.2.1 HT-ATES heat supply/demand profile and control strategy	25
4.2.2 HT-ATES model setup for HST3D.....	26
4.3 Simulation results.....	28
4.4 Conclusions.....	29
4.5 System modelling.....	30
4.5.1 CHESS.....	30
4.5.2 Heatmatcher	35
4.6 Scenario analysis.....	36
4.6.1 Demand profile.....	36
4.6.2 Control Strategies	39
4.6.3 Case Scenario	39
4.7 Simulation results.....	43
4.7.1 Time series simulation	43
4.7.2 KPI Cost information.....	50
4.8 Conclusion	51
5 System simulations on district heating networks with large scale thermal energy storage (Denmark)	52
5.1 Introduction	52
5.2 System modelling software	52
5.2.1 TRNSYS model and results.....	53
5.2.2 EnergyPRO model.....	54
5.3 System modelling.....	55
5.3.1 Heat production units and fuels	55
5.3.2 District heating network demand	56
5.3.3 Electricity prices and other economics parameters	57
5.4 Simulation results.....	61
5.4.1 Yearly energy balance	61
5.4.2 Economics results.....	61
5.5 Conclusion	62

6	System simulations at regional level for optimal development strategy (Switzerland)	64
6.1	Introduction	64
6.2	System modelling software	64
6.2.1	Simulation of energy system	64
6.2.2	Thermo-hydraulic simulation of ATES and its integration in the energy system	65
6.3	Geneva case study	66
6.3.1	Energy context and integration of geothermal energy within DH	66
6.3.2	Geological context and potential of medium-depth aquifers	67
6.4	DH model and future evolution	68
6.4.1	Input-output model	68
6.4.2	Evolution of heat demand and temperature levels	68
6.4.3	Renewable production and merit-order	69
6.4.4	Evolution of DH energy mix	70
6.5	Thermal storage design and integration aspects	70
6.5.1	Storage design	70
6.5.2	System integration and discharging techniques	75
6.6	ATES modelling	78
6.7	Simulation results for system integration	78
6.8	Limits and perspectives	81
6.9	Conclusion	81
7	Implementation of demand side management on a geothermal district heating system (Belgium)	82
7.1	Introduction	82
7.2	Storm controller	82
7.3	Demo site overview and DSM setup	83
7.4	System simulation - heat load forecasting	86
7.5	Control strategy	89
7.5.1	Default control strategy	89
7.5.2	Peak shaving and dynamic supply temperature	91
7.6	Conclusion	92
8	Concluding remarks	93
9	References	94

1 Introduction

The main objective of the work reported in this deliverable is to define and design optimal control strategies for the HEATSTORE demonstrator sites. This deliverable focusses on the system simulations that were carried out in this perspective by each demo partner. The authors of this document interpret the term 'system simulations' as computer simulations that are carried out on a system¹ level focussing on the thermal aspects which are relevant when implementing UTES technology such as:

- UTES requirements, design and components
- Heat sources (geothermal, solar, waste heat, ...)
- Building heating systems
- District heating
- Control systems

The work also builds further on conclusions and lessons learned from HEATSTORE D1.1 about UTES state-of-the-art, example cases and lessons learned [1]. For example; Storage design should take into account the heat consumer specifications and boundary conditions of the heating system where it is connected to (e.g. building heating system) and vice versa. The whole energy chain, from generation to storage and consumer should be optimized. This is where system simulations play an important role.

A brief overview of the simulation software and tools used by each partner is presented first and an overview of the simulation work and conclusions is given per demonstrator.

¹ A group of interacting components that act according to a set of rules to form a unified whole. [48, 49] .

2 System simulations for optimizing thermal energy systems with UTES

2.1 Methods and modelling approaches used at the demo sites

BRGM and Storengy made a detailed system model in TRNSYS for optimizing the integration of a BTES in a building heating system, taking into account specific component models such as solar thermal collectors, thermal energy storage tanks, heat pump and heat exchangers. Different rule-based control strategies were evaluated, and the influence of certain design parameters is discussed.

In the Netherlands a high-temperature ATES system is integrated in a horticulture heating network. After the test drilling at ECW² in 2019, the subsurface properties of the storage aquifer were mapped in detail. Also, by this time, the design pumping scheme was derived from the expected heat supply/demand profile. This information was then used to perform subsurface heat transport simulations with the HST3D software of IF Technology, which offered insights in both the underground thermal effects of the HT-ATES system and the thermal recovery efficiency that could be expected at ECW. Specifically for this HEATSTORE Demonstration project at ECW, models were constructed to find the optimal distance between the hot and cold well, offering the optimal thermal recovery efficiency.

While IF Technology focussed on finding the optimal ATES configuration, TNO carried out system simulations to find out how the ATES can be operated in the thermal network. TNO used their own CHES software which is used to design and simulate an energy system infrastructure. A simplified and fast numerical model was derived from a more detailed ATES model created in DoubletCalc3D. In addition, the Heatmatcher control algorithm was applied for optimizing demand and supply on the network.

PlanEnergi (Denmark) uses TRNSYS to make calculations of heat production systems, often including a thermal storage, whether it is a Pit Thermal Energy Storage (PTES) or a Borehole Thermal Energy Storage (BTES). For this purpose, commercially available components that simulate accurately the behaviour of such installations are used, in connection with local weather conditions (windspeed, air temperature, etc.). Results from TRNSYS calculations regarding heat production from a combination of solar thermal and a PTES or a BTES can be used as user-made inputs for systems calculations in energyPRO. This procedure is described in the present document. Both tools are mostly used for site-size calculations but can also be used for small to medium scale calculations (site size up to municipality level), and for short-term calculations (from 1 year up to 20 years).

At the Geneva site, feasibility studies for the implementation of an aquifer thermal energy storage (ATES) are still under investigation. Integration aspects of an ATES are being analysed along with hydro-geological studies, to evaluate its possible impacts on the energy system. Energy system integration as well as thermo-hydraulic simulations were made with different specific software, while taking into account the interface between surface and subsurface facilities, namely in terms of temperature constraints. UNIGE and SIG simulated prospective scenarios for the heating energy system of Geneva [2, 3] with a software developed by UNIGE and inspired from EnergyPLAN [4].

In the Belgian demosite, VITO and Noda implemented a Demand Side Management (DSM) platform to optimize the geothermal district heating system in Mol, Belgium. This platform is hosted on a cloud platform while specific components of the system are developed in Python. From a system simulation perspective, the focus of the Belgian case in this document is mainly on the forecaster component. The control strategies are described briefly.

2.2 Research questions

For each demo site certain research questions were answered by performing system simulations. An overview of these questions is given in Table 1:

² ECW Energy, Energy company in Middenmeer, The Netherlands (<https://www.ecwenergy.nl/>)

Table 1: Research questions mapped on the demonstrators.

Country, partner	Demo	Research questions
FR, BRGM & Storengy	Design and integration of BTES in building heating system	<ul style="list-style-type: none"> How to design a heating production system with solar thermal panels, a BTES and a heat pump (HP) How should the control strategy be tuned to make the best of every component? How does every operating mode contribute to the final energy delivery?
IF, TNO	Design of HT-ATES	<ul style="list-style-type: none"> What is the optimal distance between extraction and injection well?
NL, TNO	Implementation and integration of HT-ATES in geothermal DHN	<ul style="list-style-type: none"> How can the HT-ATES be integrated in the horticulture heating network at ECW and operated in an optimal way?
DK, PE	Design and integration of UTES and PTES in DHN	<ul style="list-style-type: none"> What is the impact of new energy price schemes on operational costs for the Dronninglund heating system?
CH, UNIGE & SIG	Planning the integration of a UTES in DH on regional level	<ul style="list-style-type: none"> How can ATES systems support the district heating network in Geneva in order to reach the 2035 energy efficiency targets?
BE, VITO	Implementation of DSM on geothermal DHN	<ul style="list-style-type: none"> How to increase the share of renewable heat from the geothermal source on the existing DHN? How to reduce the temperature regime of the DHN?

2.3 Background on the simulation tools and software

2.3.1 Overview

In order to answer the research questions summarized in Table 1, each partner performed system simulations with their preferred software package or simulation tool. A brief overview of the software and tools used by the project partners is given in Table 2. More details on the simulation environment and results is given per demonstrator later in the document.

Table 2: Overview of the simulation software and tools used at the demonstrator sites.

Software - tool	Scope	Manufacturer	Demosite	Reference
TRNSYS	Transient system simulations	Thermal Energy System Specialists, LLC	FR, DK	http://www.trnsys.com/
energyPRO	Energy system modelling	EMD International A/S	DK	https://www.emd.dk/energypro/
DoubletCalc3D	Detailed ATES simulations	TNO	NL	https://www.nlog.nl/tools
Smart Heat Grid - Storm	Smart control of thermal networks	Noda, VITO	BE	https://noda.se/ https://storm-dhc.eu/en/storm-controller

Heatmatcher	Smart control of thermal systems	TNO, Zonenergie	NL	https://www.tno.nl
CHESS	Energy system modelling	TNO	NL	https://www.tno.nl
UNIGE tool based on EnergyPLAN	Energy system modelling	UNIGE	CH	
Nexus-CSMP++	Detailed ATEs simulations	ETHZ	CH	https://mineralsystems.ethz.ch/software/csmp.html
HST3D	Detailed ATEs simulations	USGS	NL	https://www.brr.cr.usgs.gov/projects/GW_Solute/hst/

2.3.2 Application level

Although the demonstrators in the HEATSTORE project are very different, there are certain aspects and criteria on which the different cases can be compared and oriented. This is visualized in Figure 1 where the system simulation framework for each country is mapped on two dimensions: the time horizon and application level.

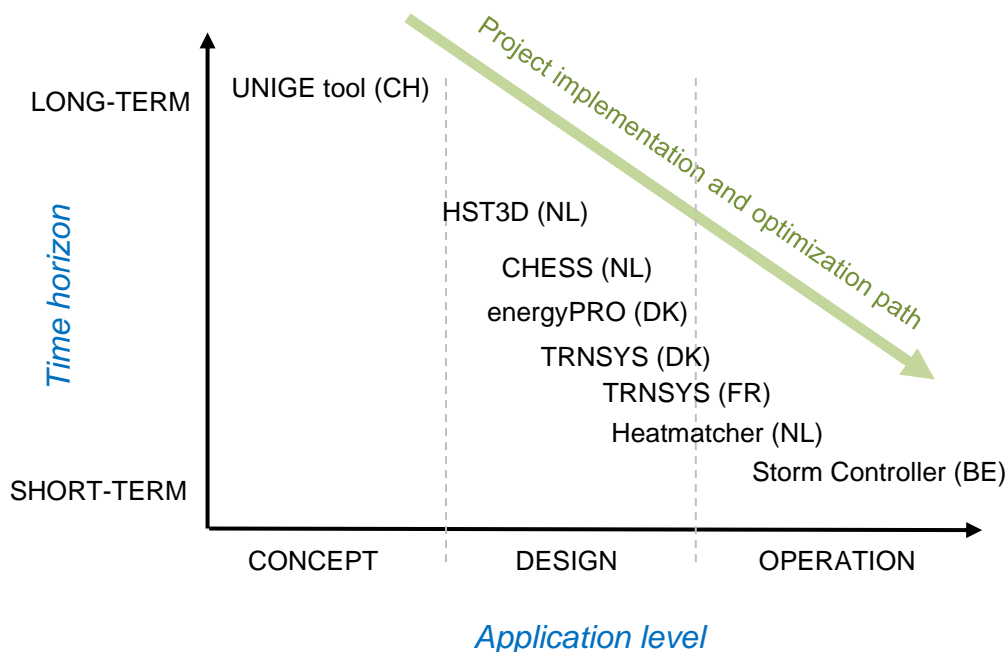


Figure 1: Mapping of the different simulation software and tools according to the time horizon and application at the demosites.

Application level (horizontal-axis):

The application level is a measure for the concreteness of a project. 3 distinct phases can be identified in which system simulations are relevant:

- The concept phase: Which technologies should be used, where should they be implemented and what are long term effects and benefits?
- The design phase: How should these technologies be implemented and integrated in a larger system.

- The operational phase: How can an existing, operational system be optimized further and what are the optimal settings of the control system and boundary conditions to operate within?

Time horizon (vertical-axis):

The time horizon on which system simulations are performed can vary and is typically linked with the application level. During the concept phase it is likely that simulations are performed with a long-term perspective while system simulations for optimizing operations are performed on a short term basis.

- Long-term: Planning, strategical, typically a time-horizon of more than 20 years.
- Mid-term: Typically up to 20 years³, related with the design phase.
- Short-term: Intraday or day – ahead.

Although the time horizon can vary significantly, the timestep or time resolution used in the system simulation environment can be comparable (typically 15 – 60min).

³ Time horizon is also linked with infrastructure life expectancy, for larger and more expensive infrastructure such as DHN or UTES this period can be longer.

3 System simulations with HT-BTES (France)

3.1 Introduction & base-case definition

BRGM and STORENGY studied a building whose heating is covered by a multi-energy system. The main components of this system are Solar Panels, a Solar Tank, a Borehole Thermal Energy Storage (BTES) and a Heat Pump (HP). The system is controlled so that the “best” energy source (i.e. the one at the higher temperature) should always be mobilized to cover the heat demand first. These sources are direct solar, solar heat pump, direct BTES, BTES through heat pump and backup heater. The solar excess heat can then be stored into the BTES when the demand is covered. The system has been modelled in the TRNSYS commercial software v18 (see Figure 2). TRNSYS is an extremely flexible graphically based software environment used to simulate the behaviour of transient systems (<http://www.trnsys.com/>). All simulations are run on 15 years with a time step of 7.5 minutes. The typical duration of one simulation is about 2 h.

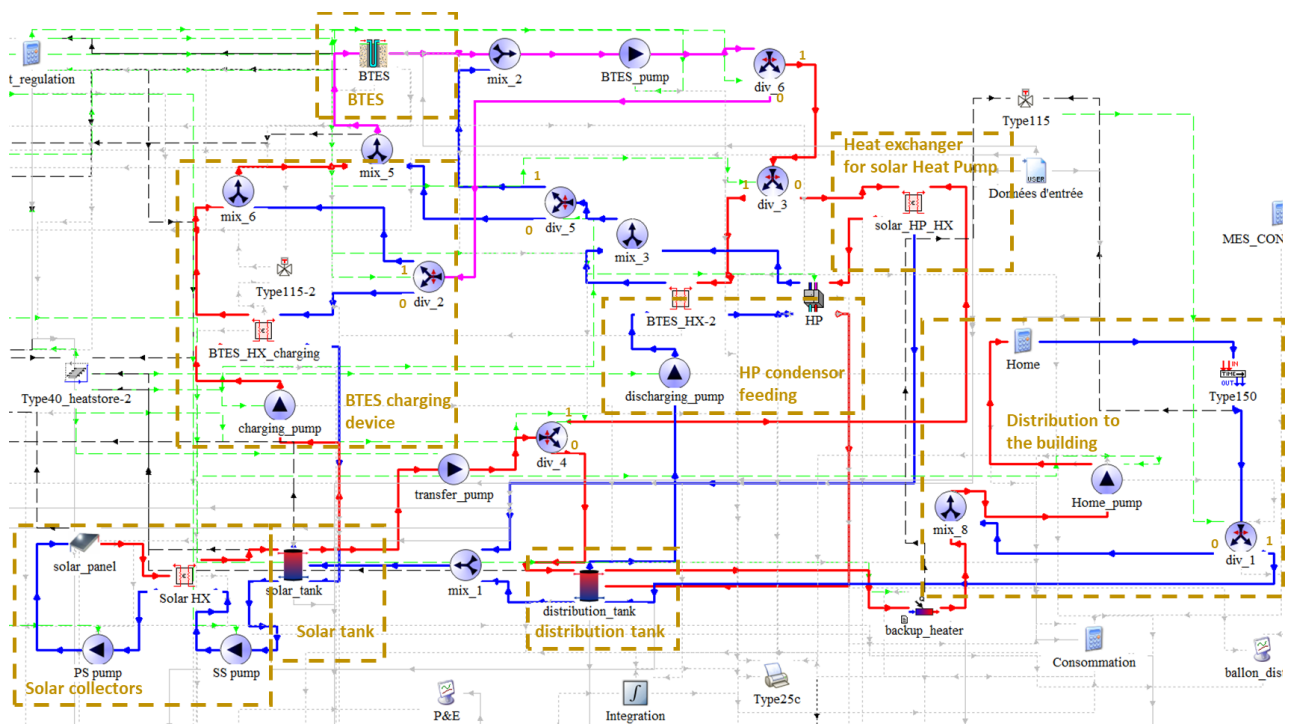


Figure 2: System overview. For every diverter div_i , the outlet as a function of the control function (from 0 to 1) is indicated.

3.2 System modelling

3.2.1 Building

The French thermal regulation RT2012 has divided the national territory into 8 climatic zones (cf. Figure 3). Climatic data are available at an hourly time step in every zone, including the air temperature, direct normal beam radiation and diffuse radiation on horizontal surface. We used the H1a climate which encompasses Paris region and a simple building model, which assumes that the thermal power required by the building P_{build} is proportional to the difference between the building setpoint temperature and the outside air temperature through a heat loss coefficient. The detailed modelling of a building through dynamic thermal simulations is outside of the scope of this study. The resulting peak power is 242 kW for a yearly energy of 584 MWh (see Figure 4).



Figure 3: the climatic zones of the French regulation⁴. H1a is in dark blue.

Table 3: Building parameters used for the thermal power required.

Minimum outside air temperature [°C]	-7.0
Building internal temperature [°C]	19.0
Building surficial heat loss coefficient G_{sv} [$W.m^{-2}.K^{-1}$]	1.3
Building surface [m^2]	10'000 m^2
Outside air cutoff temperature [°C]	16.0

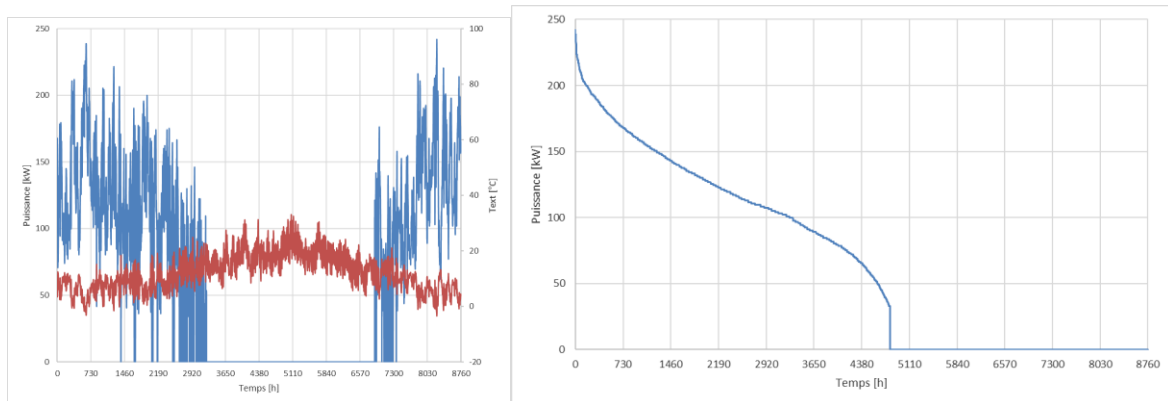


Figure 4: Power required by the building and air temperature on one year (left). Monotonic curve (right).

The building is assumed to be equipped with low temperature emitters (see. Figure 5). In what follows, the “set point temperature” refers to the temperature required in the inlet of the emitter.

⁴ Source : Arrêté du 26 octobre 2010 relatif aux caractéristiques thermiques et aux exigences de performance énergétique des bâtiments nouveaux et des parties nouvelles de bâtiments.

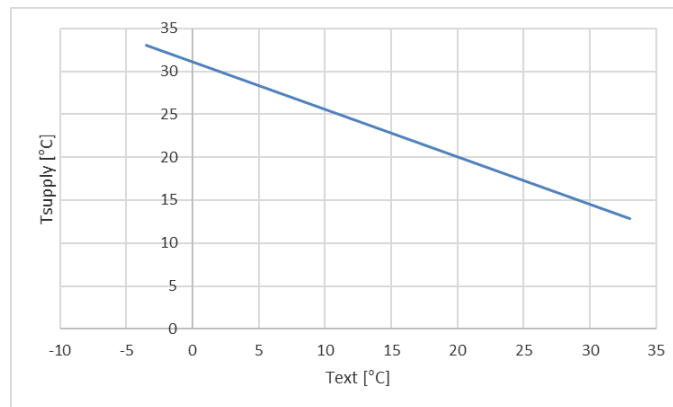


Figure 5: Emitter set point temperature as a function of the outside air temperature

3.2.2 Distribution to the building

The distribution tank is modelled with Type 534 with no internal heat exchanger (see Figure 2). The discharging and distribution pumps are fed by the top of the tank (since hot fluid is required), while *mix_1* valve is fed by the bottom since it evacuates cooled fluid back to the solar tank.

Table 4: Solar tank parameters.

Volume [m ³]	10
Height [m]	3.0
Insulation [W.K ⁻¹ .m ²]	0.55

A backup heater (type 138) after the distribution tank ensures that the set point is met in case the water leaving the distribution tank was below this point. When the heat demand is greater than zero, the pump *home_pump* operates.

3.2.3 Borehole Thermal Energy Storage (BTES)

The BTES is modelled with the Type 557b (Duct Thermal Energy Storage), see Figure 2. The model parameters are summarized in Table 5.

Table 5: BTES parameters.

Storage volume [m ³]	40'000
Borehole depth [m]	35
Spacing between adjacent boreholes [m]	3
Area of the storage volume [m ²]	1'143
Radius of the storage [m]	19
Number of boreholes [-]	144
Number of boreholes in series [-]	6
Borehole resistance [K.m.W ⁻¹]	0.08
Number of radial regions [-]	6
Number of vertical regions [-]	20
Storage (ground) thermal conductivity [W.K ⁻¹ .m ⁻¹]	1.3
Storage (ground) heat capacity [kJ.K ⁻¹ .kg ⁻¹]	2'200
Insulation radius at the surface [m]	20
Insulation thickness at the surface [m]	0.5

Insulation thermal conductivity [W.K ⁻¹ .m ⁻¹]	0.1
Initial Temperature [°C]	12
Number of years to determine the mesh size [-]	10
Thickness of the ground around the storage [m]	2'000

3.2.4 Solar panels and solar tank

The solar panels are modelled with the Type 1b (see Figure 2). The type computes the panel efficiency η as:

$$\eta = \frac{P}{\phi_{rad}S} = a_0 - a_1 \frac{T_{in} - T_{amb}}{\phi_{rad}} - a_2 \left(\frac{T_{in} - T_{amb}}{\phi_{rad}} \right)^2 \quad (1)$$

Where :

- P : power delivered by the panels [W]
- ϕ_{rad} : incoming flux on the panels [W.m⁻²]
- T_{in} : inlet temperature [°C]
- T_{amb} : ambient temperature [°C]
- S : Surface

Table 6: Solar panels parameters. ^(a): see TRNSYS manual.

Intercept efficiency a_0 [-]	0.814
Efficiency slope a_1 [W.m ⁻² .K ⁻¹]	4.81
Efficiency curvature a_2 [W.m ⁻² .K ⁻²]	0.0230
Tested flow rate [kg.h ⁻¹ .m ⁻²]	76.8
Surface S [m ²]	1'500
1 st order IAM ^(a)	0.198
2 nd order IAM ^(a)	0

The solar tank is modelled as the distribution tank, except that its volume is set to 200 m³ and its height to 8.3 m. The charging and transfer pumps are fed by the top of the tank (since hot fluid is required), while the solar heat exchanger *solar_HX* is fed by the bottom since it evacuates cooled fluid back to the solar panels.

3.2.5 Heat Pump

The HP is modelled with the Type 927 with a nominal calorific power set to 250 kW. The calorific power which the HP can provide depends upon the condenser and evaporator inlet temperatures (see. Figure 6, based on the Dynaciat HP technical data build by the CIAT manufacturer). A small difference of temperature between condenser and evaporator may damage the HP condenser. Though no technical documentation could be found on this acceptable limitation, a "recirculation zone" was modelled where the properties remain constant. Physically, a recirculation valve at the evaporator or the condenser would ensure the constraint is met. To save computational time, this was not modelled in TRNSYS, but integrated into the HP property maps.

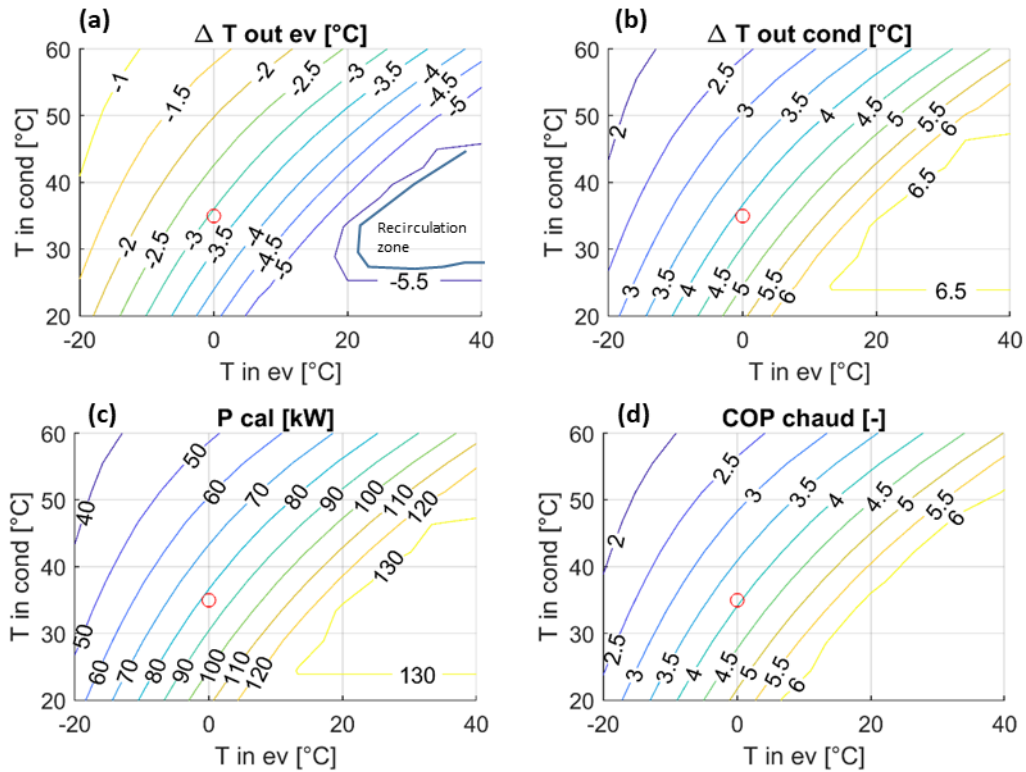


Figure 6: Heat pump properties as a function of the evaporator and condenser inlet temperatures $T_{in, ev}$ and $T_{in, cond}$: Temperature difference at the evaporator (a) and condenser (b); HP calorific power (c) and coefficient of performance (d). The red dot indicates the nominal point. Note that subplot (c) represents a HP with nominal power 100 kW, while in this study the nominal power is 250 kW. The power surface is scaled accordingly.

3.2.6 Miscellaneous hydraulic components

The 3 heat exchangers are modelled with Type 91 “effectiveness heat exchanger” which avoids to model the thermal process inside the exchanger. The efficiency is set to 75 %.

The heat-carrier fluid is water for the BTES loop and the loop from the solar tank to distribution, while it is a mixture of anti-freezing and water in the solar panels (see Table 7).

Table 7: Heat carrier fluid properties.

	Water	Water + anti-freezing
Density [kg.m ⁻³]	4.19	3.795
Heat capacity [kJ.K ⁻¹ .kg ⁻¹]	1'000	<i>Not used</i>

The pumps are On/Off pumps (see Table 8).

Table 8: Pumps parameters.

Pump	Rated flow rate [ton.h ⁻¹]	Rated power [kW]	Motor heat loss fraction [-]	Overall pump efficiency [-]	Motor efficiency [-]
<i>PS_pump</i>	37.5	1.39	0.1	0.6	0.9
<i>SS_pump</i>	37.5	0.76	0.1	0.6	0.9
<i>charging_pump</i>	35.0	0.71	0.1	0.6	0.9
<i>transfer_pump</i>	35.0	0	0.1	0.6	0.9
<i>discharging_pump</i>	48.0	1.42	0.1	0.6	0.9
<i>home_pump</i>	42.0	2.14	0.1	0.6	0.9
<i>BTES_pump</i>	35.0	3.24	0.1	0.6	0.9

3.3 Control strategy

The control strategy uses “differential controllers with hysteresis” (Type 165b of TRNSYS). Differential controllers compare two inputs (here temperatures) to return a control function γ_o equal to 0 or 1. The decisions are based on the temperatures at a given time and not on a prediction of their future status. The value of γ_o is chosen as a function of the difference between upper and lower temperatures (T_H and T_L) compared with two dead band temperature differences. The controller is ON if it was previously OFF and $T_H - T_L$ is greater than an “upper dead band” (UDB). The controller is ON if it was previously ON and $T_H - T_L$ is greater than a “lower dead band”. Otherwise the controller is OFF (see. Figure 7). In most cases, the upper dead band is higher than the lower dead band. Typically, a differential controller starts a pump to transfer the heat from a hot tank to a cold tank when the temperature difference between the hot and the cold tanks exceeds the upper dead band, and stops when the temperature difference drops below the lower dead band.

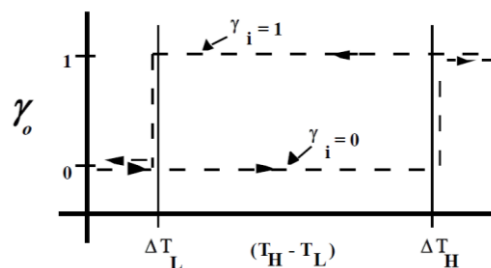


Figure 7 : Controller function (TRNSYS documentation)

The solar pumps *SP_pumps* and *SS_pumps* are controlled by a controller comparing the solar panel outlet temperature with the temperature at the top of the solar tank. If the difference is higher than 5 °C, the pumps starts, then stops when the difference drops below 0°C.

A more advanced version of the differential controller, called “microprocessor controller” (Type 40) has been used to control the pumps *charging_pump*, *discharging_pump*, *transfer_pump* and diverter *div4*. Instead of carrying one comparison to return one output function as Type 165b, Type 40 carries out several comparisons and applies a logical table to determine the outputs. The 4 hereby mentioned actuators can operate in 6 modes (see Table 9). Note that in mode 6 (Solar Heat Pump), the solar tank is connected to the HP evaporator which cools it down. This mode will be preferred over mode 4 (BTES charging) if the solar tank temperature is greater than the BTES outlet temperature, so if the solar tank is a better cold source for the HP.

Table 9: Operating modes and output functions of the microprocessor.

Modes	Mode decription	<i>transfer_pump</i>	<i>discharging_pump</i>	<i>charging pump</i>	<i>div_4</i>
1	Standby	0	0	0	0
2	BTES charging only	0	0	1	0
3	BTES discharging (with or without heat pump)	0	1	0	0
4	Transferring energy from solar tank to distribution tank (= Direct Solar)	1	0	0	0
5	Transferring energy from solar tank to distribution tank & BTES charging (not operational)	1	0	1	0
6	Solar Heat Pump	1	1	0	1

The mode is determined based on 5 comparisons of 4 temperatures (see Table 10):

- Comparator 1 compares the temperature at the top of the solar tank with the temperature at the top of the distribution tank.
- Comparator 2 compares the set point temperature required by the building with the temperature at the top of the distribution tank.

- Comparator 3 compares the temperature at the top of the solar tank with the BTES outlet temperature. Note that the BTES pump is operated continuously, so that to ensure a continuous measurement of the fluid temperature
- Comparator 4 does the same as Comparator 3, but with higher temperature dead bands. The underlying idea was to simultaneously allow energy transfer from the solar tank to the distribution tank and BTES charging if the solar tank was very hot (mode 5). However, for this report the dead bands have been set to a very large unreachable value. Therefore, mode 5 is not operational.
- Comparator 5 compares the set point temperature to the solar tank temperature.

Note that the dead bands of comparators 2 and 5 are negative. Both comparators compare a temperature to the set point temperature to warm up the distribution tank through the mode 3, 4 or 6. The dead band values have been determined by manually ensuring that the backup contribution will be negligible. Their negative values mean that the temperature at the top of the distribution tank must be kept at a temperature a bit higher than the set point temperature, by typically 3-5 °C so that to match the set point temperature at any time.

Table 10: Definition of the comparators used by the microprocessor.

<i>Comparator</i>	<i>Input 1 (= upper T)</i>	<i>Input 2 (= lower T)</i>	<i>Upper dead band [°C]</i>	<i>Lower dead band [°C]</i>
1	$T_{top_solar_tank}$	$T_{top_distribution_tank}$	5	0
2	$T_{setpoint}$	$T_{top_distribution_tank}$	-3	-5
3	$T_{top_solar_tank}$	T_{out_BTES}	5	0
4	$T_{top_solar_tank}$	T_{out_BTES}	205	200
5	$T_{setpoint}$	$T_{top_solar_tank}$	-3	-5

Table 11: Logic states of the microprocessor and resulting operating mode.

Logic state	Comparator					Mode	Relative positions of temperatures
	1	2	3	4	5		
1	0	0	0	0	-1	1	
2	0	0	0	1	-1	2	
3	0	0	1	0	-1	2	
4	0	1	0	0	1	3	
5	1	1	0	0	-1	3	
6	1	0	0	0	0	4	
7	1	1	0	1	0	4	
8	1	1	1	-1	0	4	
9	1	0	0	1	0	5	
10	1	0	1	0	0	5	
11	-1	1	0	1	1	6	
12	-1	1	1	0	1	6	

When the BTES charging pump is activated, the diverter *div_6* is in position 0, allowing the BTES outlet fluid to flow back to the charging heat exchanger. Regulations may impose a limitation on the BTES inlet temperature. For instance, in France, a 40 °C threshold is a condition for a simplified regulatory regime. The tempering valve *type 115-2* ensures an arbitrary temperature limitation is matched by diverting a part of the cooled flow coming back from the BTES trough *div_2*, avoiding it to be overheated by *BTES_HX_charging* heat exchanger. Though the functionality has been validated, the limitation temperature has been set to an arbitrary high value for this report and do not play any role. Besides, in charging mode the fluid flows from the heart to the outside of the BTES and the other way around in discharging mode.

When the discharging pump is activated, the diverter *div_6* switches to position 1. The status of diverters *div_3*, *div_5* and the heat pump (on or off) depends upon the following conditions:

- If the microprocessor is in mode 6 (Solar Heat Pump), *div_4* is in position 0 and the transfer pump is activated (see Table 11). The HP is on, *div_3* switches to 0 and heat from the solar tank is retrieved through *Solar_HP_HX* heat exchanger to feed the HP evaporator. *div_5* switches to position 1 to bypass the BTES, while *BTES_pump* circulates the fluid to the HP.
- If the microprocessor is in mode 3 (BTES discharging), *div_3* feeds the HP (outlet 0) or the discharging heat exchanger *BTES_HX-2* (outlet 1) if the BTES outlet fluid is hot enough. More specifically, *div_3* is controlled by a differential controller which lower and upper dead bands have been set to 2 °C and 7 °C respectively to ensure that the heat flows through the heat exchanger from the BTES to the distribution tank, as expected, and not in the other way around. If the output of this controller is 1, *div_3* switches to 1 and the HP is off. Conversely, if the controller output is 0, *div_3*

switches to 1 and the HP is on, provided that the BTES outlet temperature is above a temperature cutoff set to 6 °C. If the HP is turned off, it will start again when the BTES outlet temperature exceeds 8 °C.

3.4 Simulation results

The heat provided to the building is the sum of six contributions:

- The electricity feeding the compressor of the heat pump
- The solar energy used as a cold source of the heat pump
- The BTES energy used as a cold source of the heat pump
- The direct BTES energy
- The direct solar energy
- The backup energy.

The system experiences a transitory phase that lasts for about 6-10 years, when the BTES is warmed up. Then the energy mix reaches a permanent state (cf. Figure 8). Throughout the simulated lifespan, the HP-BTES is the main energy source delivered to the building. During the 15th year, 66 % of the heat injected into the BTES is retrieved, 79 % of which through the heat pump (cf. Figure 9).

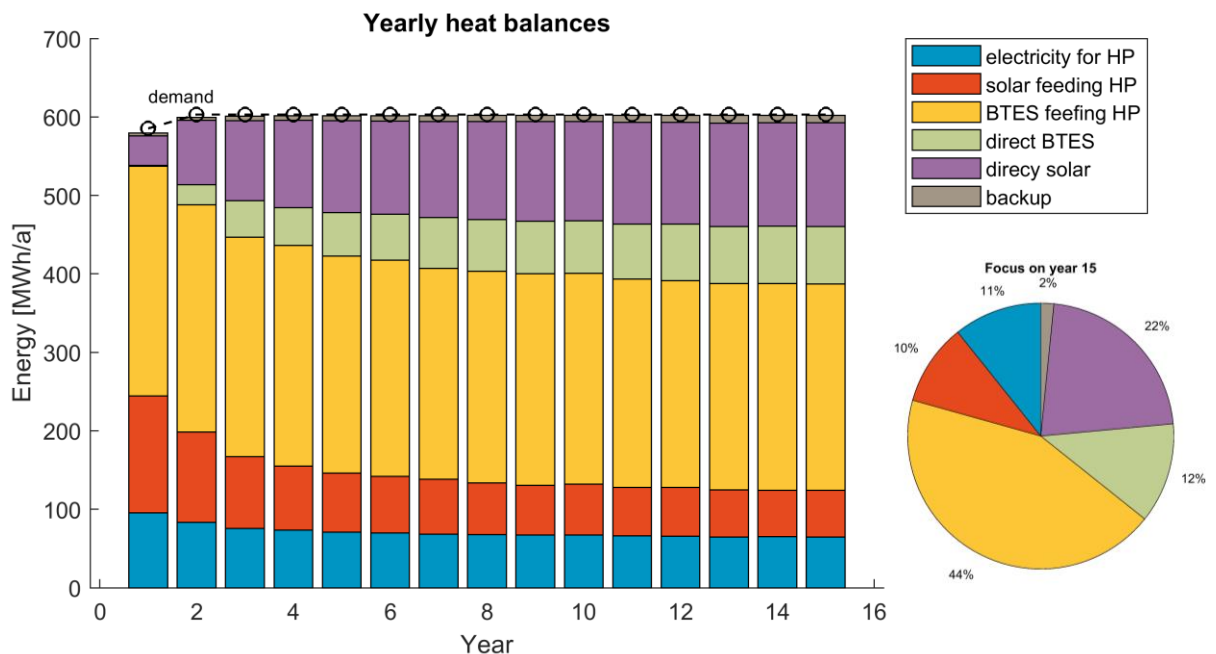


Figure 8: Origin of the heat provided every year for the reference configuration.

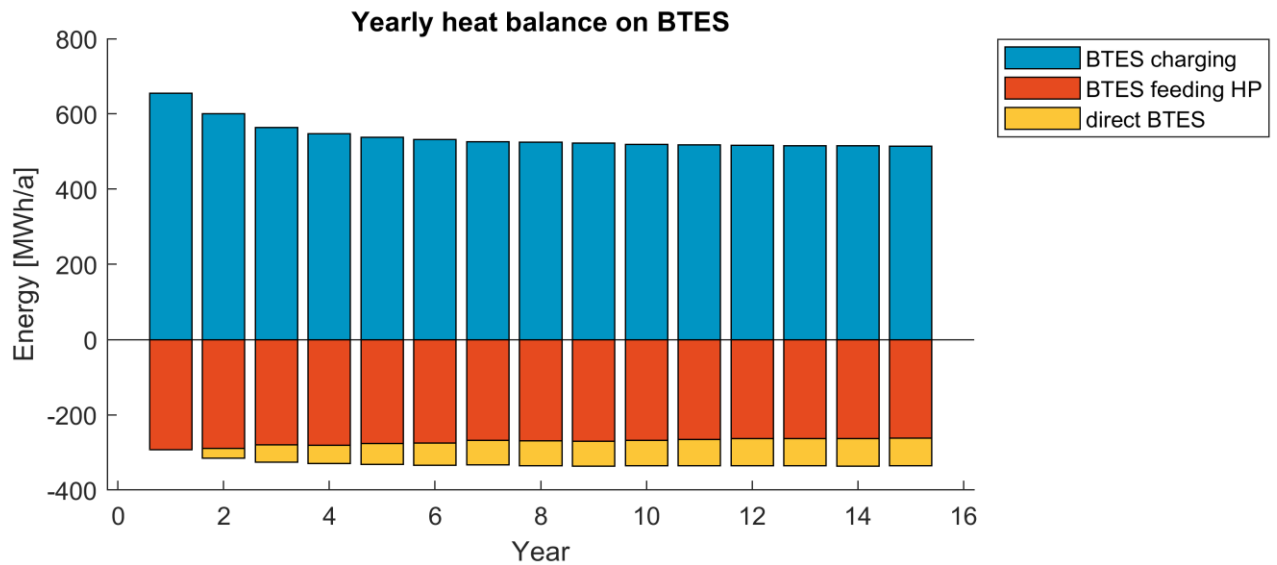


Figure 9: Yearly heat balance on BTES.

3.5 Analysis of sensitivity towards the design parameters

The influence of 4 design parameters on averaged heat balances modelled on 15 years is analysed:

- BTES volume
- Solar collector area
- Solar tank volume
- Distance between boreholes

The BTES volume V_{BTES} and solar collector area A_{coll} have been varied from 15 000 m³ to 140 000 m³ (ref. config.: 40 000 m³) and from 0 to 2000 m² (ref. config.: 1500 m²). Whatever the BTES volume, the backup consumption significantly increases when the solar collector area drops below a 800 m² threshold. The system is no longer able to cover the building needs, which is associated with a drop of the HP contribution. Meanwhile, above this threshold, the overall contribution of the HP decreases since more solar energy and BTES energy can be used directly (cf. Figure 10 and Figure 11).

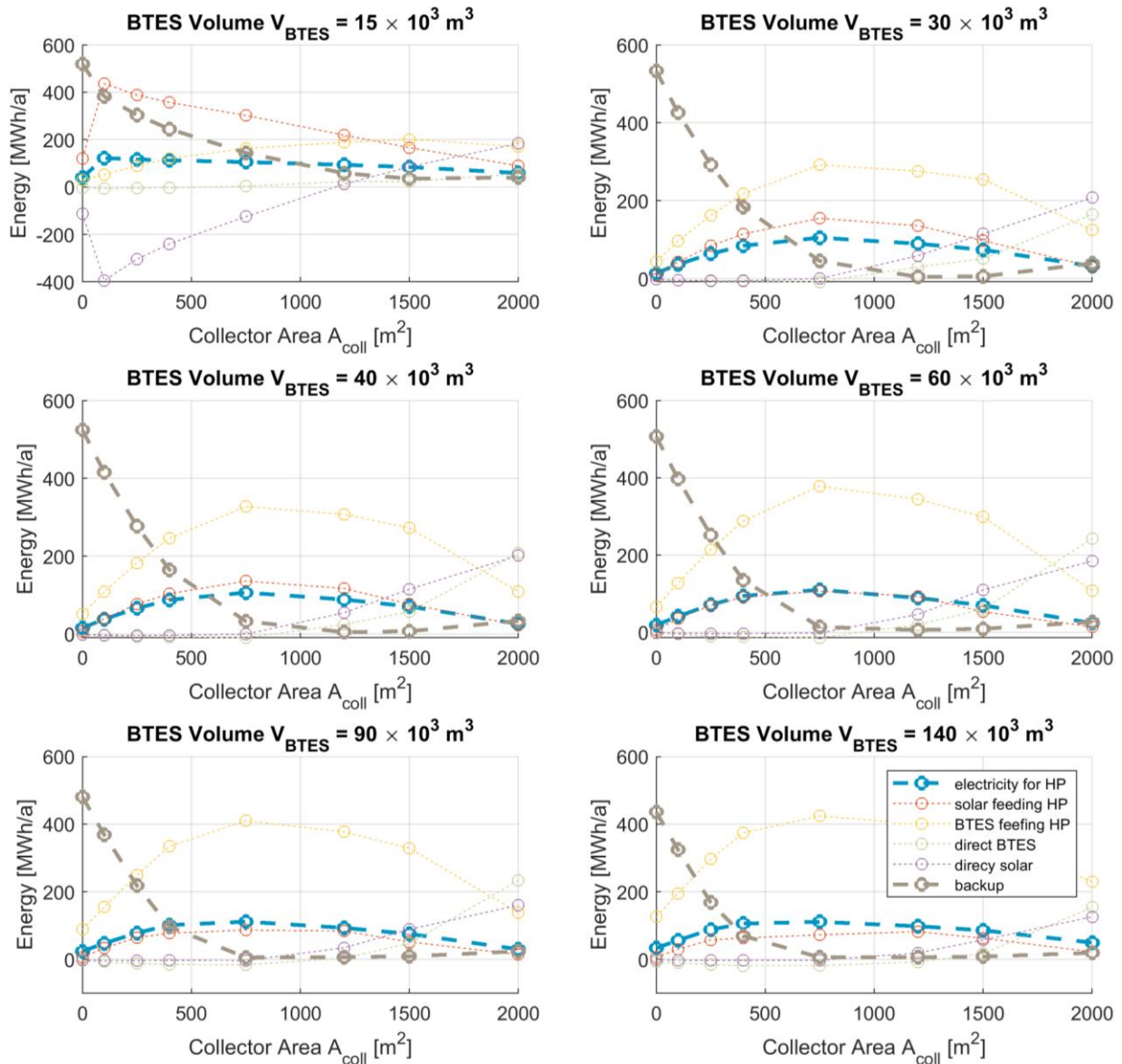


Figure 10: Energy mix as a function of the BTES volume V_{BTES} and solar collector area A_{coll} .

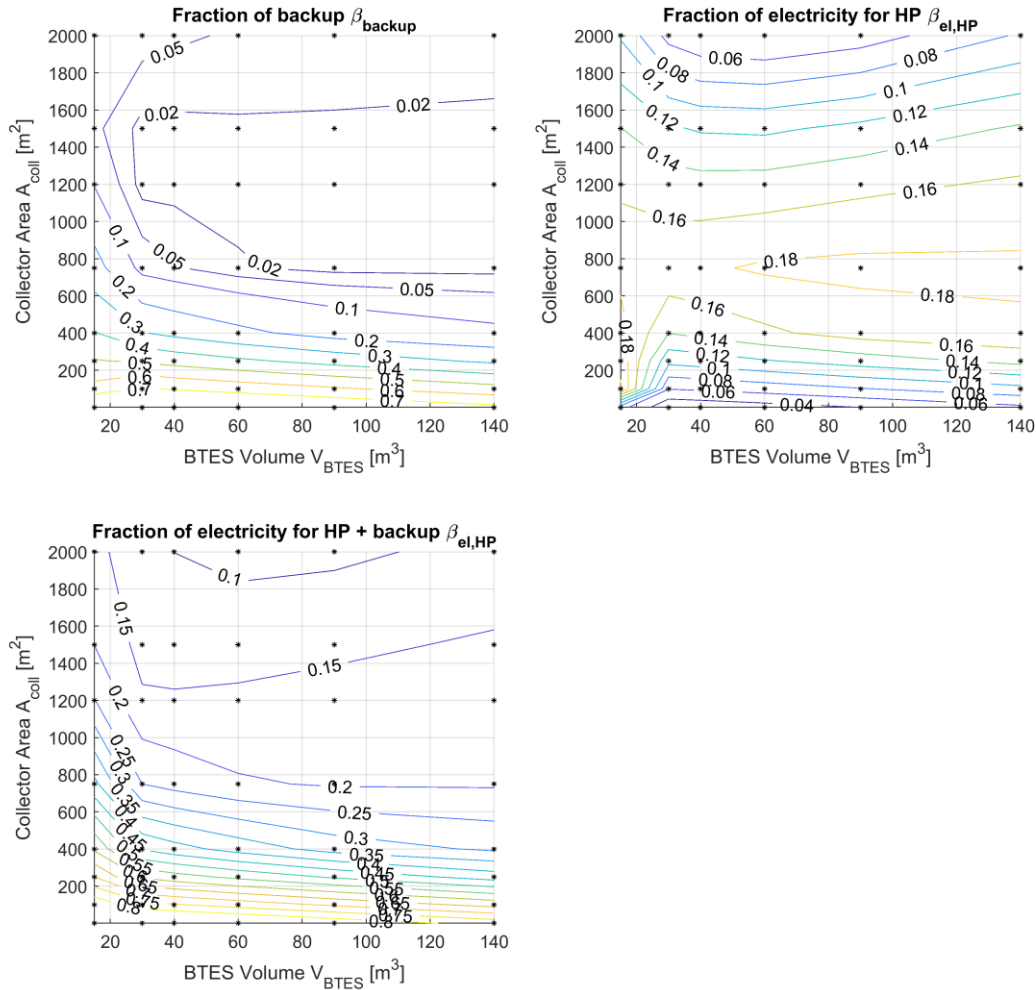


Figure 11: Focus on the fraction of electricity used by the backup burner (a), the HP (b) and the sum of them (c) as a function of the BTES volume V_{BTES} and solar collector area A_{coll} .

The solar tank volume has, indeed, a little influence on the system performance (cf. Figure 12). Between 20 m³ and 300 m³, the HP electricity consumption and backup consumption changes from 12.8 % to 11.8 % and 1.5 % to 1.1 % of the energy delivered to the building respectively. Increasing the solar tank size mostly results in replacing the BTES with solar energy to feed the HP. The distance between boreholes will play a much larger role. Increasing the distance between the boreholes from 3 m to 4 m has a negligible impact on the backup contribution, and slightly increases the HP contribution from 11.7 % to 13.9 % of the heat demand. If the boreholes are set further away, the backup consumption will further increase.

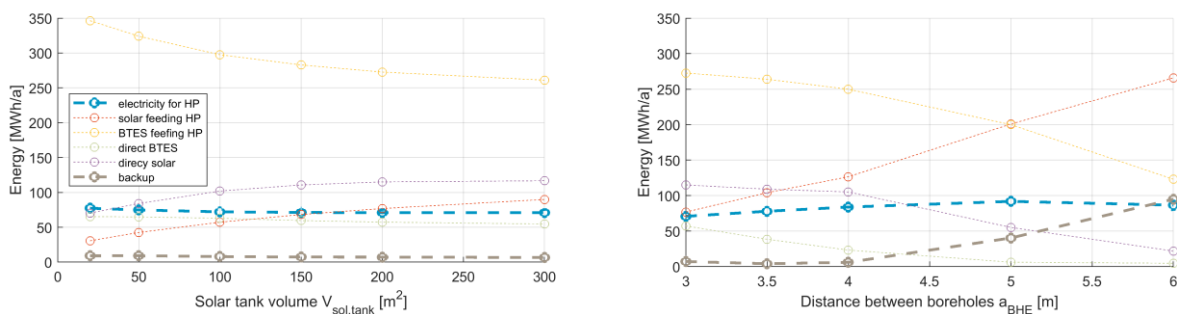


Figure 12: Energy mix as a function of the solar tank volume (left, ref. value: 200 m³) and distance between boreholes (right, ref. value: 3 m).

Based on the sensitivity analysis, a pre-optimized design can be proposed (Table 12).

Table 12: Proposition of an optimized design.

	Initial design	Pre-optimized design
BTES volume [m ³]	40'000	35'000
Solar collector area [m ²]	1'500	1'300
Solar tank volume [m ³]	200	25
Distance between boreholes [m]	3	4

3.6 Conclusion

The main findings of the current system modelling are:

- Building the largest BTES can be counter-productive since for a fixed collector area, HP electrical consumption increases if the BTES volume cannot be fully warmed up by solar heat (cf. Figure 11).
- Increasing the solar tank size mostly results in replacing the BTES with solar energy to feed the HP, with no significant changes of the HP electrical and backup consumptions.
- The distance between boreholes play a much larger role than the solar tank size. If the boreholes are set further away, the backup consumption will further increase as the BTES volume is too large to be fully warmed.

4 System simulations and smart control on a district heating network with HT-ATES (The Netherlands)

4.1 Introduction

For the Dutch HT-ATES Demonstration project in Middenmeer, the Netherlands, modelling studies were performed by IF Technology to optimize the initial well design. More specifically, the aim was to find the optimal distance between the hot and the cold HT-ATES wells. Placing the wells far apart would cause relatively high heat losses to the surroundings, but placing the wells too close would cause interference between the hot and cold well, affecting the thermal performance of the system. The optimal well distance should be small enough to prevent large-scale heat losses to the surroundings, while keeping the well interference within an acceptable range. Several scenarios were simulated, each with different well distance, to learn about the thermal processes that influence the performance of the HT-ATES system, and to find the optimal well distance for the HT-ATES system.

The amounts of energy and groundwater that are to be pumped by the HT-ATES system of ECW depend on the heat supply from the heating grid and the heat demand from the greenhouses. Therefore, a schematized heat supply/demand profile was constructed first, based on the heat flows that were to be expected at ECW, as described in section 4.2.1.

Using the profile as input, several scenarios were simulated using the subsurface Heat and Solute Transport 3D (HST3D) software of IF Technology to see what well distance offered the optimal thermal recovery efficiency of the HT-ATES system, while keeping thermal interference acceptable. The model setup and results are described in sections 4.2.2 and 4.3.

While IF Technology focussed on the optimization of the well configuration in order to start the construction process, TNO used a reduced and faster ATES model for the overall system simulation framework.

4.2 HT-ATES modelling with HST

4.2.1 HT-ATES heat supply/demand profile and control strategy

For the greenhouse horticulture area Agriport in Middenmeer, a HT-ATES (high temperature aquifer thermal energy storage) in combination with a district heating net is used for heat supply. The HT-ATES is currently (April 2021) being realized at the horticulture business of Helderman in Middenmeer on behalf of ECW.

Helderman has 10 ha of greenhouses and currently, 10 additional ha of greenhouses are under construction. This will be completed by the end of 2021. The existing area of greenhouses was built before the HT-ATES was designed, and therefore the design of the heat supply was not optimal for HT-ATES integration. For the greenhouses under construction however, the heat supply design was set up in synergy with the HT-ATES, enabling low temperature heat supply and increasing the HT-ATES storage efficiency.

From about May to August, surplus heat from the district heating network is charged in the HT-ATES. The flow rate applied at the HT-ATES during charging depends on the overcapacity of the heating grid, but is approximately 150 m³/h for the duration of four months. When there is no more overcapacity of the heating grid, charging is stopped by the operator (ECW). The supply of heat from the heating grid to the HT-ATES is stopped for the rest of the year, and the HT-ATES system starts supplying heat to Helderman.

During the cold season (approximately from September to March), on request of Helderman, the HT-ATES will supply heat to their greenhouse. The flow-rate is determined based on the heat demand of the greenhouse in the past hour. When there is limited or no heat demand, the HT-ATES continues to supply heat at a minimum flow rate (about 30 m³/h). Excess heat is stored in Helderman's above-ground heat buffer. The minimum flow rate is expectedly applied in the first three months after charging, i.e. from about September to November. During the mid-winter months, the heat demand from the greenhouses is significantly higher (100 m³/h on average), resulting in higher flow rates applied to the HT-ATES. Heat supply from the HT-ATES to the greenhouse continues until the production temperature of the hot well drops below 55°C (cut-off temperature). The operator receives a notification and stops discharging the HT-ATES.

This control strategy is used to minimize the number of start-stops of the ESP (electric submersible pump). Fewer start-stops will increase the lifetime of the ESP. When the cut-off temperature is reached, the HT-ATES system will be in rest until heat can be charged again in spring.

The heat supply and demand pattern of the HT-ATES system, described above in a qualitative way, was translated to the following simplified pumping scheme for the HT-ATES wells:

- Loading the HT-ATES for 4 months at 150 m³/h
- Discharged for 7 months
 - 3 months low flow rate (30 m³/h), applying a cut-off temperature at 55 °C
 - 4 months high flow rate 100 m³/h), applying a cut-off temperature at 55 °C
- 1 month rest (maintenance, etc.)

This scheme is based on monthly averaged flow rates at the wells. Hourly fluctuations were not taken into account. Together with the subsurface information gathered during the test drilling at ECW of 2019, this pumping scheme forms the input for subsurface heat transport models that were used to find the optimal well distance.

4.2.2 HT-ATES model setup for HST3D

HST3D software

The Heat and Solute Transport 3D (HST3D) software of IF Technology is capable of simulating heat and solute transport in 3D water-saturated groundwater systems [5]. The model numerically solves the fluid, heat and solute transport equations. The model includes dependency of both fluid viscosity and fluid density on temperature, which makes it suitable for HT-ATES simulations. Using HST3D, the thermal effects of HT-ATES on the subsurface can be simulated and visualized. Also, production temperatures from the wells, which are dependent on subsurface heat processes, can be derived from the simulations, offering insights in the thermal recovery efficiency of a HT-ATES system.

Simulation of several scenarios

The aim was to find the optimal distance between the hot and the cold HT-ATES well. Placing the wells far apart would cause relatively high heat losses to the surroundings, but placing the wells too close would cause interference between the hot and cold well, affecting the thermal performance of the system. The optimal well distance should be small enough to prevent large-scale heat losses to the surroundings, while keeping the well interference within an acceptable range. Although the well distance was varied for the different scenarios, the subsurface properties and the pumping scheme applied to the scenarios remained constant.

Subsurface input parameters

The subsurface input parameters provided to the model were derived from the results of the test drilling (2019). The heat storages takes place in a horizontal and relatively homogeneous aquifer at a depth of 360 – 383 mbgs, between two thick clay layers. The aquifer has a horizontal hydraulic conductivity of 12.7 m/d, with a vertical hydraulic conductivity 4 times smaller, and a natural groundwater temperature of 15.5 °C. The volumetric heat capacity of the solid phase is 2.0 MJ/ (m³ °C) for both sand and clay. Bulk thermal conductivity is 2.4 and 1.9 W/(m °C) for water-saturated sand and clay respectively. Porosity is 0.35 for the complete model domain.

Pumping scheme

Based on the heat supply/demand profile as described in the previous section, a pumping scheme was derived, as visualized in the figure below. Note that the flow rate during charging is lower in the first year, compared to the following years, and that the flow rate during discharging is relatively low in the first three years, because the heat demand from the greenhouses is low until the construction of the new greenhouse is finalized. As from the fourth year onwards, the pumping scheme remains constant. The injection temperatures are 85 °C and 30 °C at the hot well and cold well respectively. Note that during discharging of the hot well, a cut-off temperature of 55 °C is applied. This means that the discharging of heat stops when the production temperature of 55 °C is reached at the hot well, and that the HTATES system is in rest until the next charging period starts again in May.

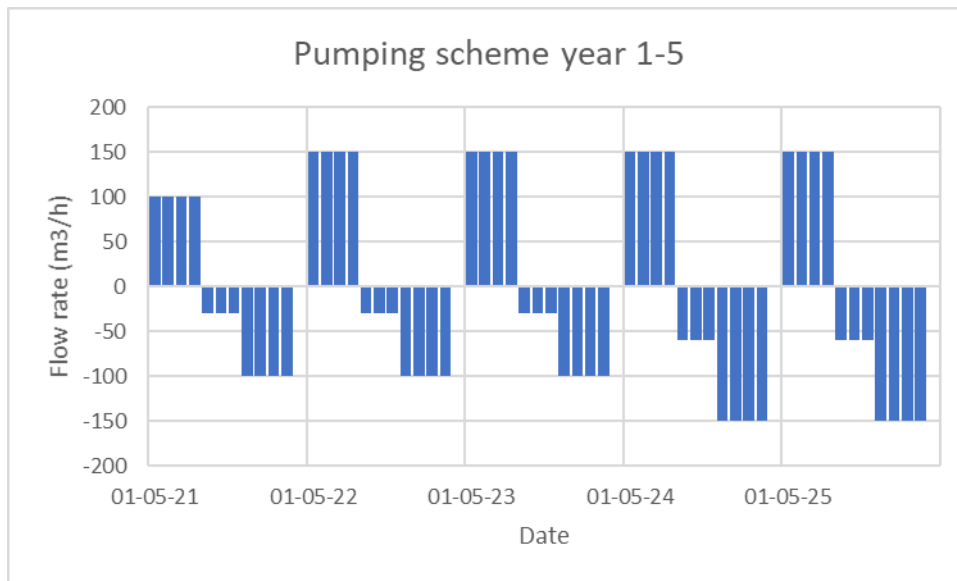


Figure 13: Pumping scheme applied in the first five years of the simulations. Positive flow rates represents charging, while negative flowrates represent discharging of the hot well.

The pumping scheme used for the simulations were somewhat uncertain. Therefore, it was not only investigated what well distance offered optimal results based on the basic pumping scheme as shown above, but it was also checked whether this well distance would also be optimal if all monthly flow rates would be increased/decreased by a factor 0.75. This means that the optimal well distance should offer satisfactory results for the basic pumping scheme, but also if the applied flow rates would be a factor 0.75 higher or lower than expected. The following table shows the pumping schemes applied:

Table 13: Various pumping schemes applied during the simulations. The basic pumping scheme is shown without color mark. The two additional pumping schemes differ slightly from the basic scheme, as shown in red (0.75*basic scheme) and yellow (basic scheme/0.75).

Phase → Jaar	Phase 1: Charge (4 mnth) m³/h	Phase 2: Discharge (3 mnth) m³/h	Phase 3 Discharge (4 mnth) m³/h	Phase 4 Rest
1	75/100/133	30	100	0
2	113/150/200	30	100	0
3	113/150/200	30	100	0
4 - 10	113/150/200	45/60/80	113/150/200	0

Scenarios

For each scenario, the subsurface properties and the pumping scheme described above were applied to the model, while the well distances were varied.

Assuming that heat is charged in the hot well with a flow rate of 150 m³/h for 4 months (basic pumping scheme), this means that about 440'000 m³ of hot water (85 °C) is injected in the hot well each year. Given the aquifer dimensions, the thermal radius corresponding to this storage volume is about 100 m. Various scenarios were constructed with well distances of 1.5 -2.5 times the thermal radius of the hot storage, i.e. with well distances of 150 – 250 m.

Output parameters

To find the optimal well distance, the following modelling results were visualized and assessed:

- Thermal recovery efficiency
- Thermal interference between the wells, based on production temperatures at the hot and cold wells.

4.3 Simulation results

The thermal recovery efficiency and the thermal interference between the hot and cold wells were assessed, for a number of simulations with various well distances. Based on the results, the optimal well distance seemed to be around 220 m. Below, only the results for this well distance is shown.

Thermal recovery efficiency

Figure 14 shows the thermal recovery efficiencies corresponding to a well distance of 220 m. Both the basic pumping scheme (orange) and the other schemes show satisfactory results. Note that from the fourth year onwards, more water is produced from the hot well (see Figure 13) hence more heat, compared to earlier years. This results in higher thermal recovery efficiencies. As becomes clear from the figure too, the scenario with large storage volume (charging 4 months with 200 m³/h) offers high recovery efficiencies, which is in accordance with the advise of the HT-ATES State of the Art report [6], which states that larger heat storage systems generally offer larger recovery efficiencies.

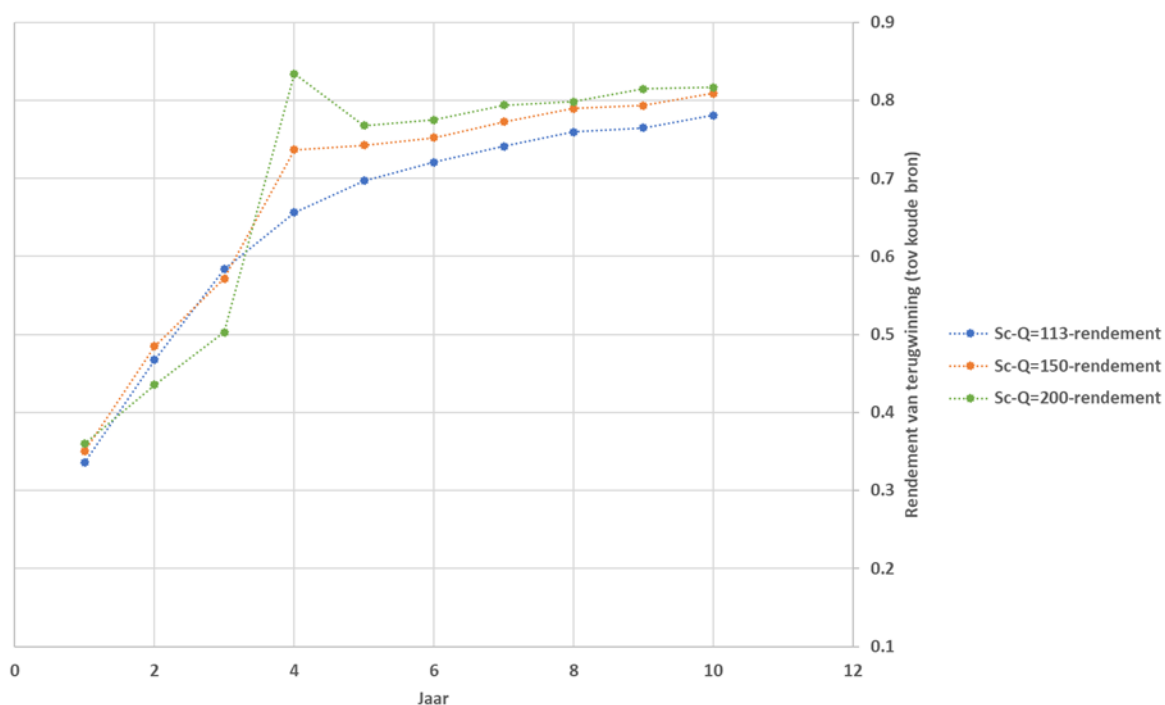


Figure 14: Thermal recovery efficiencies corresponding to a well distance of 220 m. The three lines represent the efficiencies that correspond to the three different pumping schemes, with orange as the basic scheme.

Thermal interference

Although the thermal recovery efficiencies seem satisfactory for a well distance of 220 m, it is still to be checked whether thermal interference between the hot and cold well remains within an acceptable range. To this end, it was looked at the production temperatures of the hot and the cold wells, as shown in Figure 15 for the scenarios with well distance of 220 m.

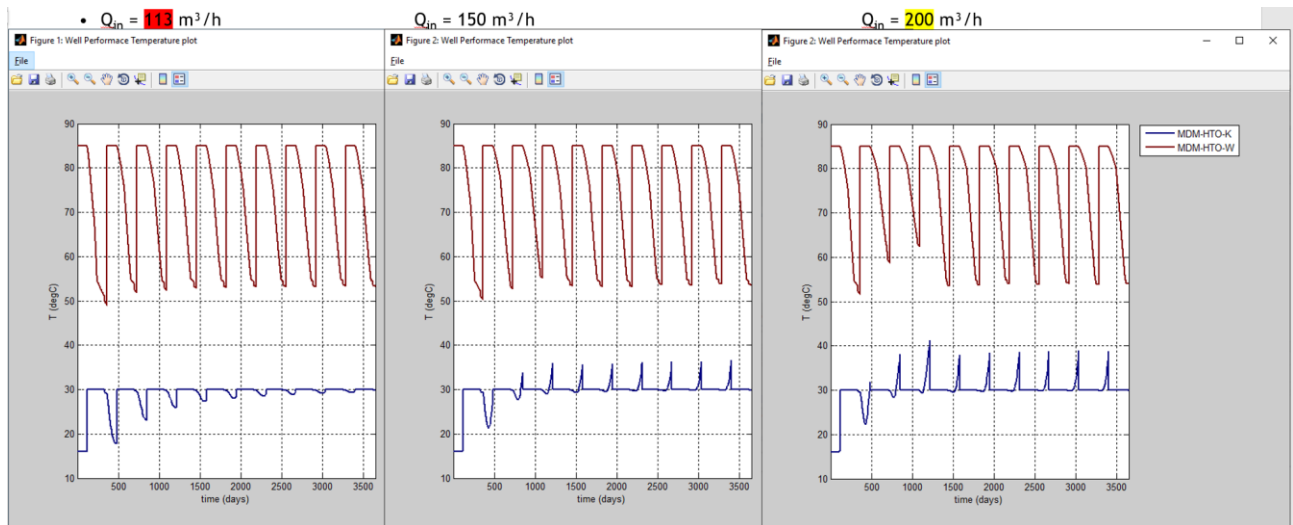


Figure 15: Well temperatures at the hot (red) and cold (blue) well of the HT-ATES system. The graph in the middle shows the well temperatures resulting from the basic pumping scheme, and the left/right graphs show the results for the lower/higher flow rates. Injection temperatures are 85 °C and 30 °C at the hot and cold wells respectively. Production temperatures are influenced by heat transported processes, as simulated by the HST3D model.

The figure shows that the production temperature at the hot well decreases during the recovery of heat from the hot well (red lines), until the cut-off temperature of 55 °C is reached. For the scenario with a high storage volume (right hand side of Figure 15), the production temperatures remain above 55 °C in the first three years (when heat demand is limited) compared to later years.

Looking at the production temperatures at the cold well, it becomes clear that scenarios with larger heat storage volumes (i.e. pumping schemes applying higher flow rates) show higher production temperatures at the cold well. This is because the heat injected at the hot well reaches the cold well filters. This may advocate for a larger well distance. However, the low production temperatures at the cold well in the scenario with low flow rates (left hand side of Figure 15) shows that the production temperature remains relatively low during the first years. Placing the wells farther apart would further decrease the production temperature at the cold well. It is important to note that the heat storage capacity of the HT-ATES system is typically limited by the minimum temperature at the cold HT-ATES well, because of the high viscosity of the cold water. In the Netherlands, norms are applied to determine the maximum flow velocity at the borehole wall to prevent sand production. The critical flow velocity (hence the critical flow rate) is defined by hydraulic conductivity, which is in turn sensitive to viscosity and the temperature of the produced water. Therefore, the temperature at the cold well should remain high enough to facilitate a sufficient flow rate for the HT-ATES system during charging of heat. Because of this consideration, larger well distances would pose risks for the maximum flow rate applied to the HT-ATES system, because of relative low production temperatures at the cold wells. Note that the HT-ATES system in Middenmeer is designed for flow rates exceeding the Dutch norms [7].

4.4 Conclusions

Based on the results and the considerations described there, it was concluded that for a well distance of 220 m, both the thermal recovery efficiencies and the thermal interference between the hot and cold wells were satisfactory for the ECW case, for both the basic pumping scheme and the uncertainty that applies to it. This well distance corresponds to approximately 2.2 times the thermal radius of the hot storage. The well distance of 220 m was chosen as the optimal well distance and this conclusion was subsequently used as input for the technical well design.

4.5 System modelling

4.5.1 CHESS

CHESS (Controlled Hybrid Energy Systems Simulator) is a proprietary software tool developed by TNO to design and simulate an energy system infrastructure. In the transition towards a sustainable energy system the latter becomes increasingly complex. Intermittent unpredictable energy sources, such as wind and solar power create challenges for supply/demand management. Conversion and storage technologies, such as heat pumps and geothermal storage can be used to overcome this problem, creating interaction between various energy infrastructures (i.e. thermal and electrical grids). Novel control algorithms are being developed to enable all these pieces of technology to cooperate in a sustainable, affordable and reliable energy system.

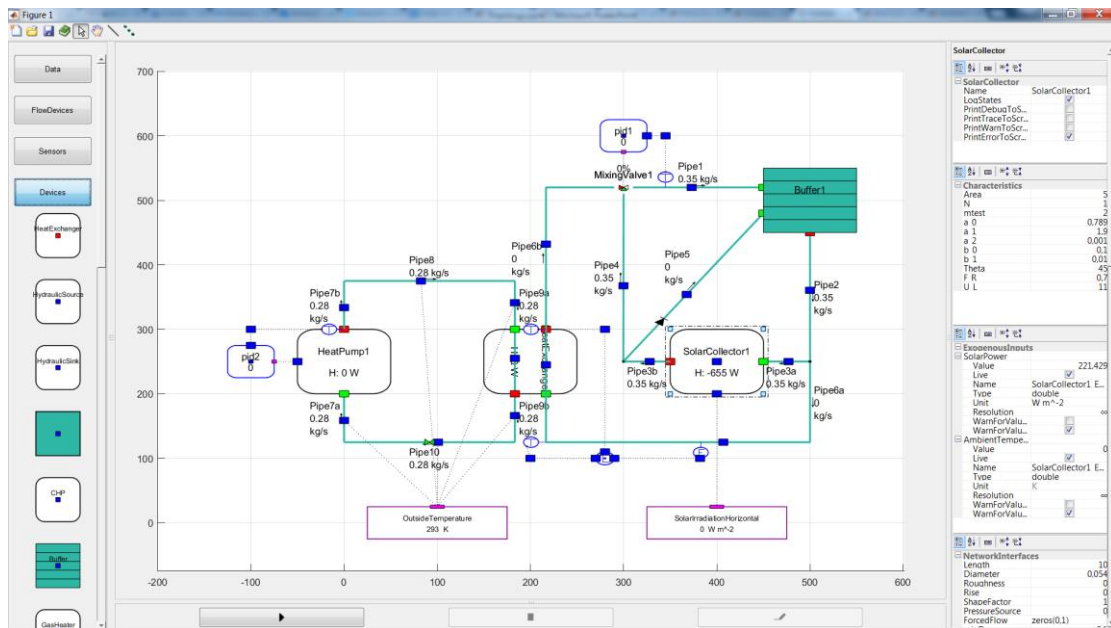


Figure 16: CHESS software tool at a glance.

The goal of CHESS is to allow the user to design energy systems, by connecting components in *any* way he or she sees fit, using a drag & drop interface (Figure 16). Control algorithms can be easily selected to operate the various components, providing a range of conventional and modern (smart) controllers. Scenarios are conveniently created by defining external conditions like weather and commodity prices. With the system created and the boundary conditions set, a dynamic simulation of the system can be started, calculating all energy flows, temperatures, fuel consumptions, losses, efficiencies and – if defined – KPI's at a component or system level, throughout time. The system in operation is visualized in animation, leading to insight into the dynamics at hand. Operationally relevant parameters can be logged over the simulated time period. This way, various system designs can be quickly and objectively compared.

CHESS combines the following solvers to enable full system simulation:

- a detailed hydraulic solver (pipe flow and pressure drop, valve, pump, etc.)
- a detailed thermal solver (thermal losses, thermal transport)
- a simple electrical network (electricity power)
- a detailed simulation of device dynamics (ramp-up time, setpoint control, etc.)

a) HT-ATES model

Aquifer Thermal Energy Storage (ATES) plays an important role in the integrated heat network by storing the excess heat for example from geothermal source during low demand season (summer time) and producing the heat during peak load (winter time). The physical model of ATES for ECW case has been developed in

the numerical software DoubletCalc3D [8]. Using this software it is possible to calculate the temperature and pressure around two or more geothermal wells, in three dimensions (3D) and over the course of time. In this study, we use the initial design parameters of the ECW ATEs model before optimization with dimensions of 400m x 400m x 480m (depth) with a well spacing of 120m between hot and cold well (Figure 17). The numerical model is simulated for 15 years using assumption constant flow rate of 50, 100 and 150 m³/h (during injection and production) and supply temperature 83 °C with the following scenario⁵: 3 months injection, 3 months rest, 3 months production and 3 months rest for each cycle.

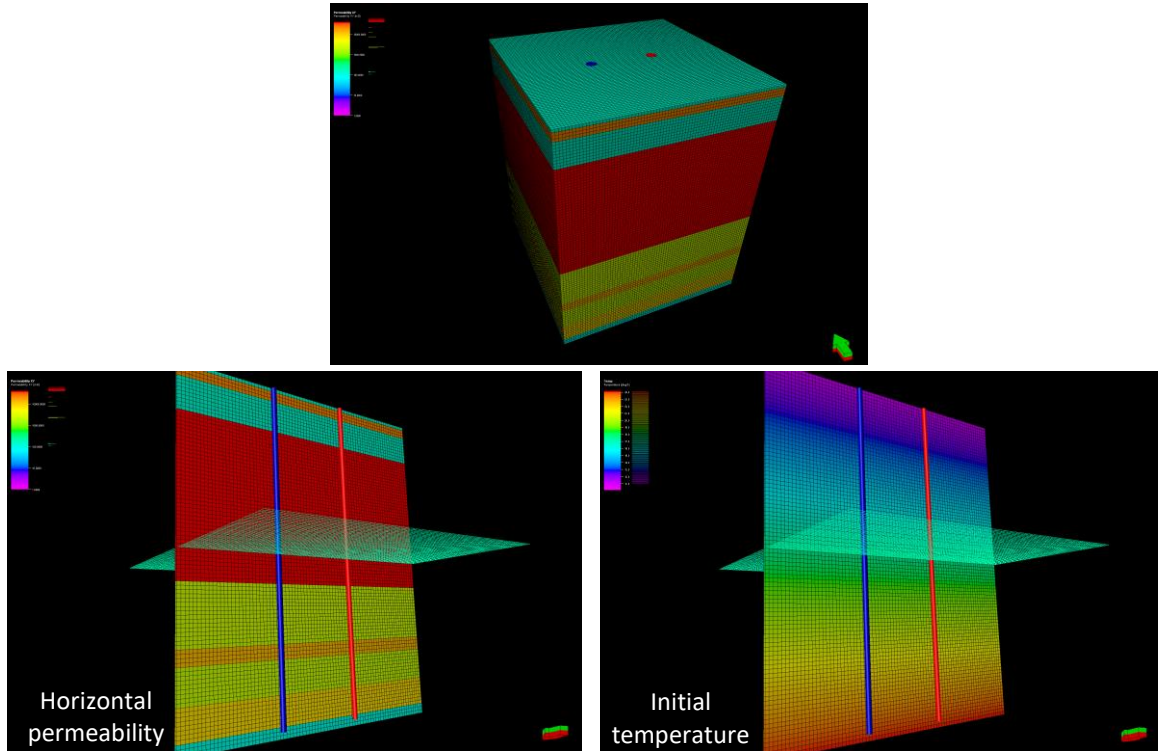


Figure 17: Numerical model of ATEs of ECW case in DoubletCalc3D.

However this model is computational expensive and requires several hours to calculate the simulation which is not really convenient to be used for an integrated heat network analysis. Thus, a proxy (fast) model was developed in CHESS and calibrated to the result of the numerical model. A simplified analytical model to predict storage well temperatures are made based on mixing of injected and in situ water and dispersion of heat in subsurface [9]. Two similar models are developed for warm well and cold well.

The model uses F_{mix} (as a function of volume ratio) for predicting temperature drops during production and F_{temp} (as a function of cycle year) to replace the volume left behind in each cycle injection and production.

$$T_{startcycle} = T_{soil} + F_{temp}(T_{injection} - T_{soil})$$

$$T_{well} = T_{startcycle} F_{mix} + T_{soil}(1 - F_{mix,warm})$$

Where,

- $T_{injection}$ is the injection temperature to ATEs
- T_{soil} is the soil temperature
- $T_{startcycle}$ the initial temperature of the well for each cycle year
- T_{well} is the well temperature
- F_{temp} is a fit function for initial temperature as a function of cycle year
- F_{mix} is a fit function for temperature drops as a function of volume produced

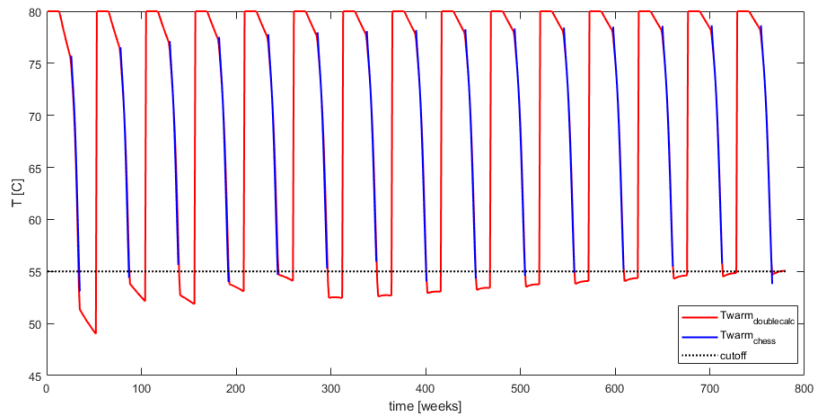
⁵ During the study, the actual flowrate strategy to fill in and use the ATEs is unknown. Thus, for validation of the proxy model with the numerical model, we assume this operational flowrate strategy.

4th order polynomial is used to represents both F_{mix} and F_{temp}

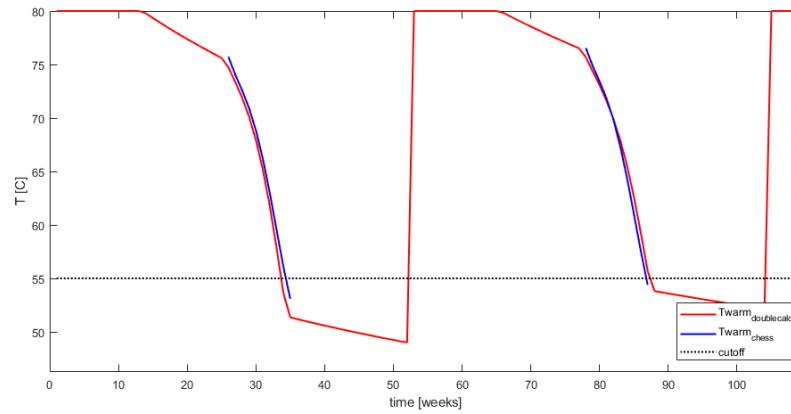
$$F = a x^4 + b x^3 + c x^2 + d x + e$$

Table 14: Coefficient of 4th order polynomial fit function ATES proxy model.

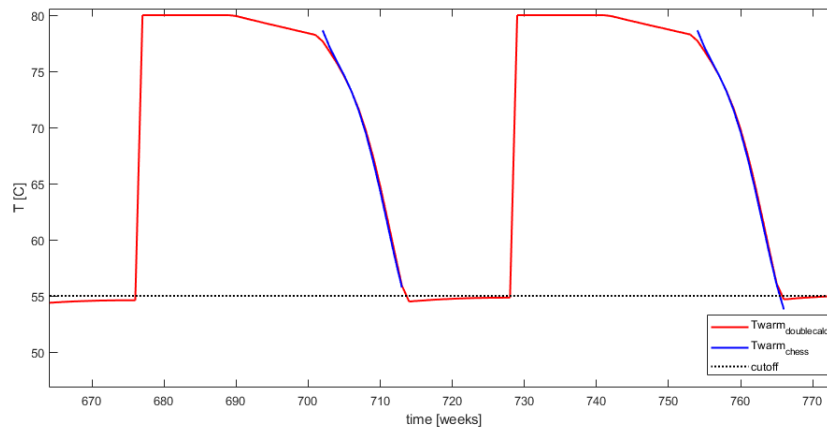
	a	b	c	d	e
F_{temp}	-5.163e-06	0.0002074	-0.003059	0.02067	0.912
F_{mix}	3.216	-5.198	2.268	-0.7335	1.042



(a)



(b)



(c)

Figure 18 Temperature comparison between DoubleCalc2D (red line) and CHES proxy model (blue line) at flowrate 150 m³/h. (a) Full 15 years simulation, (b) at year 1st and 2nd, and (c) at year 14th and 15th year.

The ATEs proxy model has good accuracy with root mean squared error (RMSE) of 0.83°C, mean error of 0.22°C and standard deviation of 0.79°C for the hot well. This model runs with computational speed less than 10 seconds. The proxy model was then integrated as a new asset in CHES framework, an example of the implementation of this ATEs model in a heat network is shown in Figure 19.

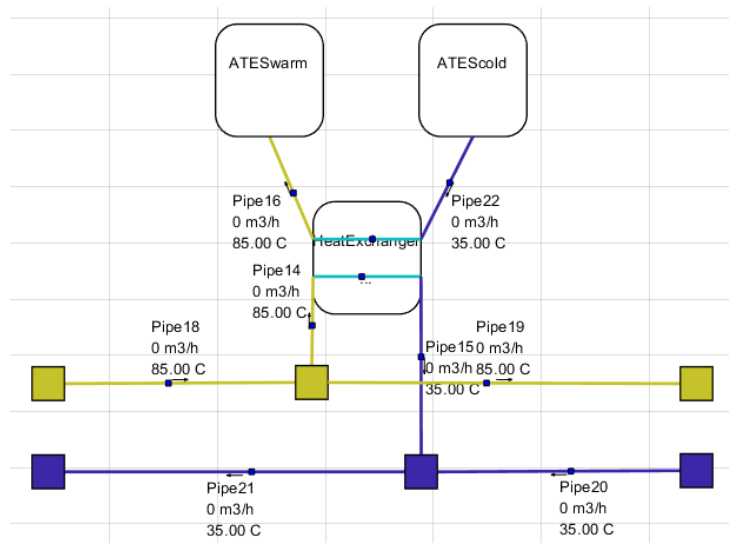


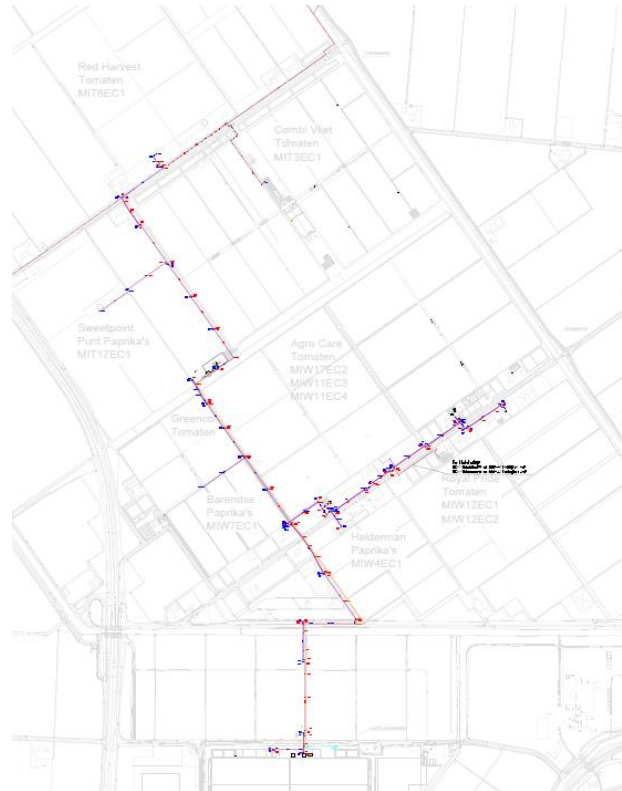
Figure 19: ATEs model in CHES and its connection to the heat network.

b) Network modelling

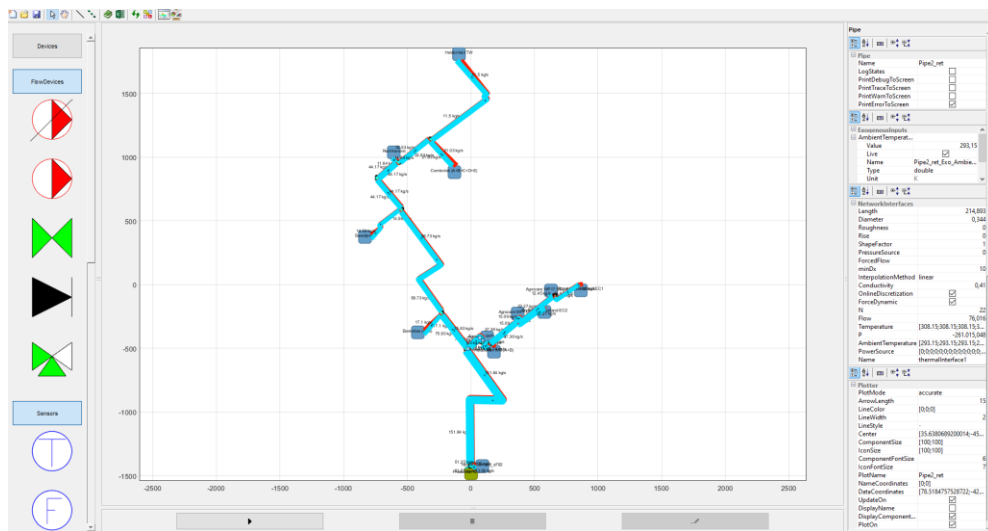
The existing ECW heat network consists of 3 geothermal doublets with a maximum thermal production capacity of 43 MW. This network has several greenhouse customers with peak demand reaching 70 MW. They are aggregated to 12 Demand Clusters. The network has an operating temperature of 85 °C for the supply line and 35 °C for the return line. The pipe diagram was derived from a CAD drawing and the LOGSTOR pipe catalogue [10] was used as a reference for specific piping details.



(a)



(b)



(c)

Figure 20: (a) Satellite view of ECW heat network (b) CAD diagram piping layout of ECW heat network (c) CHES model of ECW heat network.

Before running scenario analysis, we would like to validate our heat network model based on measurement data of Distributed Control System (DCS) data on 11th January 2019 at 11:46. The operational strategy of ECW is to have a setpoint flowrate based on weekly demand request. Thus this measurement values hold for 1 week. We compare the flowrate and temperature passing through the heat exchanger of the greenhouse. We also compare the total pressure drop of the heat network at the distribution pump and temperature at the heat exchanger of the geothermal source. During the study, measurement data for the summer period was not available.

Table 15: Comparison measured value and simulated value at 11th January 2019.

Demand Clusters	Measured Flowrate (m3/h)	Simulated Flowrate (m3/h)	Difference (%)	Measured Temperature (C)	Simulated Temperature (C)	Difference (%)
0	176.4	177.49	+0.62	84.6	84.89	+0.34
1	52.3	52.23	-0.13	84.4	84.76	+0.43
2	81.2	80.92	-0.34	84.6	84.85	+0.30
3	53	52.89	-0.21	84.6	84.86	+0.31
4	43.3	43.11	-0.44	84.3	84.72	+0.50
5	0	0	0	84.2	84.61	+0.49
6	34.1	33.99	-0.32	84.2	84.61	+0.49
7	59.4	59.19	-0.35	84.6	84.88	+0.33
8	50.5	50.41	-0.18	84.2	84.42	+0.26
9	40.4	40.29	-0.27	84.2	84.39	+0.23
10	72.9	72.79	-0.15	84.1	84.24	+0.17
11	39.9	39.80	-0.25	84.1	84.23	+0.15

at Geothermal	Measured	Simulated	Difference (%)
Temperature Supply (C)	84.6	84.92	+0.38
Temperature Return (C)	32.8	32.87	+0.21
Supply pressure (bar)	8	8	0%
Return pressure (bar)	2	2.09	+4.09
Total Pressure Drop (bar)	6	5.91	-1.5

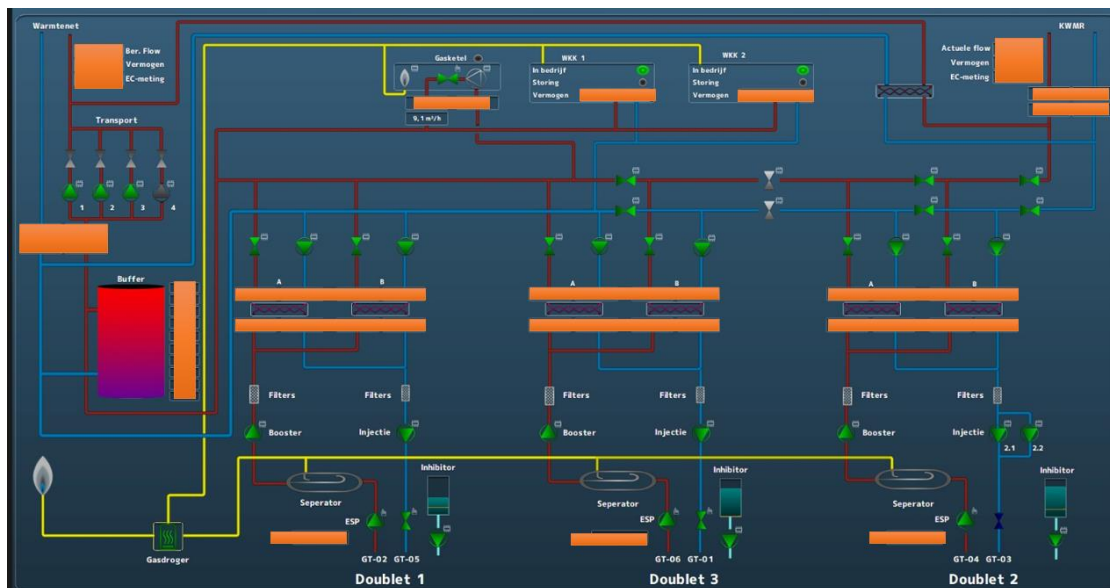


Figure 21: Schematic diagram geothermal doublets DCS system.

4.5.2 Heatmatcher

HeatMatcher is an innovative controller for heat networks [11, 12]. The initial focus of the HeatMatcher controller was controlling heat networks in buildings and apartment complexes. Several field trials with HeatMatcher were performed on heating systems with gas boilers, heat pumps and thermal storage tanks. Results show that HeatMatcher outperforms standard rule-based control systems by 20%. This is due to a better dispatching of sustainable sources and smarter utilization of the thermal storage systems in those buildings. This results in a 20% reduction in gas consumption and 12% reduction in energy costs [13].

HeatMatcher is an agent-based controller. This means that each heat producing component (sources) and consuming component (demands) is represented by an agent in the controller. This agent is responsible for the control of the component and exchanges information with the controller to optimize its dispatch.

HeatMatcher's control algorithm is market-based. A market is a virtual trading place where energy is exchanged. The agents act on this market and express their demand and/or supply in terms of a bid. This bid defines information at which price a certain energy volume is consumed or produced. When all bids are received, HeatMatcher calculates for each market the optimal dispatch such that consumption and production are equal. The agents are subsequently required to implement this dispatch.

Since HeatMatcher is aimed for use in buildings, several aspects were not taken into account in the algorithm which are, however, relevant for heat networks. These aspects are:

1. Distances between sources and demands are significantly larger. This means that the time between dispatch and consumption, delays and thermal inertia become relevant when flexible temperature regimes are used.
2. Thermal losses in pipes cannot be neglected and should be taken into account.
3. Capacity constraints of the pipes

This means that sources nearby should take preference over sources further away when their marginal costs are equal. The topology of the network is the originator of these aspects, i.e. when the topology changes these aspects also change. Therefore, the HeatMatcher algorithm should take the topology of the network into account when optimizing the dispatch in heat networks.

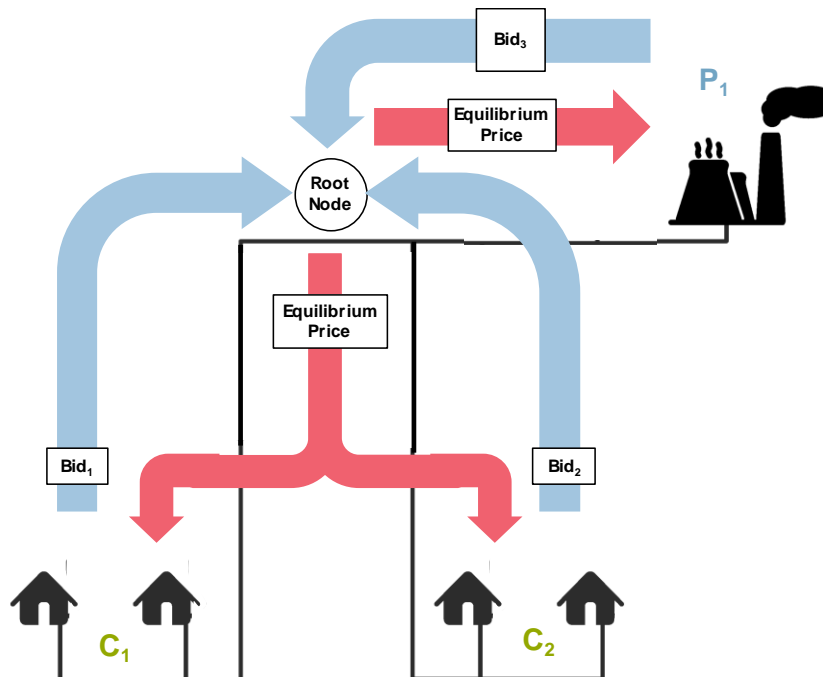
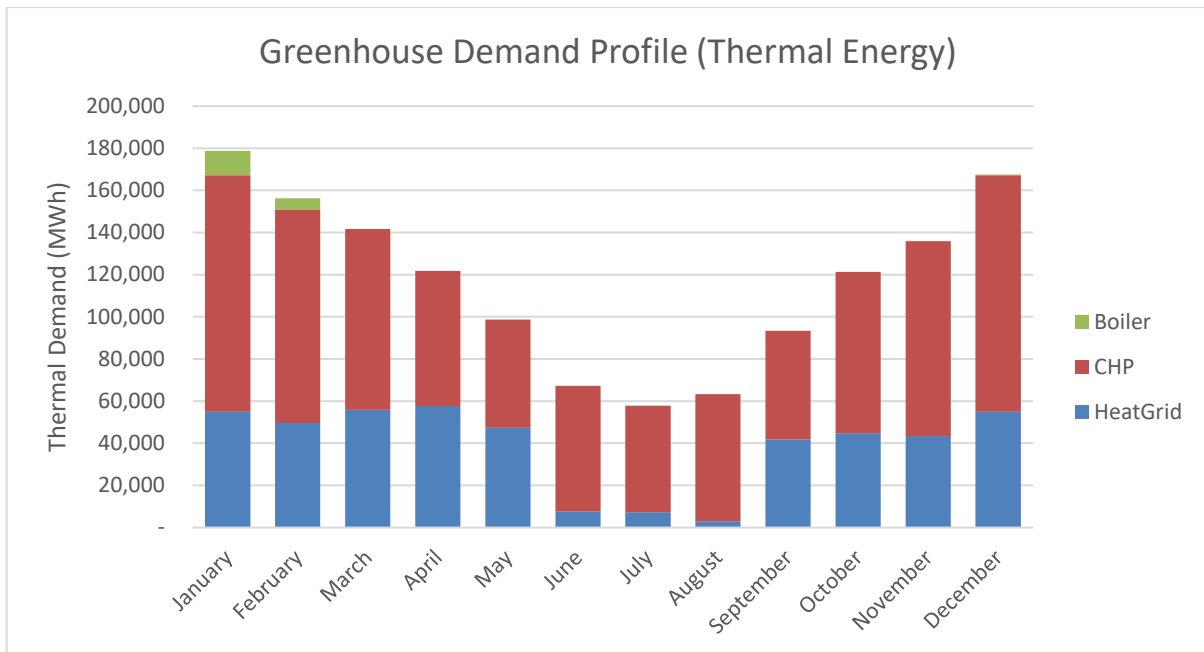


Figure 22: Example of algorithm with one producer and two consumers. First, bids are sent to the root node (blue). There, the equilibrium price is calculated and sent back to the consumers and producer (red).

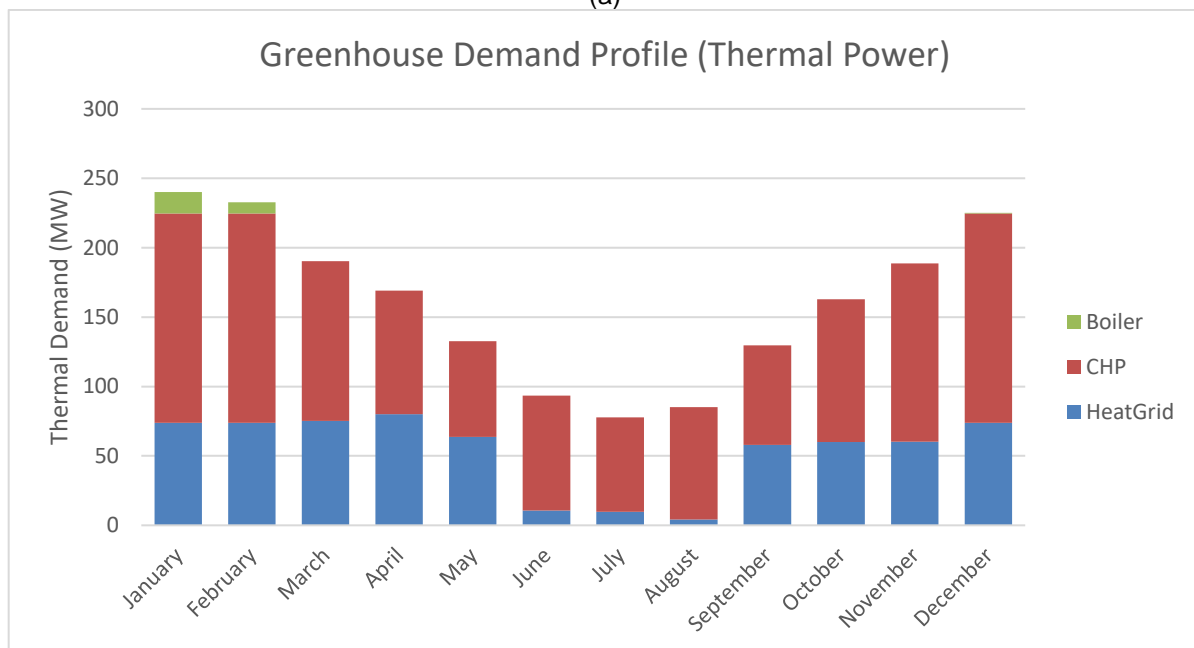
4.6 Scenario analysis

4.6.1 Demand profile

The total heat demand for all greenhouses for each month in entire year is presented in Figure 23. In order to be used in CHESS, we need to divide this total demand into each individual greenhouse with a finer time resolution.



(a)



(b)

Figure 23: Total heat demand profile of ECW heat network. (a) Thermal Energy (b) Thermal Power.

Workflow :

- For each individual greenhouse, the areas (ha of lit and unlit crops) are multiplied by their respective energy demand per ha figures based on crop type. This gives the **total thermal demand of a green house**. This demand can be satisfied by the heat grid, the CHP and the boiler.
- The monthly heat grid thermal demand is found by subtracting the CHP/boiler generated heat from the total thermal demand. The heat grid thermal demand is compared to the total in order to determine how much thermal demand is satisfied by the heat grid compared to other sources (**percentage heat grid usage per month**).
- Then, the **total thermal demand of a green house** is scaled with the **percentage heat grid usage per month** to come to the demand of each greenhouse from the heat grid per month.

- Monthly figures (12 for each greenhouse) are then fitted with smoothing Piecewise Cubic Hermite Interpolating Polynomial (fits) to get to a finer resolution (365 for each greenhouse) – in this case days.

Table 16: Lit and unlit area of each greenhouse.

Demand Cluster	Crop	Area (ha)	Area lit (ha)	Area Unlit (ha)
0	Paprika	40	0	40
1	Tomato	27	27	0
2	Paprika	24	0	24
3	Tomato	27	27	0
4	Tomato	5	45	9
5	Tomato	30	30	0
6	Tomato	30	15	15
7	Paprika + Tomato	28	9	19
8	Paprika	13.5	0	13.5
9	Tomato	30.8	23.3	8
10	Tomato	75	75	0
11	Paprika	10	0	10
Total		391	251	140

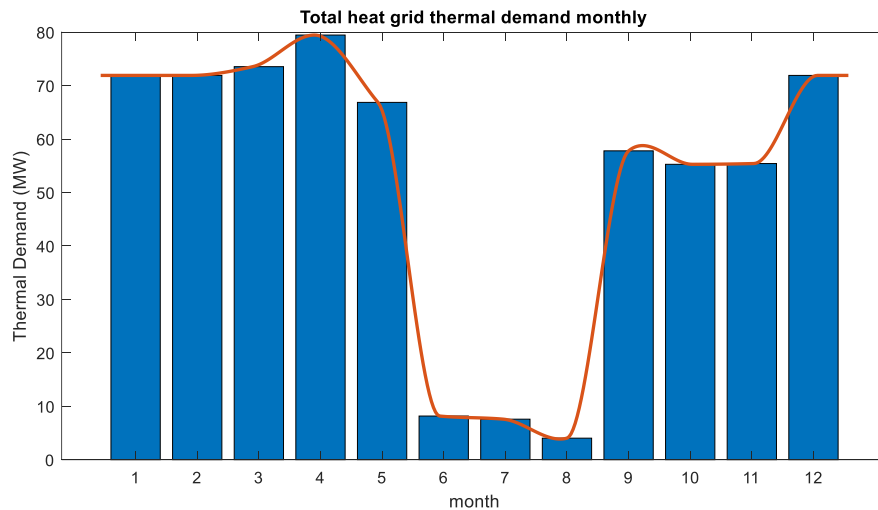


Figure 24: Monthly total heat grid thermal demand (blue bar chart) and daily total heat grid thermal demand (red line).

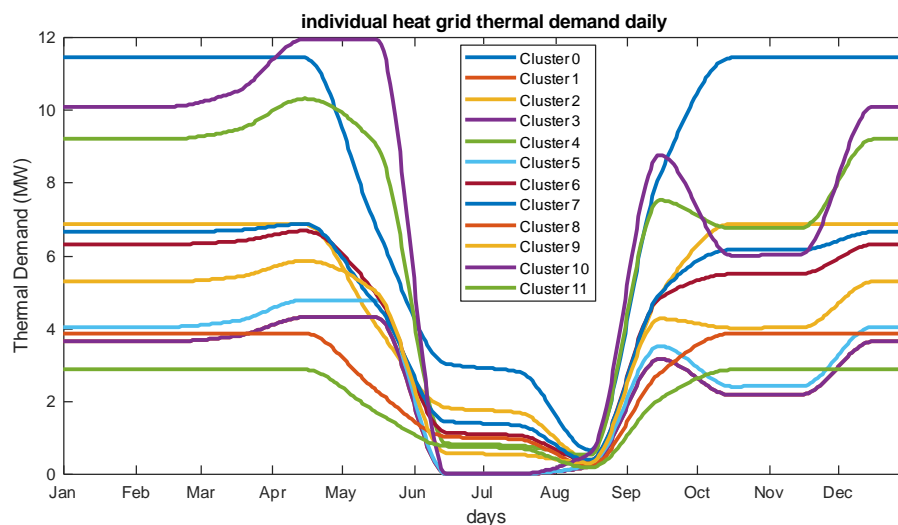


Figure 25: Daily heat grid thermal demand for each individual greenhouse.

4.6.2 Control Strategies

Current heat network operation strategy is to calculate setpoint flowrate for each customer on weekly basis based on desired heat demand. Then, the production is fixed per week. The control valve of heat exchanger regulates delta temperature (ΔT) at 1°C between primary and secondary side. The distribution pump ensures that there is no customer's delta pressure (ΔP) over control valve below 1 bar.

In CHESS, we can use a rule-based controller for supply and demand allocation or use HeatMatcher to calculate supply and demand matching based on bid curves. For source allocation, there is a requirement that geothermal sources have a high priority and should be running at least 7'000 hours in a year. For demand allocation, we assume each individual consumer has the same purchasing price, thus the same priority. If the consumer has a different set of requirements, for example priority based on "first come first serve" basis or based on a specific contract (minimum delivery), this can be easily implemented in the bid curve of HeatMatcher.

4.6.3 Case Scenario

The main objective of WP3 is to define the design and operational strategies for ATES and demand side management (DSM) based on the above-surface conditions (DHC networks, surplus of thermal production) of geothermal district heating networks and to assess the economic viability of the proposed district heating schemes.

To answer this objective, we will assess several case scenarios from implementing possible integration options of different types of ATES, finding optimal ATES configuration and supporting business case of ECW for future heat sources and demands. List of scenarios are defined below:

a) Direct coupling ATES with greenhouse

This is a default implementation, where ATES is deployed next to Demand Cluster 11 (the farthest consumer in the heat network) and is used directly to supply this greenhouse (Figure 26). The ATES system cannot supply heat to the heat network directly because the ATES supply temperature decreases over time during production ($T_{\text{ates}} < T_{\text{heatgrid}}$). 3 different flowrates⁶ are assessed: 50 m³/h, 100 m³/h and 150 m³/h. An operational cut off temperature of 55°C is implemented. The greenhouse requires a minimum temperature supply of 55°C . When the temperature of the ATES is below the cut off temperature, the heat production from the ATES is stopped.

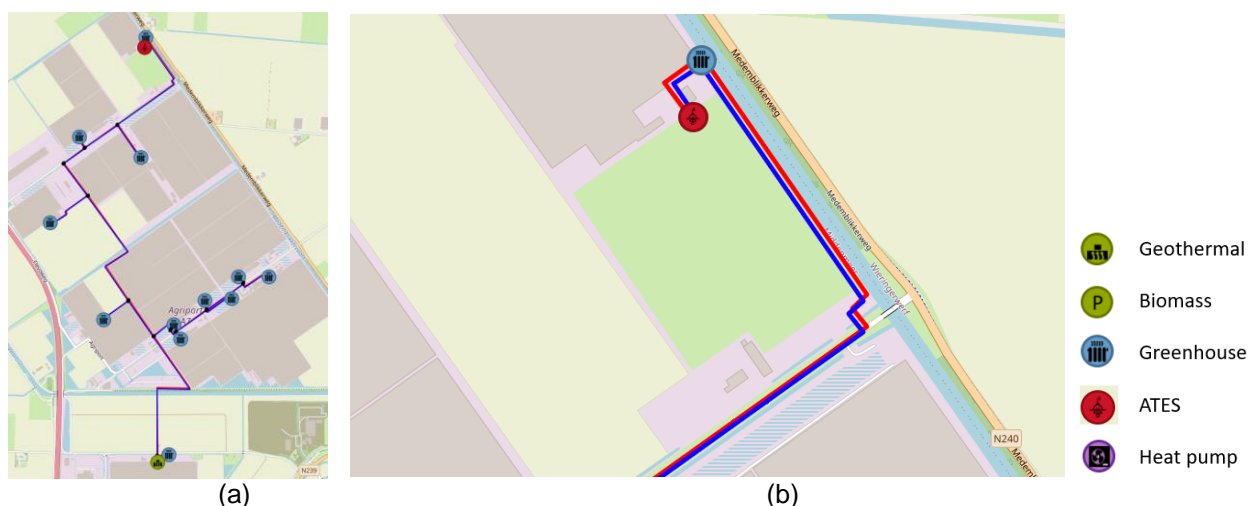


Figure 26: (a) Zoom-out overview ATES location (b) ATES direct coupling to supply green house.

⁶ The maximum flow rate of the real ATES at ECW is not known as the well not in operation yet; current estimates range from 50 to 150 m³/h. For these values a sensitivity analysis was conducted to validate the CHESS model.

b) Coupling ATES with heat pump to the heat grid

In this case scenario, there is a direct coupling between ATES and the heat network. A heat pump is used to stabilize the supply temperature to the heat grid during production period. We will assess 3 different flowrates : 50 m³/h, 100 m³/h and 150 m³/h. Again, an operational cut off temperature of 55°C is implemented.

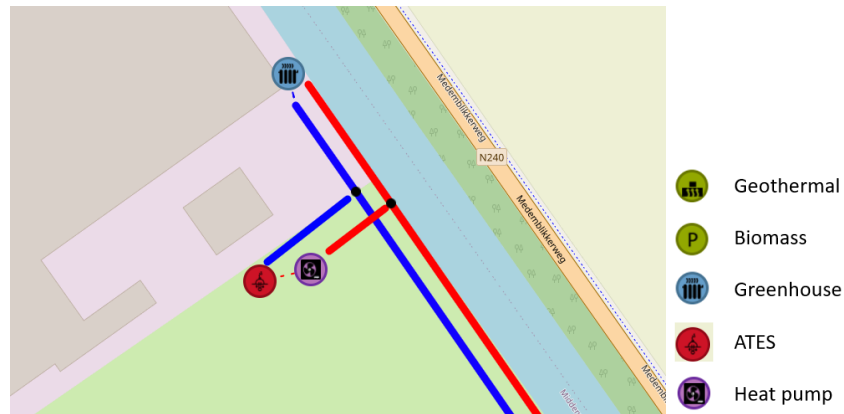


Figure 27: ATES direct coupling to heat grid via a heat pump.

c) Adding additional biomass heat source

There is a plan to add an additional heat source next to geothermal heat sources. This biomass heat source is located in the North-West (Figure 28) and capable to deliver 18 MW. This additional heat source will give more flexibility and leverage in delivering heat to the customer (Figure 29).

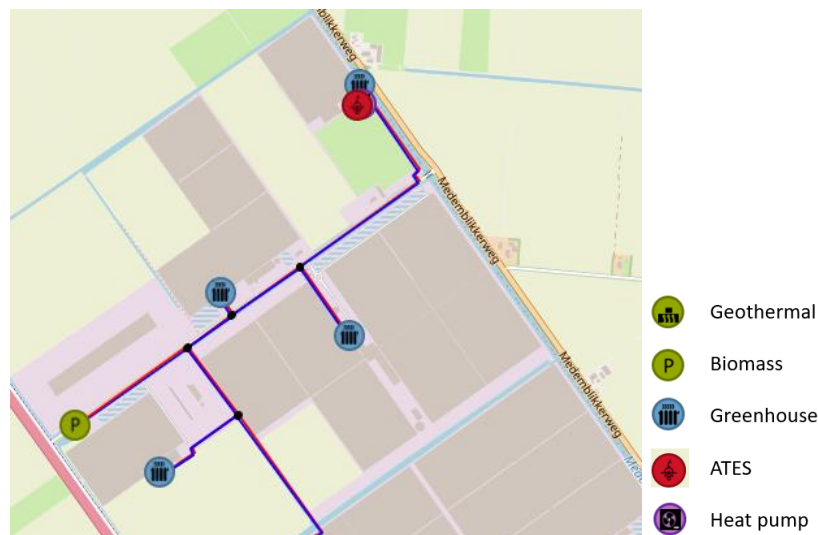


Figure 28: Additional biomass heat source in the ECW heat network.

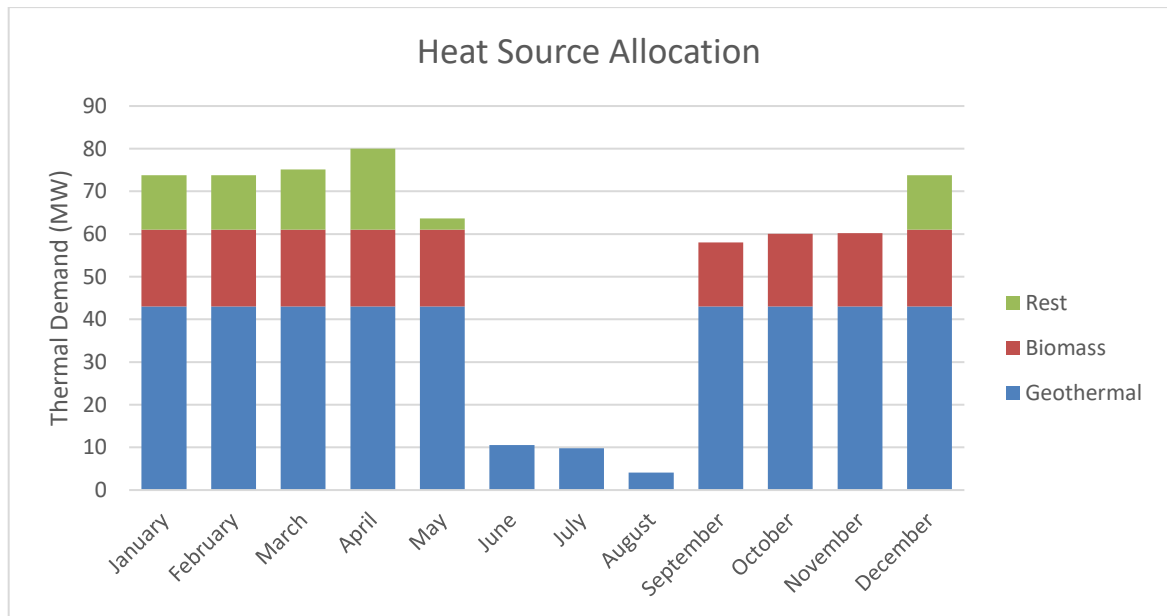


Figure 29: Example heat source allocation without ATES.

d) Using centralized large ATES

Introducing 8 ATES wells (3 warm wells and 5 cold wells) with flowrate up to 400 m³/h (~ 23 MW). The possible location of these wells is at the end of the first branch on the west side of the heat network.

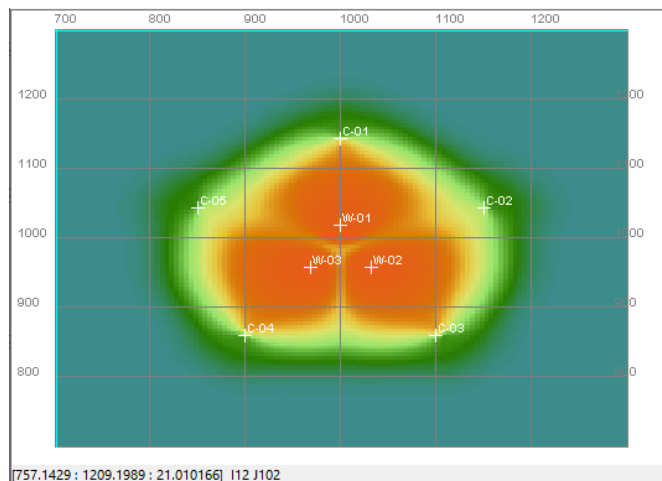


Figure 30: Top view schematic 8 wells ATES.

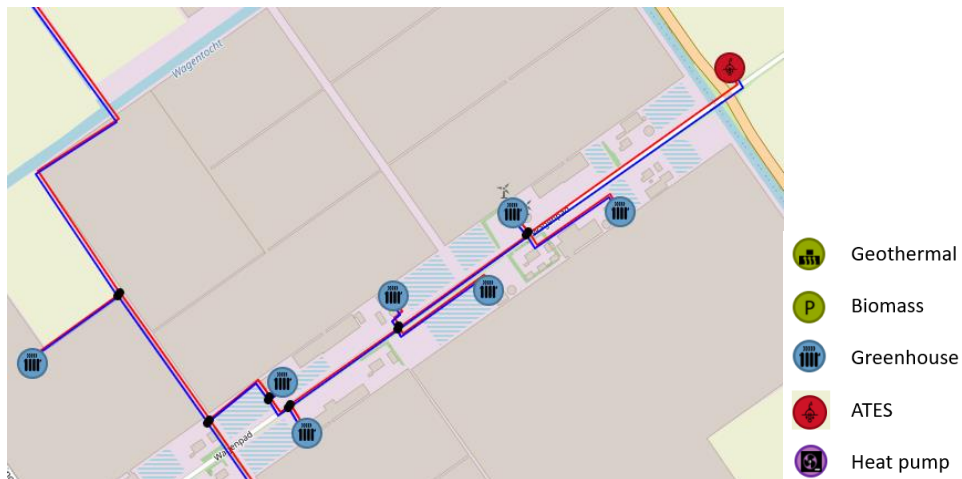


Figure 31: A large ATES integration into ECW network.

e) Using decentralized small ATES

Another possibility is by replicating a doublet well ATES and distribute them into several locations in the heat network. As presented in Figure 32, there are 3 additional ATES wells integrated in the system. A flowrate of 100 m³/h is used for each ATES.

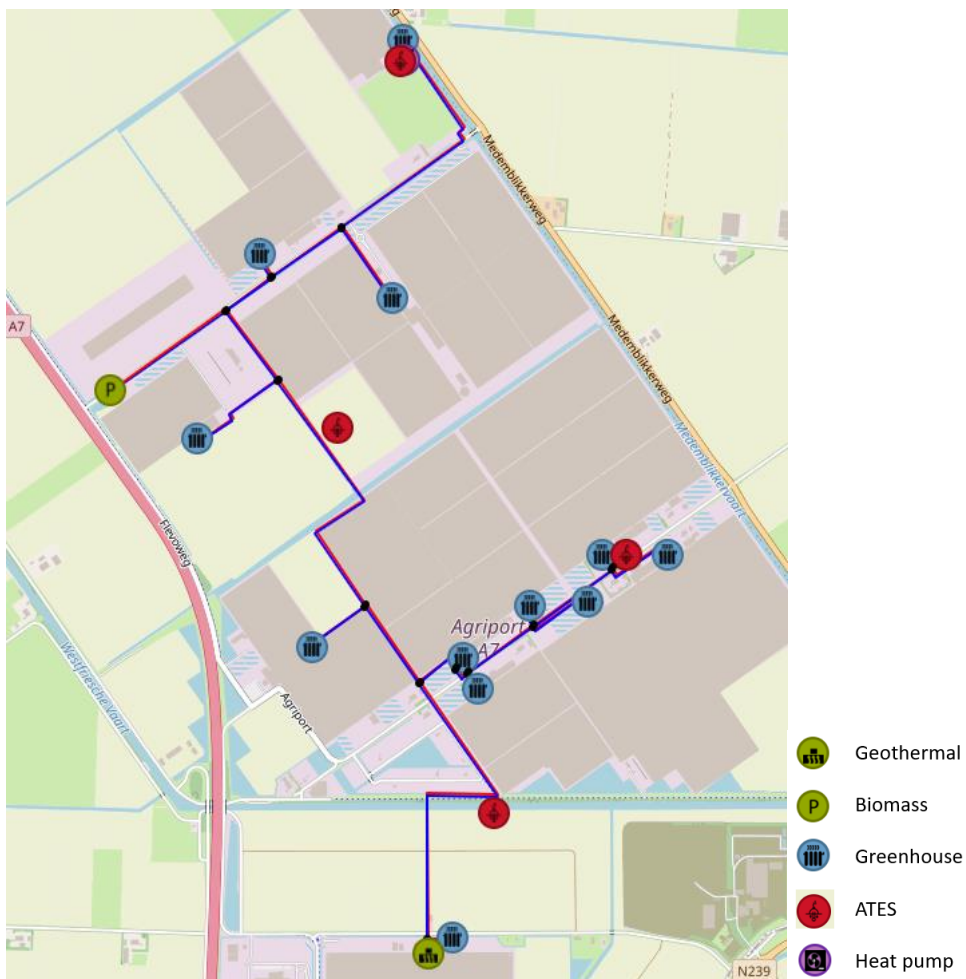


Figure 32: Several distributed small ATES into ECW network.

4.7 Simulation results

4.7.1 Time series simulation

In this section we will present the time series information for a simulation period of 1 year (starting from 1st of June) and make some comparison to the current existing heat network (base case). The “thermal demand” is the requested power by the greenhouses and “thermal consumption” is the actual power based on flowrate passing through the greenhouses. During the winter time due to limited production supply, the actual consumption is lower than the thermal demand. Thus, each greenhouse will be supplied with a lower flowrate based on ratio utilization. In Figure 33 the thermal balance of the heat network is given for the base case. Allocation ratio utilization for each demand cluster is set equal each other (Figure 34). Where ratio utilization is thermal consumption divided by thermal demand.

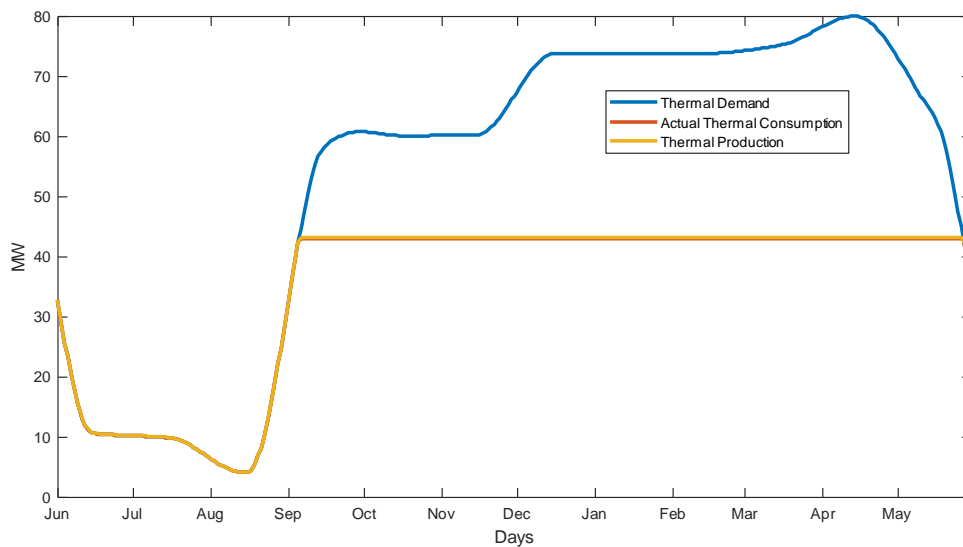


Figure 33: Total thermal balance of the heat network for base case.

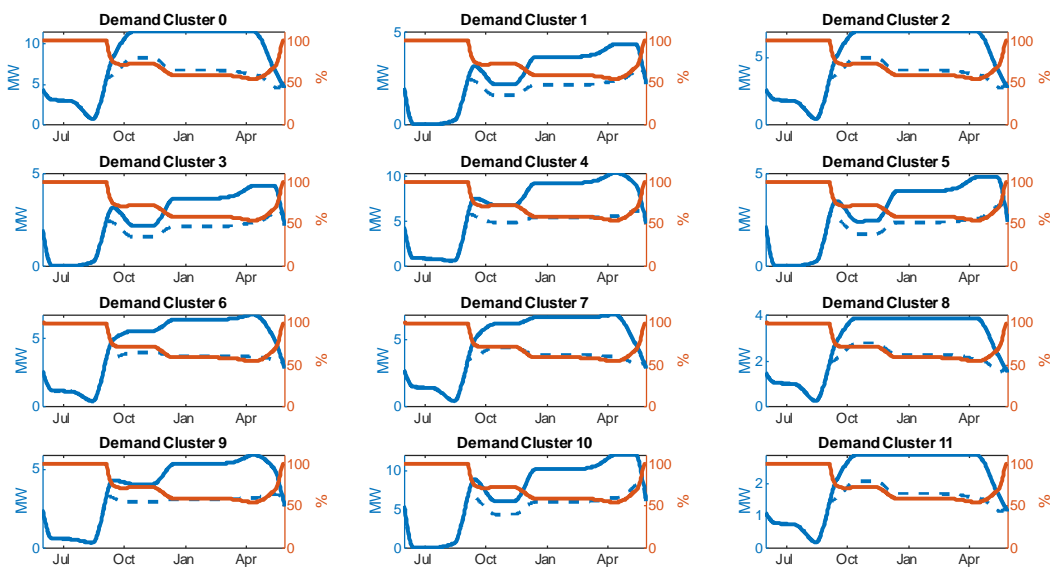


Figure 34: Thermal demand (blue line), thermal allocation (blue dot line) and ratio utilization (red line) of each demand cluster for base case.

Since the pump curve specifications are usually unknown in the design phase, the theoretical hydraulic distribution pump shaft power was calculated taking into account a pump efficiency of 80%.

$$P_h = \frac{q \Delta p}{3.6 \cdot 10^3} \quad P_s = P_h / \eta$$

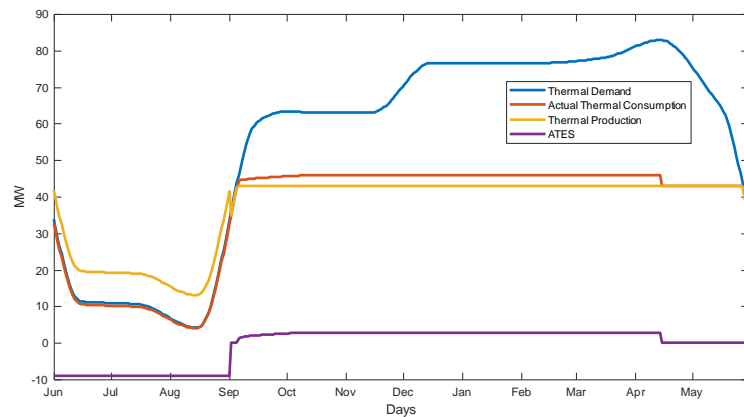
Where,

- P_h = hydraulic power (W)
- q = flow (m³/h)
- Δp = differential pressure (Pa)
- P_s = shaft power (W)
- η = pump efficiency

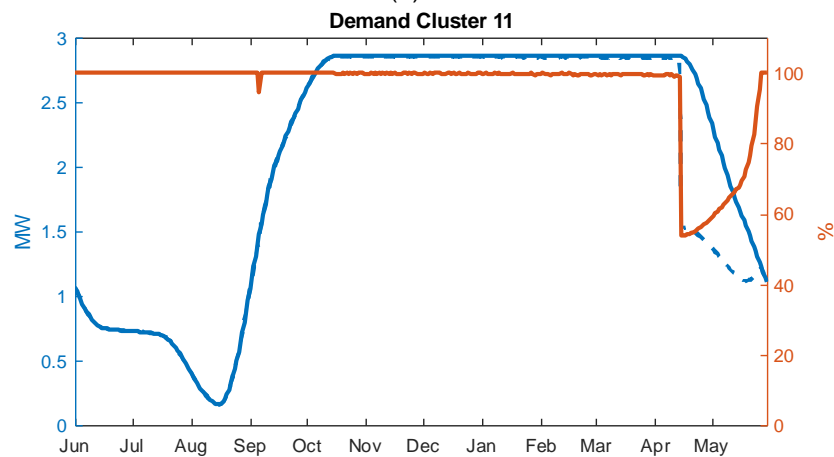
For the Electronic Submersible Pump (ESP) in the geothermal doublet, a pump efficiency of 70% and a differential pressure of 50 bar was assumed.

a) Direct coupling ATES with greenhouse

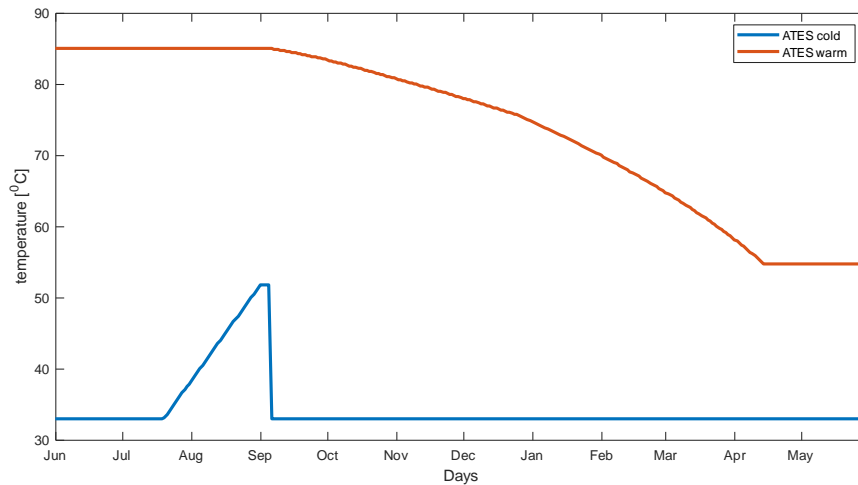
ATES is located next to Demand Cluster 11 and is used directly to supply this greenhouse. Since ATES can't deliver back the excess power to the heat grid, the production flowrate will be set equal to thermal demand of this greenhouse. Once ATES reaches cut-off temperature, this greenhouse is supplied back by the heat grid.



(a)



(b)

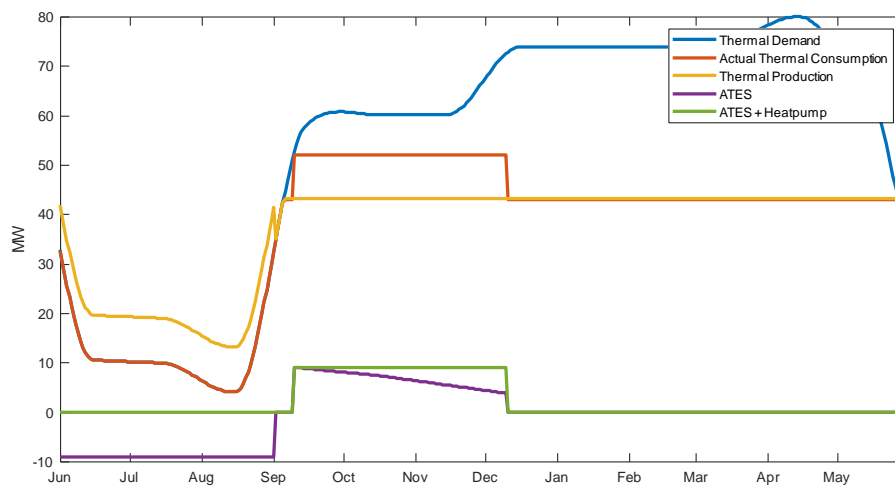


(b)

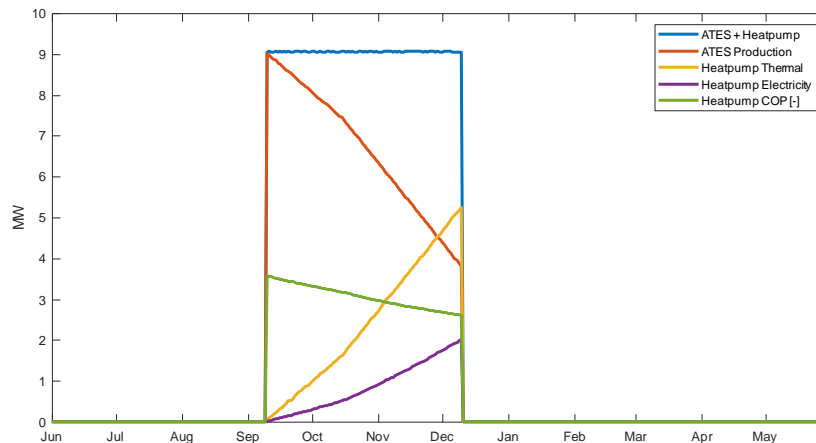
Figure 35: (a) Total thermal balance of the heat network for direct coupling ATES with flowrate 150 m³/h (b) Thermal demand (blue line), actual thermal consumption (dash blue line) and ratio thermal consumption and thermal demand (red line) of Demand Cluster 11 (c) temperature warm and cold well during injection and production.

b) Coupling ATES with heat pump to the heat grid

A heat pump is coupled with the output of ATES to boost the supply temperature when it is below the heat grid temperature. This combination will give a possibility to supply back the surplus heat when the thermal demand from Demand Cluster 11 is low. A time series simulation results for ATES with flowrate 150 m³/h and 5 MW heat pump is presented in Figure 36.



(a)



(b)

Figure 36: (a) Total thermal balance of the heat network for coupling ATES + heat pump with flowrate 150 m³/h (b) Heat pump thermal power and electricity power.

c) Adding additional biomass heat source

There is business case to add additional 18 MW heat source (biomass⁷) next to geothermal sources. We simulate the case using ATES + heat pump with flowrate 150 m³/h (Figure 37). This additional heat source helps to provide more heat during winter period to customers.

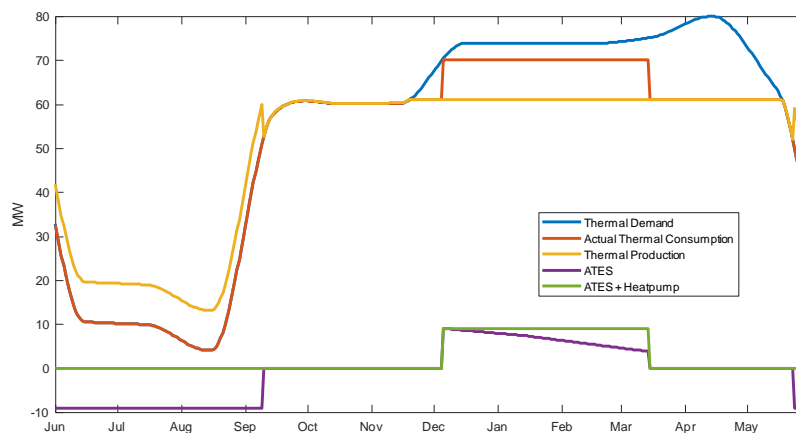


Figure 37: Total thermal balance of the heat network with additional biomass heat source for coupling ATES + heat pump with flowrate 150 m³/h.

d) Using centralized large ATES

For the next 2 cases we will compare between 1 large centralized ATES and 4 small decentralized ATES with the same maximum combine flowrate 400 m³/h. Since the total combine thermal production (geothermal, biomass and ATES) exceeds current demand profile, thus we increase all the thermal demand from the heat grid by factor 20%.

⁷ There is a plan to build an additional heat source (biomass plant) which requires a minimum operational time in order to be cost-efficient. Therefore, we assume the biomass plant has a higher priority merit-order than ATES.

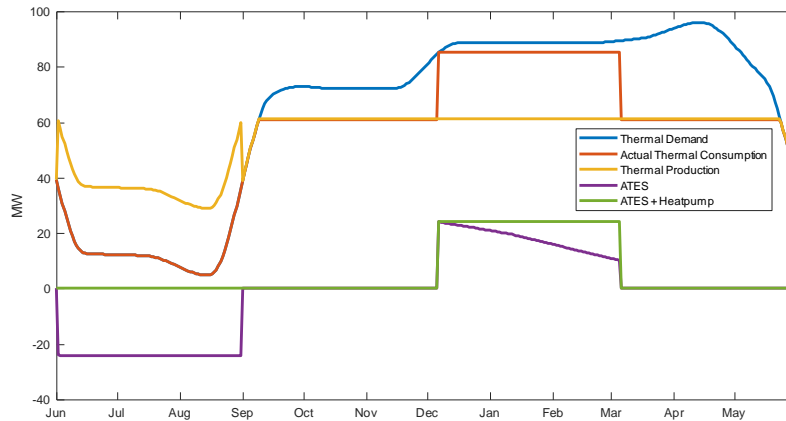
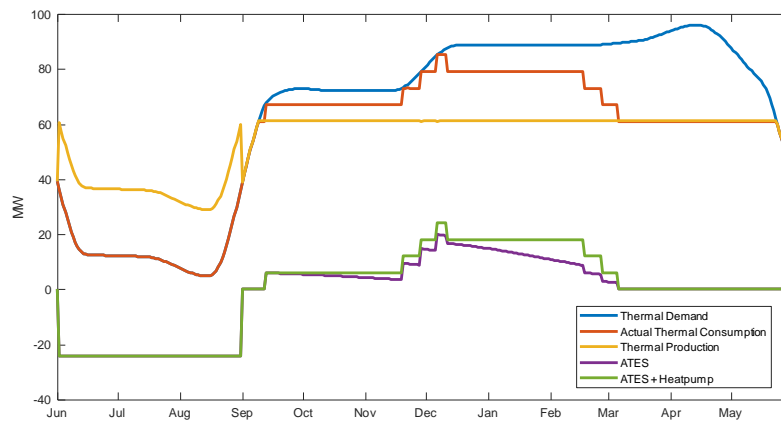


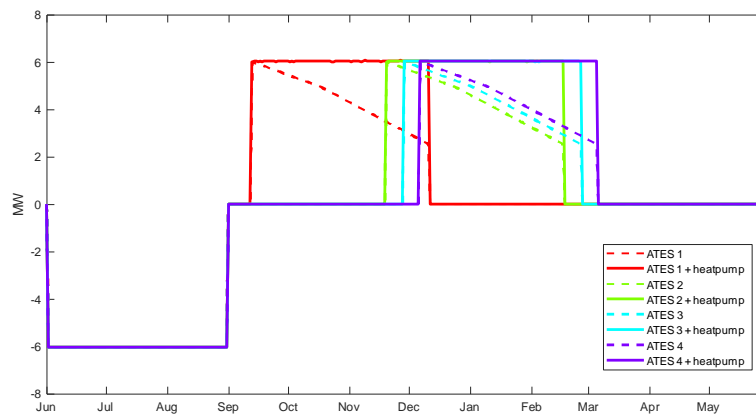
Figure 38: Total thermal balance of the heat network with 1 large ATES flowrate 400 m³/h.

e) Using decentralized small ATES

Using decentralized ATES gives more flexibility since the usage of each individual ATES can be controlled separately. As can be seen in Figure 39, the ATES is used with different time period and also a specific ATES can be used to the closest demand, thus the pressure drop during production period is lower compared to a large ATES configuration.



(a)



(b)

Figure 39: (a) Total thermal balance of the heat network with 4 small ATES flowrate 100 m³/h (b) Thermal power during injection and production of different ATES.

f) Comparison results

In this section, the simulation results of each scenario are compared. The total energy balance (heat production and consumption) on the heat network and the system properties like pressure drop, thermal losses and electricity used are given.

Table 17: Comparison results several possible scenario for ATES integration.

	Base Case	Case A			Case B			Case C
		50 m3/h	100 m3/h	150 m3/h	50 m3/h	100 m3/h	150 m3/h	
Production								
Geothermal Energy (GWh)	305.77	312.87	319.55	325.99	312.88	319.56	326.01	327.00
ESP production & injection electricity (GWh)	16.07	16.44	16.79	17.13	16.44	16.79	17.13	17.18
Biomass Energy (GWh)	-	-	-	-	-	-	-	111.62
Consumption								
Greenhouse (GWh)	305.27	310.31	315.18	319.97	312.15	318.75	325.27	436.18
Storage								
ATES injection energy (GWh)	-	7.09	13.75	20.18	7.09	13.75	20.19	23.44
ATES production energy (GWh)	-	5.03	9.90	14.70	5.03	9.86	14.63	15.903
Transport								
Pump electricity (GWh)	1.26	1.27	1.30	1.37	1.23	1.24	1.37	1.58
Maximum Δp (bar)	9.31	9.31	9.31	9.31	9.31	9.31	9.31	7.83
Transport Losses	0.506	0.505	0.521	0.531	0.518	0.532	0.549	0.731
Conversion								
Heatpump thermal energy (GWh)	-	-	-	-	1.84	3.61	5.36	5.83
Heatpump electricity (GWh)	-	-	-	-	0.64	1.26	1.88	2.04
Maximum Heatpump COP	-	-	-	-	3.57	3.57	3.57	3.57
Minimum Heatpump COP	-	-			2.61	2.61	2.61	2.61

	Case D	Case E
Production		
Geothermal Energy (GWh)	361.69	361.69
ESP production & injection electricity (GWh)	19.01	19.01
Biomass Energy (GWh)	117.06	117.06
Consumption		
Greenhouse (GWh)	477.43	477.42
Storage		
ATES injection energy (GWh)	52.67	52.68
ATES production energy (GWh)	38.16	38.16
Transport		
Pump electricity (GWh)	2.54	1.66
Maximum Δp (bar)	16	8.9
Transport Losses	0.813	0.813
Conversion		
Heatpump thermal energy (GWh)	13.99	13.99
Heatpump electricity (GWh)	4.89	4.89
Maximum Heatpump COP	3.56	3.56
Minimum Heatpump COP	2.61	2.61

As shown in Table 17, introducing ATES to the heat network can give more flexibility in supplying greenhouse demand during peak load (winter time) by injecting excess energy to ATES during base load (summer time). The customer can get more renewable heat compared to base load and also geothermal source can be operated with higher utilization during summer time.

Implementing a centralized ATES in an existing heating network can lead to a high pressure drop in the system due to a high flowrate. Normally, this should be taken into account when dimensioning the piping for the heating network. The pressure drop can be reduced by distributing multiple smaller ATES systems over the network trajectory.

4.7.2 KPI Cost information

In this section a cashflow analysis is presented for the different scenarios (cases A - E) described above. The following assumptions were made:

1. CAPEX

- Geothermal = 1.2 M €/MW
- Biomass = 1.4 M €/MW
- ATES = 0.4 M €/MW
- Heat pump = 0.25 M €/MW

2. OPEX

- Geothermal = 80 k €/MW
- Biomass = 20 k €/MW
- ATES = 10 k €/MW

3. Price

- Electricity price = 0.08 €/kWh
- Subsidy Geothermal = 34 €/MWh
- Subsidy Biomass = 50 €/MWh
- Grower heat price = 6 €/MWh
- Discount Rate 6%

Table 18: Comparison result cashflow analysis for different scenario.

		Unit	Base Case	Case A			Case B		
				50 m3/h	100 m3/h	150 m3/h	50 m3/h	100 m3/h	150 m3/h
CAPEX	Geothermal	M€	51.6	51.6	51.6	51.6	51.6	51.6	51.6
	Biomass	M€							
	ATES	M€	2.5	2.5	2.5	2.5	2.5	2.5	2.5
	Heatpump	M€					0.4	0.9	1.3
OPEX	Geothermal	M€/year	3.44	3.44	3.44	3.44	3.44	3.44	3.44
	Biomass	M€/year							
	ATES	M€/year		0.05	0.05	0.05	0.05	0.05	0.05
	ESP electricity	M€/year	1.29	1.32	1.34	1.37	1.32	1.34	1.37
	Distribution pump electricity	M€/year	0.10	0.10	0.10	0.11	0.10	0.10	0.11
	Heatpump electricity	M€/year					0.05	0.10	0.15
REVENUE	Greenhouse	M€/year	1.83	1.86	1.89	1.92	1.87	1.91	1.95
	Geothermal subsidy	M€/year	10.40	10.64	10.86	11.08	10.64	10.87	11.08
	Biomass subsidy	M€/year							
CASHFLOW	TOTAL CAPEX	M€	51.60	54.10	54.10	54.10	54.53	54.98	55.40
	TOTAL OPEX	M€/year	4.83	4.91	4.94	4.97	4.95	5.03	5.12
	TOTAL REVENUE	M€/year	12.23	12.50	12.76	13.00	12.51	12.78	13.04
	PROFIT	M€/year	7.40	7.59	7.82	8.03	7.56	7.74	7.92
	PAYBACK PERIOD	years	6.97	7.13	6.92	6.73	7.22	7.10	7.00
	NPV 10 YEARS	M€	2.87	1.78	3.45	5.03	1.09	2.02	2.86

		Unit	Case C	Case D	Case E
CAPEX	Geothermal	M€	51.6	51.6	51.6
	Biomass	M€	25.2	25.2	25.2
	ATES	M€	2.5	10	10
	Heatpump	M€	1.3	3.5	3.5
OPEX	Geothermal	M€/year	3.44	3.44	3.44
	Biomass	M€/year	0.36	0.36	0.36
	ATES	M€/year	0.05	0.20	0.20
	ESP electricity	M€/year	1.37	1.52	1.52
	Distribution pump electricity	M€/year	0.13	0.20	0.13
	Heatpump electricity	M€/year	3.44	3.44	3.44
REVENUE	Greenhouse	M€/year	2.62	2.86	2.86
	Geothermal subsidy	M€/year	11.12	12.30	12.30
	Biomass subsidy	M€/year	5.58	5.85	5.85
CASHFLOW	TOTAL CAPEX	M€	80.60	90.30	90.30
	TOTAL OPEX	M€/year	5.51	6.12	6.04
	TOTAL REVENUE	M€/year	19.32	21.02	21.01
	PROFIT	M€/year	13.80	14.90	14.97
	PAYBACK PERIOD	years	5.84	6.06	6.03
	NPV 10 YEARS	M€	20.98	19.36	19.88

Adding a heat pump to the existing ATES configuration in order to supply more heat to the heat grid does not improve the economic feasibility in comparison to the original design. This is due to the capacity of the ATES which is too small. When the ATES capacity is increased, the configuration with heat pump becomes more interesting.

Adding a large central ATES to an existing heating network can result in a significant increase of the overall pressure drop and electricity consumption of the distribution pumps during the charging cycle of the ATES as a result of higher flowrates.. Distributing a large ATES into smaller ATES systems over the piping network can be beneficial for implementing an ATES in an existing heating network.

4.8 Conclusion

The design specifications and operational strategies for the integration of an ATES in the existing heat network at ECW were evaluated with CHES and HeatMatcher. Several possible integration options and scenarios were assessed. The simulation results provide a better understanding of the interaction between the ATES and the heat network and also give more insight in the business cases.

5 System simulations on district heating networks with large scale thermal energy storage (Denmark)

5.1 Introduction

Between 2000 and 2020, Solar District Heating (SDH) systems have known a very fast development in Denmark and can typically supply 20% of the yearly local heat demand from solar heat. During the same years, the will to increase this solar fraction by means of seasonal thermal energy storage grew, and several projects were started after 2008. In this context, thermal design of heat storages as a part of a heating system has proven crucial to determining the feasibility of a project, and was carried out, among other projects for a PTES in Dronninglund, in Northern Denmark.

During the early design phase of the PTES study in Dronninglund [14], as well as in the final design and implementation phase [15], TRNSYS has been used to make the main system calculation design and optimization [16]. Internally at PlanEnergi, it was also chosen to make some price-scheme sensitivity analysis through the setup of an energyPRO model, which would use some of the TRNSYS calculations results as inputs to run the model. The context at the time of the study was that fixed-price schemes were about to be abolished in Denmark, and it was interesting to evaluate if switching to a spot-price scheme earlier than the law change would make sense from an economics point of view.

5.2 System modelling software

To begin with, energyPRO is a modelling software developed by the Danish company EMD International A/S, used for analysis of various types of energy systems on an hourly basis, down to a one-minute timestep. It is able to calculate both energy balance (non-dynamic calculations) and operations costs. It has a long range of built-in components such as solar collectors, a load/heat demand component, Combined Heat and Power (CHP) plants or boilers (with a standard range of fuels that can be imported).

It can make yearly calculations quite fast and therefore enable the study of a great variety of scenarios. It offers access to online data for technical and economics information, as well as time series (such as local weather data) and can be therefore very relevant for local studies. It also enables the use of user-made inputs, functions and/or time series, to account for specific components, energy tariffs, etc.

Then TRNSYS is used, for more detailed energy balance calculations. TRNSYS is a complete and extensible simulation environment for the transient simulation of energy systems, developed at the University of Wisconsin. It is used by engineers and researchers around the world to validate new energy concepts, from simple domestic hot water systems to the design and simulation of buildings and their equipment, including control strategies, occupant behaviour, renewable energy systems (wind, solar, photovoltaic, hydrogen systems), etc. It simulates the energy system balance starting from an hourly timestep, down to a timestep of a few milliseconds.

A TRNSYS project is typically set up by connecting components graphically in the program called 'Simulation Studio'. Each Type of component is described by a mathematical model in the TRNSYS simulation engine and has a set of matching 'Proformas' in Simulation Studio. The proforma has a black-box description of a component: inputs, outputs, parameters, etc. TRNSYS components are often referred to as 'Types' (e.g. Type 1 is a solar collector). TRNSYS also enables the use of user-made inputs, functions and/or time series.

At PlanEnergi, TRNSYS is used to make calculations of heat production systems, often including a thermal storage, whether it is a Pit Thermal Energy Storage (PTES) or a Borehole Thermal Energy Storage (BTES) [17]. For this purpose, commercially available components that simulate accurately the behaviour of such installations are used, in connection with local weather conditions (windspeed, air temperature, etc.).

Results from TRNSYS calculations regarding production of heat from a combination of solar thermal with a PTES or a BTES can be used as user-made inputs in systems calculations in energyPRO. This procedure is described in the following. Both tools are mostly used for site-size calculations but can also be used for small to medium scale calculations (site size up to municipality level), and for short to mid-term calculations (from a few hours up to 20 years).

System simulations including large scale seasonal thermal energy storage using TRNSYS was thoroughly described in deliverable D2.1 of HEATSTORE project [18]. However, to the best of our knowledge, the use of heat delivered by a large scale seasonal thermal energy storage in energyPRO hasn't been reported before. The following sections describe the main results from the TRNSYS study and how they have been used as inputs to an energyPRO model.

5.2.1 TRNSYS model and results

The TRNSYS model used for the study of Dronninglund is shown in Figure 40. The main components are the gas motor ("Motor"), the Solar Collector Field ("SCF"), the PTES, the heat pump, the bio-oil boiler and the heat exchangers ("HX-1&2"). Refer to Heatstore deliverable D2.1 for more details.

Main results of the optimized (and final) calculations showed an optimum Absorption Heat Pump (AHP) size of 2.1 MW cooling capacity. The main energy balance calculations are shown in Table 19. The calculated heat delivered to the district heating network (at Søndervang) is 16'302 MWh per year. It is this value that is being reused in the energyPRO model.

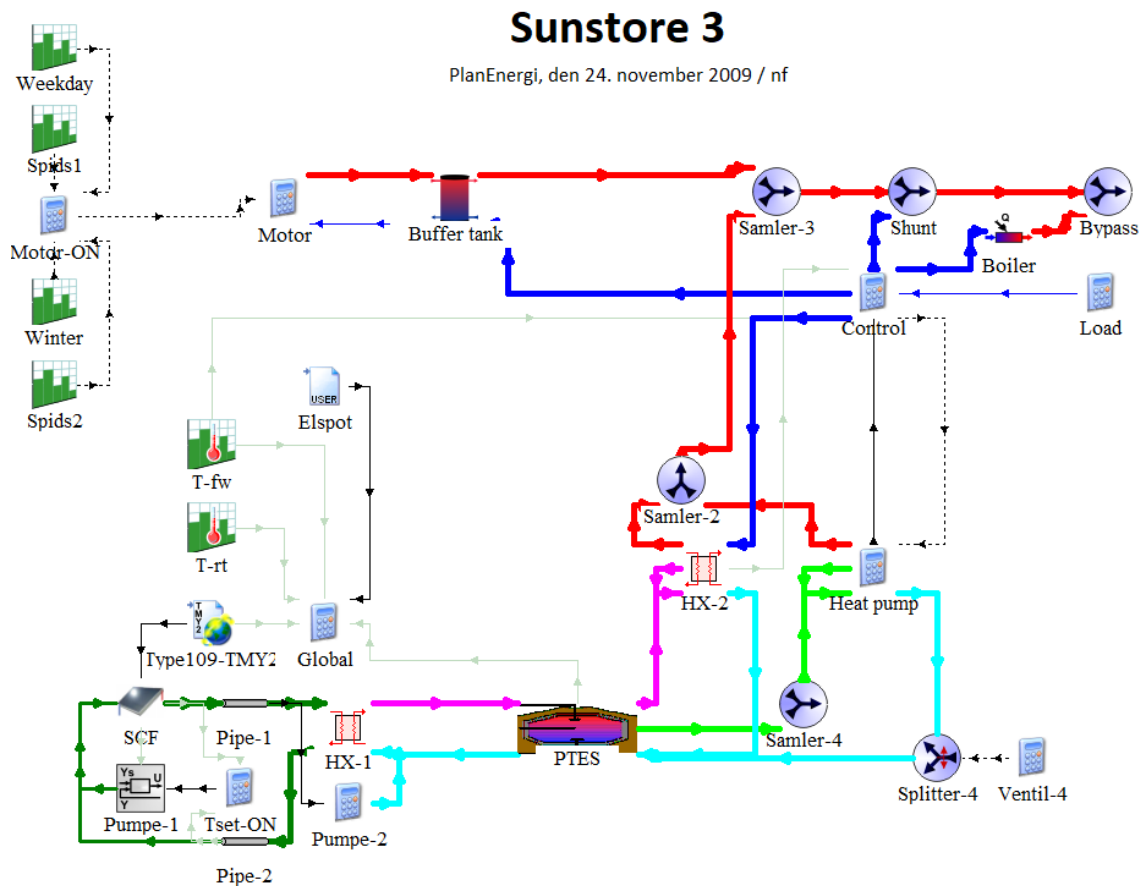


Figure 40: Components and connections in the TRNSYS model for Dronninglund. Thick lines represent water flows, and thin lines represents the control signals.

Table 19: Calculated heat contributions from the TRNSYS calculations, phase 2.

	Reference	With AHP
Energy, unit		
Heat demand, MWh	40'000	40'000
Degree day dependent heat, %	65	65
Heat production, engines, peak load, MWh	7'086	7'086
Heat production, engines, high load, MWh	6'626	6'626
Heat production, bio oil boilers, MWh	26'288	9'986
Heat from solar collectors, MWh	0	18'500
Heat loss from storage, MWh	0	-1'602
Energy change in storage, MWh	0	38
Heat delivered by the SHS (SCF + PTES), MWh	0	16'860
Heat loss from transmission line, MWh	0	-558
Heat delivered at Søndervang, MWh	0	16'302
Heat via heat exchanger, MWh	0	10'478
Absorption heat pump, cooling, MWh	0	5'824
Electricity production, peak load, MWh	4'204	4'204
Electricity production, high load, MWh	3'931	3'931
Natural gas consumption, MWh	23'240	23'240
Bio oil consumption, MWh	28'574	10'623

5.2.2 EnergyPRO model

The model built in energyPRO has two main variations: one including fixed-prices for the electricity, and another one with spot-prices. The main interface of the model using fixed-prices is shown in Figure 41. Its main components are the bio-oil boilers, the gas engines, the tank TES, the district heating load and the PTES. Support components are providing fuel characteristics (bio-oil and gas), heat power delivered by the PTES and fixed electricity prices. The spot-prices layout is the same, with spot-prices instead of fixed prices.

The model uses a timestep of one hour, and the operations of the heat production system is optimized on a monthly basis, which means that the different heat sources are used in order to achieve the lowest operations costs for each month.

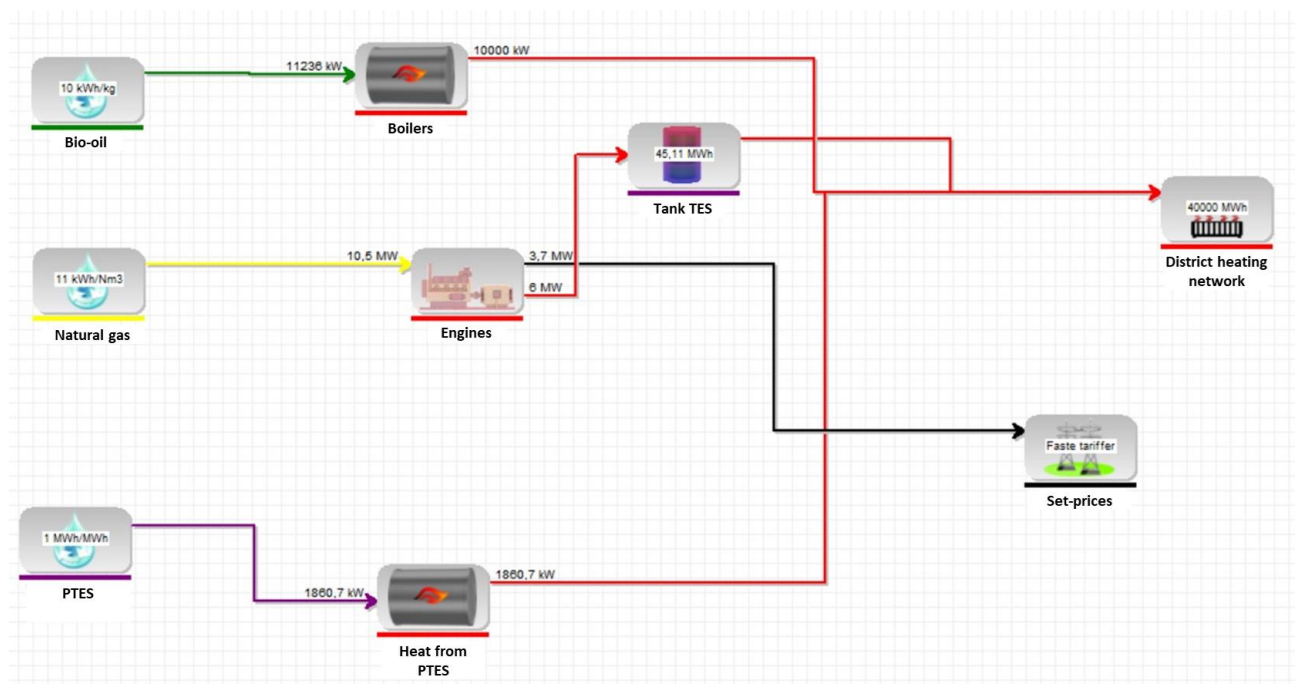


Figure 41: Components and connections in the energyPRO model for Dronninglund, with set-prices for electricity. Red lines and red components represent heat produced and delivered to the district heating or the buffer tank, purple components represent heat storages, and green and yellow represent different kinds of fuels. The black line represents the electricity production.

5.3 System modelling

5.3.1 Heat production units and fuels

a) Bio-oil boilers

Bio-oil is assumed to have a heating value of 10 kWh/kg, and the boilers have a heating capacity of 10 MW with an efficiency of 89%. Bio-oil is assumed to have a constant price of 4.186 DKK/kg for the year 2013.

b) Natural gas engines and tank TES

Natural gas is assumed to have a heating value of 11 kWh/Nm³, the gas engines have a heating capacity of 6 MW with an efficiency of 57.14%, and an electric capacity of 3.7 MW (35.24% efficiency). Natural gas is assumed to have a constant price of 2.47 DKK/Nm³ for the year 2013. Heat produced by the gas engines are stored in a tank TES assumed to have a total volume of 865 m³, a top temperature of 90°C and a bottom temperature of 40°C. Heat stored in the tank TES is assumed to be usable up to 90%, and have no thermal losses. This means that the heat storage, which has a capacity of 45.11 MWh, can only be used to a charge/discharge capacity of 40.60 MWh. This assumption comes from the fact that in practice, it is impossible to have the entire water volume heated up to 90°C or cooled down to 40°C.

c) Heat from the PTES

As shown in Section 5.2.1, TRNSYS calculations predict a 16'302 MWh annual supply of heat coming from the solar system (including the PTES and the evaporator side of the absorption heat pump). Rounded down to 16'300 MWh, this means that the PTES provides on average $\frac{16300}{8760} = 1.8607$ MWh every hour of the year. This significant approximation is justified by the fact that energyPRO is here used to study global impact of using the PTES as a part of the techno-economic system of Dronninglund, using different electricity price assumptions, not detailed energy balance calculations.

Therefore, it was decided to insert the component “PTES” which takes the heat delivered from the PTES and handles it like a fuel that is then sent to a theoretical 100 % efficiency boiler (“Heat from PTES”). The theoretical boiler receives 1.8607 MW of heat from the PTES and delivers it directly to the district heating network. It is assumed that the heat cost from the PTES is 10 DKK/MWh (operations and maintenance costs for the PTES).

5.3.2 District heating network demand

The district heating network heat demand curve is determined by the following parameters, used as inputs to the standard energyPRO load calculation component:

- Period of weather-dependent load: September 1st to May 31st.
- Reference temperature (linear dependency to outdoor temperature, see formula below): 17°C.
- Portion of weather dependence related to space heating: 50%⁸.
- Dataset used for outdoor temperature: Outdoor temperature, central Jutland, Design Reference Year (DRY) from energyPRO in 2014⁹.
- Daily variability of the demand: 80% from 9 pm to 6 am, 100% from 6 am to 9 pm.
- A yearly load of 40'000 MWh.

With the aforementioned parameters, the load profile obtained is shown in Figure 42. The way the load is calculated is based on previous parameters above and the following formula:

$$Q_{load} [MW] = A \cdot \max(17 - \overline{T_{amb}}; 0) + B$$

Where:

- $\overline{T_{amb}}$ is the ambient air temperature averaged over the day.
- A and B are constants determined by energyPRO to respect the aforementioned parameters, in respectively MW/K and MW.
- Calculations in energyPRO give the following results: $A = 0.2470$ MW/K and $B = 2.2831$ MW.

For instance, if a given day has an average temperature of 16°C, then the average daily load would be $0.247 \cdot \max(17 - 16; 0) + 2.2831 = 0.247 \cdot 1 + 2.2831 = 2.5301$ MW, and would vary during the day according to an 80%/100% distribution.

During the summer months, between May 31st and September 1st, the load has only daily variability according to an 80%/100% distribution, such that the daily load has an average of 2.2831 MW. Moreover, if during a given day, average ambient temperature is above 17°C, then the same profile as the summer profile would be observed (not the case here outside of the summer months with Danish weather conditions).

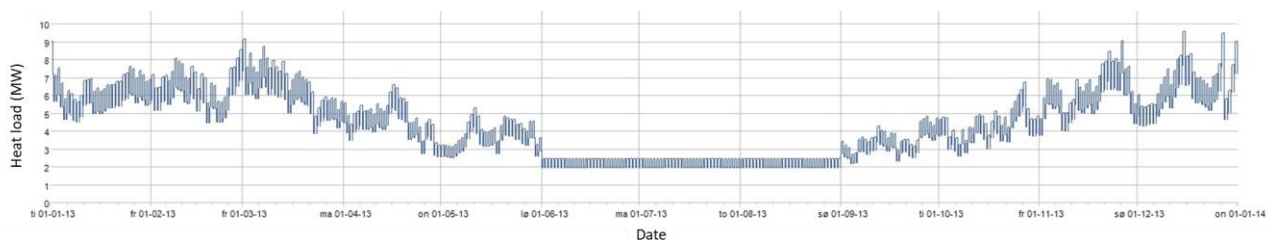


Figure 42: Load profile generated by the load calculation component in the energyPRO model for Dronninglund.

⁸ This percentage isn't the same as the 65% used in the TRNSYS model, but it allowed the minimum base load to be higher than the PTES heat delivery capacity, meaning that all of the 16'300 MWh delivered by the PTES can be transferred to the district heating network in the energyPRO simulation.

⁹ Ny Dansk Design Reference Year, Centrale Jylland - Station 6060, Flyvestation Karup, Breddegrad 56,28, længdegrad 9,12.

5.3.3 Electricity prices and other economics parameters

d) Fixed electricity prices

The reason for using the energyPRO model is to see if using spot-prices with the complete heat production system in Dronninglund (including gas motors and bio-oil boilers) could give a better economy than using the fixed-prices. Therefore, these 2 different price schemes have been implemented, starting with fixed prices.

Fixed prices have been divided into 3 categories:

- Peak-load prices.
- High-load prices.
- Low-load prices.

Peak-load and high-load prices are periodically defined during weekdays, at certain hours, and the other hours are filled with low-load prices (see Table 20 and Figure 43).

Table 20: Price category distribution of peak-load and high-load.

Price category	from hour	to hour
Peak-load	7:30	12:00
Peak-load	17:00	18:30
High-load	06:30	07:30
High-load	12:00	17:00
High-load	18:30	21:00

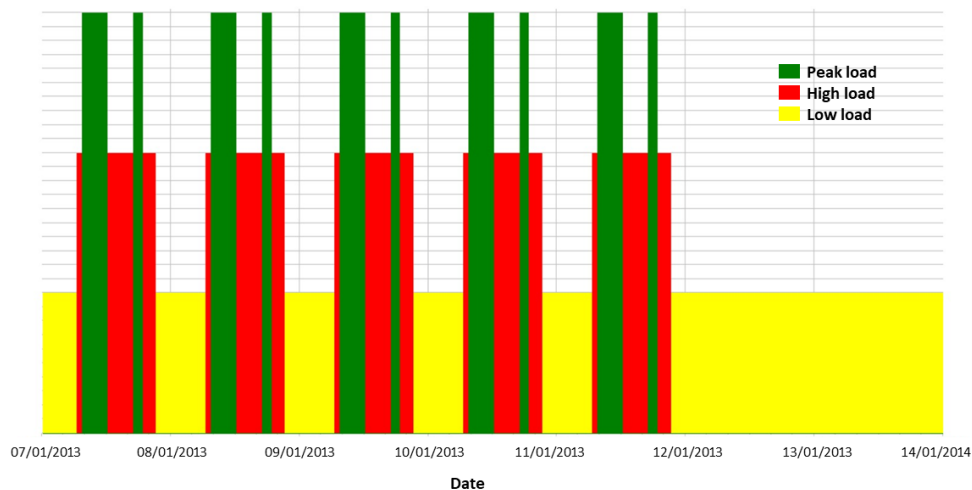


Figure 43: Weekly distribution of peak load (in green), high load (in red) and low load (in yellow) prices in the energyPRO model for Dronninglund.

These prices are then distributed over the whole year, excluding holidays. A typical week has 5 instances of peak and high load periods, but because of holidays there are some exceptions. For instance, in January 2013, January 1st is a Tuesday, and is a holiday. Therefore the first week has only three peak and high load instances (see Figure 44), while the three next weeks have 5. As for the last week of January 2013, it simply is divided over two months, as January 31st is a Thursday.

Then, each of these price categories have their own monthly variability (see Figure 45), which is used by energyPRO to set the actual price that is being applied for every given hour. In January, peak load will have a price of 894 DKK/MWh, while it will be at 885 DKK/MWh in November.

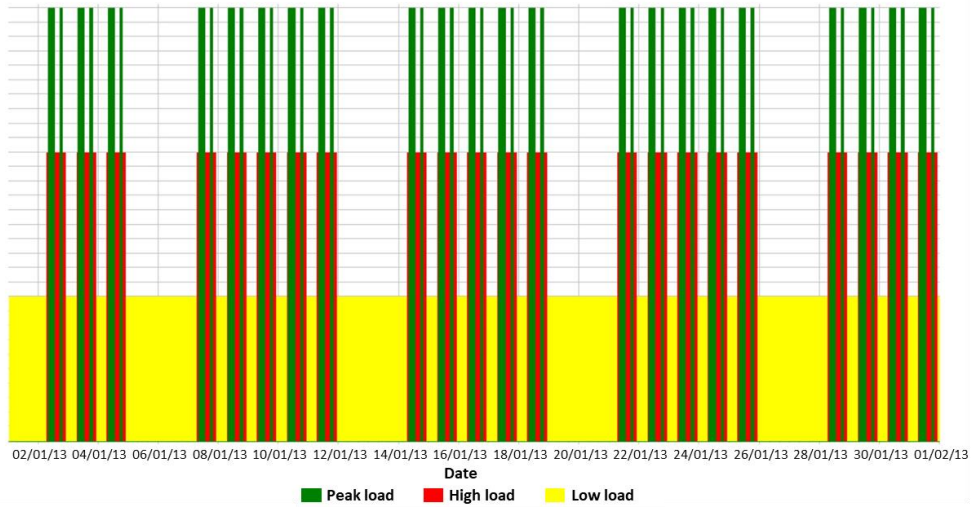


Figure 44: Monthly distribution of peak-load, high-load and low-load prices in the energyPRO model for Dronninglund, example of January.

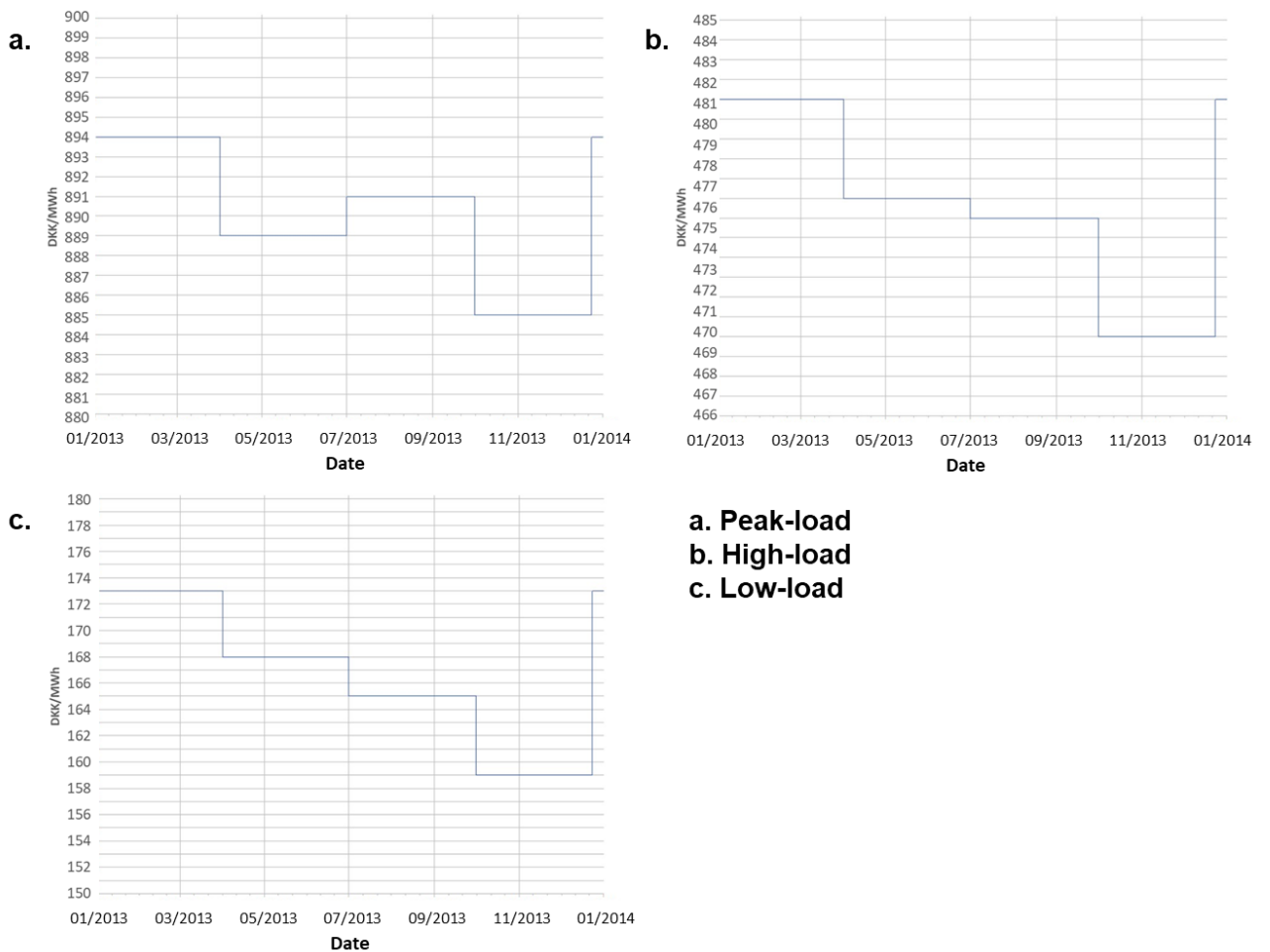


Figure 45: Price variability of peak-load, high-load and low-load prices over the year 2013.

e) Spot electricity prices

Spot prices needed a different implementation, as they vary throughout the day, but cannot be perfectly predicted in practice. Therefore, the spot-prices of electricity in 2013 have been used (see Figure 46) to make a forecast price function, which approximates the spot-price curve (see Figure 47). This curve is used by the model to choose which unit should generate heat and/or electricity in the next hour.

This forecast function is generated by energyPRO's internal function "Intervals". This function generates, based on an existing time series, a new time series with a specified number of intervals omitting a percentage of extreme values, based on monthly values. In the developed model, the function $Intervals(Elspot\ indeks; 5; 5)$ was used, and provides a time series with 5 intermediate values for each month, omitting the highest and lowest 5 percent value of the spot-price curve. The 5 intermediate values are equally distributed between the upper and lower border values, which means that for each month the curve can have a total of 7 possible values.

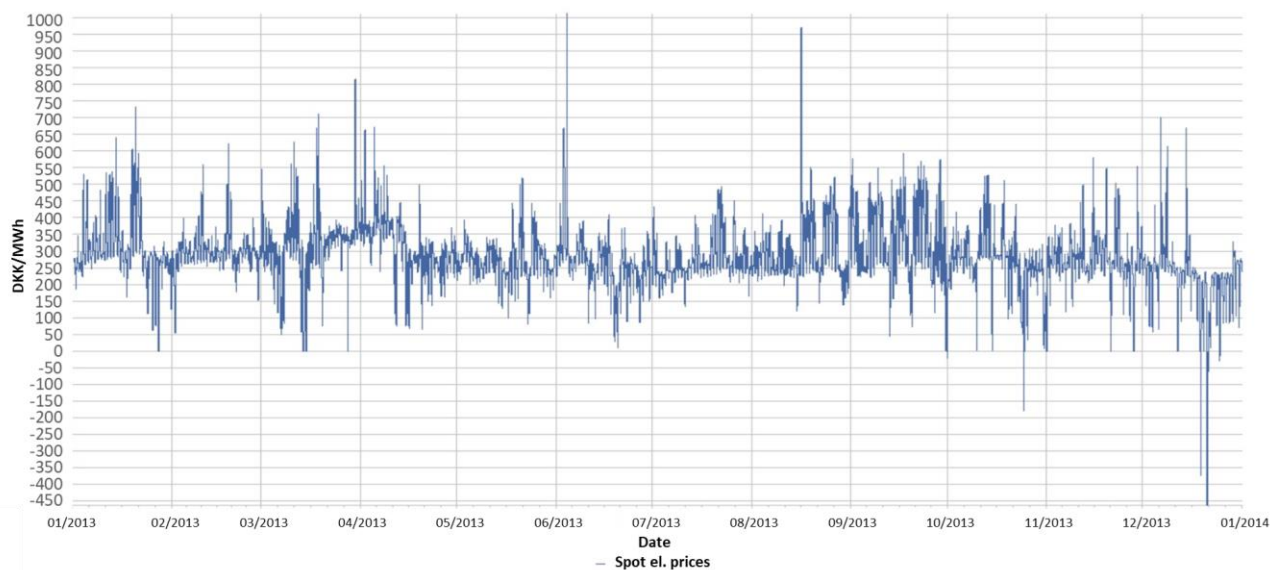


Figure 46: Spot-price curve for 2013, prices in DKK/MWh.

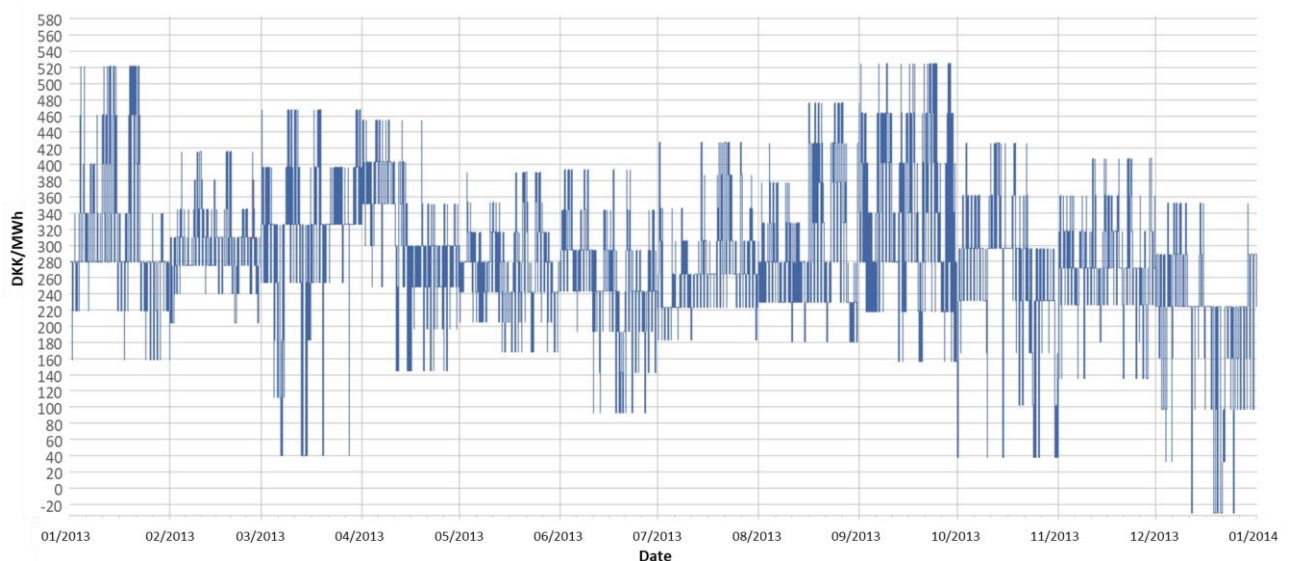


Figure 47: Spot-price forecast curve generated by energyPRO from the 2013 spot-price curve.

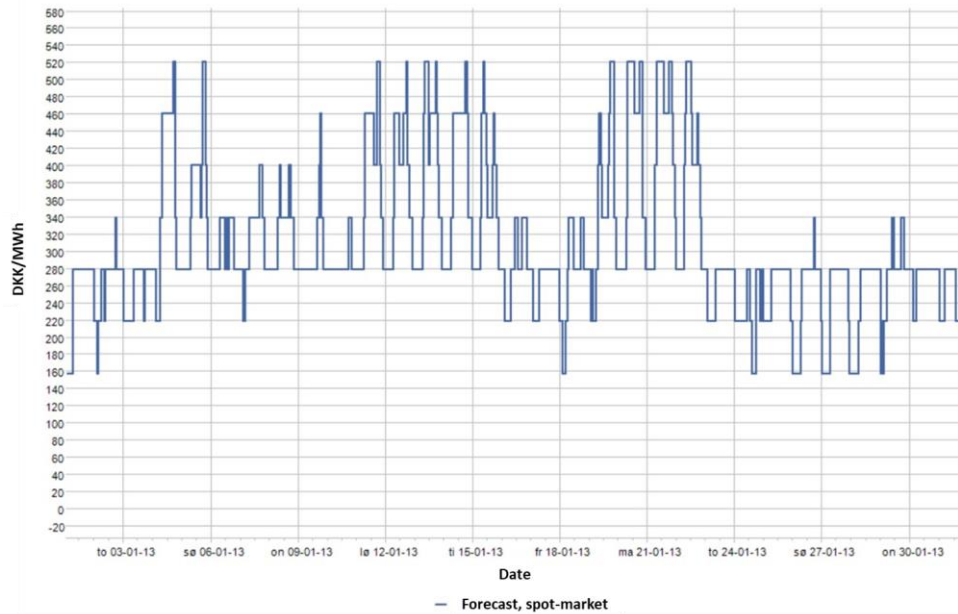


Figure 48: Detail of January 2013 from the spot-price forecast curve generated by energyPRO.

If the spot-prices curve has values in the interval $[-450 \text{ DKK/MWh}; 1'000 \text{ DKK/MWh}]$ (see Figure 46), the forecast curve only varies in the interval $[-20 \text{ DKK/MWh}; 520 \text{ DKK/MWh}]$ (see Figure 47). This is the whole purpose of the function 'Intervals'.

Details for January 2013 are shown in Figure 48 and exhibit clearly that besides from the highest and lowest values, the curve only takes 5 different possible values, equally distributed between these border values.

f) Other economics parameters

In addition to the previous techno-economic parameters for fuels, heat production units and the electricity prices, several other parameters have been used in the simulation. They are gathered in Table 21. Sales of the heat delivered to the district heating network were not considered. This means that the economics calculation results will contain Operations and Maintenance (O&M) costs minus the revenues from the electricity sales. This enables however the comparison between the two scenarios, as both systems provide the same amount of heat to the district heating network.

Table 21: Economics operations parameters used in energyPRO.

Price category	Unit	Value
Fixed electricity production subsidy ¹⁰	DKK/year	+640'000
Proportional electricity production subsidy ¹¹	DKK/MWh _{el}	+80.00
Production-independent subsidy for CHP spot-production ¹²	DKK	+3'028'518 ¹³
Gas engines, energy tax	DKK/Nm ³	-2.8450
Gas engines, CO ₂ tax	DKK/Nm ³	-0.3770
Gas engines, NO _x tax	DKK/Nm ³	-0.1440
Gas engines, CH ₄ tax	DKK/Nm ³	-0.0650
Gas engines, CO ₂ compensation	DKK/year	-457'640
Bio-oil boiler, NO _x tax	DKK/kg	-0.04680
O&M, gas engines	DKK/MWh _{el}	-120.0
O&M, bio-oil boilers	DKK/MWh _{heat}	-10.00
O&M costs for the PTES heat exchangers (el.) ¹⁴	DKK/MWh _{heat}	-6.000
O&M, PTES	DKK/MWh _{heat}	-10.00

5.4 Simulation results

5.4.1 Yearly energy balance

Running the 2 scenarios (with the different price schemes) in energyPRO provides the energy balance results shown in Table 22. These results correspond to the operations' optimization for the system, made by energyPRO, based on the different techno-economic assumptions presented in the previous section.

Table 22: Yearly energy production for both scenarios calculated with energyPRO.

Heat production	Fixed prices	Fraction	Spot prices	Fraction
Gas engines [MWh/year]	13'722.0	34.3%	4'191.0	10.5%
PTES [MWh/year]	16'300.7	40.8%	16'300.7	40.8%
Bio-oil boiler [MWh/year]	9'977.3	24.9%	19'508.3	48.8%
Total [MWh/year]	40'000.0	100%	40'000.0	100%

The scenario with fixed prices is clearly favourable to the use of the gas engines, while both scenarios successfully manage to make use of 100% of the heat coming from the PTES.

5.4.2 Economics results

Main economics results from the energyPRO calculations are gathered in Table 23.

¹⁰ For a yearly electricity production over 8'000 MWh per year.

¹¹ For a yearly electricity production below 8'000 MWh per year.

¹² This subsidy is specific for decentralized Combined Heat & Power (CHP) production units that use spot prices. It is calculated from monthly average spot prices and is proportional to a base amount. This base amount, which was enticing companies to use spot-prices, has been deleted in 2019 due to EU regulations.

¹³ Base amount for the calculation of the production independent subsidy for CHP production.

¹⁴ For the pumps and accessories' electricity consumption to transfer heat from the PTES to the district heating network.

Table 23: Main operations economics results for both scenarios calculated with energyPRO.

Expense/revenue [Mio.DKK/year]	Fixed prices	Spot prices
Fixed electricity production subsidy	0.640	0
Production-independent CHP subsidy	0	2.300
Electricity sales, spot price	0	1.150
Electricity sales, peak load	3.598	0
Electricity sales, high load	2.105	0
Electricity sales, low load	0	0
Electricity sales, total	5.703	1.150
Electricity revenue, total*	6.343	3.656
Fuel costs, total	-10.085	-10.826
Gas engines taxes, total	-3.766	-0.842
Bio-oil boilers taxes, total	-0.052	-0.103
Gas engines O&M costs, total	-1.015	-0.309
Bio-oil boilers O&M costs, total	-0.100	-0.195
PTES O&M costs, total	-0.261	-0.261
O&M costs, total*	-15.279	-12.536
Result of heating system operations (sum of *)	-8.936	-8.880

Overall, operations costs and benefits (excluding heat sales) for both scenarios provide similar yearly results, under the given assumptions. The scheme using spot prices offers an overall expense slightly smaller than the fixed price scheme, although mainly due to the production independent subsidy.

In practice, the PTES would cover a higher percentage of the heat in the summer months (up to 100%), and less in the winter months, when the gas turbines are most needed to meet heat demand. This means that revenue optimization based on fixed prices variability will be deteriorated during the winter (because of less flexible use of the gas turbines) and therefore a lower revenue/higher total expense is to be expected for the fixed price scheme.

5.5 Conclusion

Based on previous comments on the economics results of the energyPRO calculations, using spot prices already for 2014 instead of fixed prices could provide lower operations expenses, and thus have been encouraged at the time of the study.

However simplified, this energyPRO study has helped determine that using the spot price scheme early was most interesting for the heating system of Dronninglund. This kind of study in TRNSYS would have been much more complicated to obtain, as it involves plenty of economics parameters that are not standard for TRNSYS, and therefore would have needed a specific implementation. On top of this, one would have needed to implement an hourly operations cost optimization algorithm inside the TRNSYS model, where energyPRO has this feature built in.

The next level of simulation using TRNSYS inputs in energyPRO would have been to use monthly averaged values for the heat input coming from the PTES. Due to a lack of time, at the time of the study (which needed a quick estimation of the spot price scheme alternative), this solution was not pursued. It would have most likely brought to the same conclusion, as, once again, seasonality effects would degrade the economy of the fixed price scheme.

Opening new horizons for the joint use of TRNSYS and energyPRO studies involving PTES, one could find the opportunity offered by energyPRO to use hourly time series results from TRNSYS as inputs to the energyPRO model. This method, however, requires several back-and-forth runs between TRNSYS and energyPRO, as new energyPRO results would redefine the parameters used in the controls strategy of the TRNSYS model, and new TRNSYS results would change the energyPRO model inputs, etc. This method could be used for a very specific and detailed economics study, where a lot of budget is available to make economics calculations, but this hasn't been the case for the study carried out in Dronninglund.

Generally speaking, this approach could very well be reused in other contexts and is not limited to the tandem TRNSYS/energyPRO. Any kind of detailed energy model including UTES calculations and providing energy system balance results could be reused as an input to some more simple software calculations but offering the possibility to test a variety of new parameters (such as economic parameters, use of different auxiliary heat sources, use of different fuels, etc.). It is a good reflex, when making feasibility and pre-feasibility studies involving UTES, to consider using a combination of tools, one of which (at least) can model the behaviour of the UTES in a realistic way. For instance, it would not have provided trustworthy results to use energyPRO to model the solar heating system of Dronninglund in combination with the boilers and gas turbines.

6 System simulations at regional level for optimal development strategy (Switzerland)

6.1 Introduction

District heating networks (DH) are known for their capacity to integrate renewable resources into the heating system and to reduce associated CO₂ emissions [19]. Technical and economic feasibility studies for DH are normally based on the cartography of heat demand [20]. In this case, heat demand density maps are created and, together with density threshold limits, priority areas for the DH extension are defined [21]. Likewise, cartography studies can be used to identify local available renewable heat [22] and waste heat resources [23], enabling to estimate the distance of heat sources from high dense heat demand zones [24]. It becomes thereby possible to estimate annual energy values and define local resources to supply the network. In Switzerland, available geo-spatial data on local heat resources and on heat demand are publicly available at <https://map.geo.admin.ch/> (Figure 49).

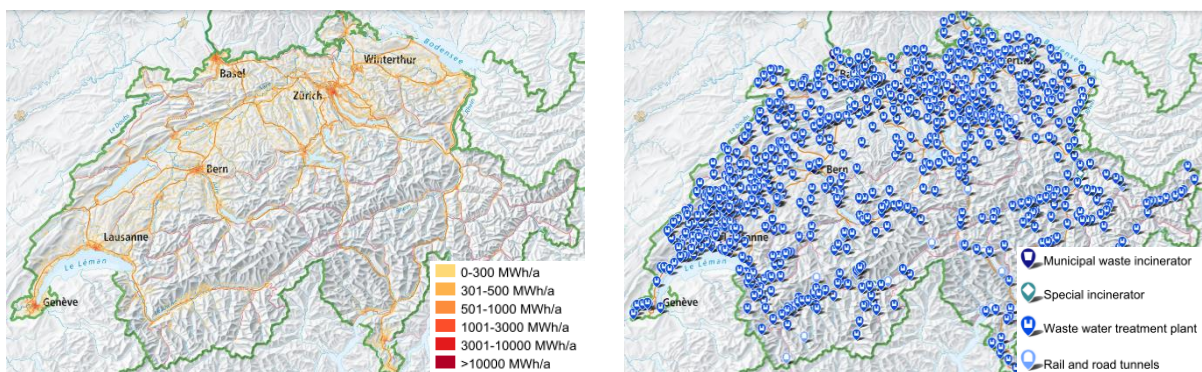


Figure 49: Examples of available GIS open-data for energy studies (Source: <https://map.geo.admin.ch/?topic=energie&lang=en>).

More specifically, in order to study the feasibility of aquifer thermal energy storage (ATES) at national level (HEATSTORE Task 1.3), geo-localized information on industrial waste heat [23] and on heat demand are cross-cut with available data on geological units and existing DH networks, for a territorial analysis of the connection potential between supply, ATES and demand.

However, the cartography of currently available sources and sinks is not enough to ensure the long-term market feasibility for an underground thermal energy storages (UTES). In fact, demand evolution can have an important impact, notably concerning the availability of energy for charging the UTES [25]. An overall view of the grid development is necessary and not only new connections must be analysed, but also the impact of global warming and building refurbishment on the future heat demand. In addition, hourly dynamics (demand and production) are necessary to evaluate the energy balance and the energy mix on the grid [2].

6.2 System modelling software

6.2.1 Simulation of energy system

The thermal energy system of the canton of Geneva is called to evolve, in particular in terms of district heating (DH) networks coverage. Based on available geo-spatial information [26, 27], the public-owned energy provider (Services Industriels de Genève - SIG) is designing the DH extension and planning the future heat production capacity. Since legislative rules impose a minimum share of renewable energy in future thermal grids, an hourly input-output energy balance model was used to estimate the annual production mix on the grids [28]. Noticing that ATES heat storage should be connected to the DH system, the same software was used in HEATSTORE project to evaluate the dynamics of the available energy, which could be charged and discharged.

The software was developed by UNIGE, inspired from EnergyPLAN [4], and was used to simulate prospective scenarios for the heating energy system of Geneva [2, 3]. It has been validated by comparing

predicted and measured data for the heating sector at cantonal level [29]. In the model, hourly profiles are used to ensure the matching between fluctuating renewable energy sources and weather-dependent heat demand.

Population evolution is used to estimate the heated surface and the associated heat demand, while current heat demand at building level [27] is used to estimate the maximum energy saving potential by way of building refurbishment. The impact of climate changes on the heating sector, assigned by the decreasing on heating degree-days (HDD), is also integrated into the model for adjusting of the annual heat demand. Production plants are characterised by a fixed efficiency, by a maximum power capacity and by a fixed production temperature.

Based on hourly measurements, space heating (SH) and domestic hot water (DHW) dynamics are rescaled in order to account for the building stock evolution (heat demand and SH / DHW share on existing, new and retrofitted buildings). PV and solar-thermal energy productions are also based on *in-situ* measured profiles.

In 2019, the model was adapted and temperature constraints were implemented to guarantee a more precise source to sink matching, especially concerning low-temperature renewable resources and geothermal energy [28].

Optimisation is based on a “what... if...” analyses, by changing some parameters like the DH coverage, the retrofit rate and quality, the heat production capacity and efficiency, the merit-order for activation of the diverse DH resources and supply plants, as well as the combined heat and power (CHP) production strategy (driven by electric or by heating markets). Scenarios are compared by way of the annual production mix, the full load capacity for each production plant, and the corresponding CO2 emissions for the entire thermal sector.

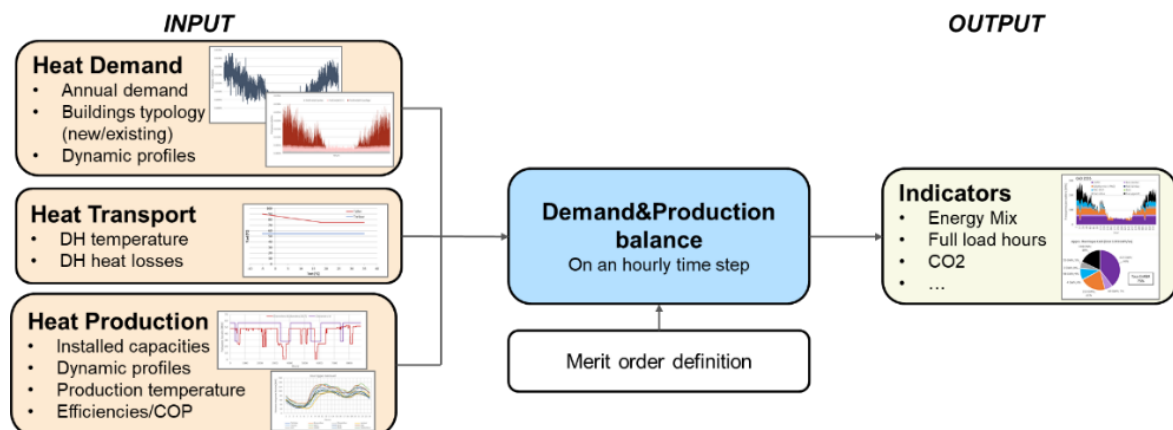


Figure 50: Input/Output of the energy balance model at hourly time-step. Source: [28].

6.2.2 Thermo-hydraulic simulation of ATES and its integration in the energy system

Aquifer thermo-hydraulic responses, after 15 years of charging and discharging, were investigated in hourly time-step with the Nexus-CSMP++ simulator [30]. The simplified model (isotropic and locally uniform porous rock) provides first results on fluid flow, by integrating both forced and natural convective processes, as well as on heat transfer interaction between the rock and the aquifer fluid [31, 32]. Based on several studies carried out in the canton of Geneva [33, 34, 35, 36, 37, 38, 39, 40], different geology and hydrology configurations were tested. Likewise, different well configurations (2 or 5 wells) and system integration approaches (direct or indirect heat extraction) were also tested.

To simulate the integration of ATES in the existing energy system and to evaluate its efficiency, a simplified charging / discharging cycle was used. Temperature constraints were also imposed on the thermo-hydraulic module to allow a realistic connection between the subsurface and the surface “worlds” in a robust, yet

simple manner. Based on existing DH temperature regimes in Switzerland [29], we assume that the ATES system is charged during summertime with 90°C (DH supply temperature) and that direct discharge is possible down to 50°C (discharge cut-off, corresponding to the DH return temperature). For extracting more energy from the storage and reduction of the re-injection temperature down to 20°C, assisted discharging by way of electric heat-pumps (HP) are also analysed [41, 42].

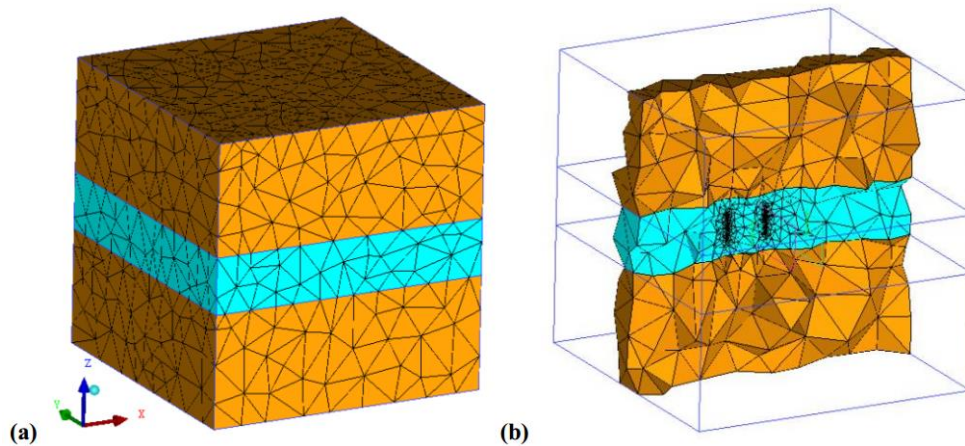


Figure 51: (a) Geological layers and mesh structures used to simulate an ATES system in a cubic volume of 1-1-1 km with (b) lattice refinement near the ATES wells. Source: [31].

6.3 Geneva case study

Currently, about 60-70 GWh/year of heat are wasted during summertime at Cheneviers, the urban solid waste incineration plant of Geneva and main non-fossil source of the existing DH. In order to maximise heat recovery energy from the plant, preliminary studies were done by the Swiss consortium of HEATSTORE to evaluate the feasibility to integrate an ATES into the DH network.

Energy scenarios were constructed based on the evolution of DH (temperature levels, demand profile and supply sources), while ATES thermo-hydraulic responses were simulated numerically to estimate its energy efficiency and the impact of the integration ATES into the DH.

Before exposing the proposed method for the ATES / DH integration analysis, geological and energy contexts will be presented

6.3.1 Energy context and integration of geothermal energy within DH

Currently, more than 50% of total final energy in Geneva is used to cover space heating (SH) and domestic hot water (DHW) demand. Despite the importance of the heating sector and the high heat demand density [2], less than 15% of total thermal demand is covered by district heating networks (DH) (Figure 52 - left).

By 2035, the DH coverage is bound to supply 35% of the total heat demand, with at least 80% of it supplied by renewable energy and waste heat recovery. A prospective scenario for 2035 is shown in Figure 52 (right), where one can easily see the increasing importance of renewable resources into the cantonal heating energy system, as well as the development of DH ("CAD" in French) [3].

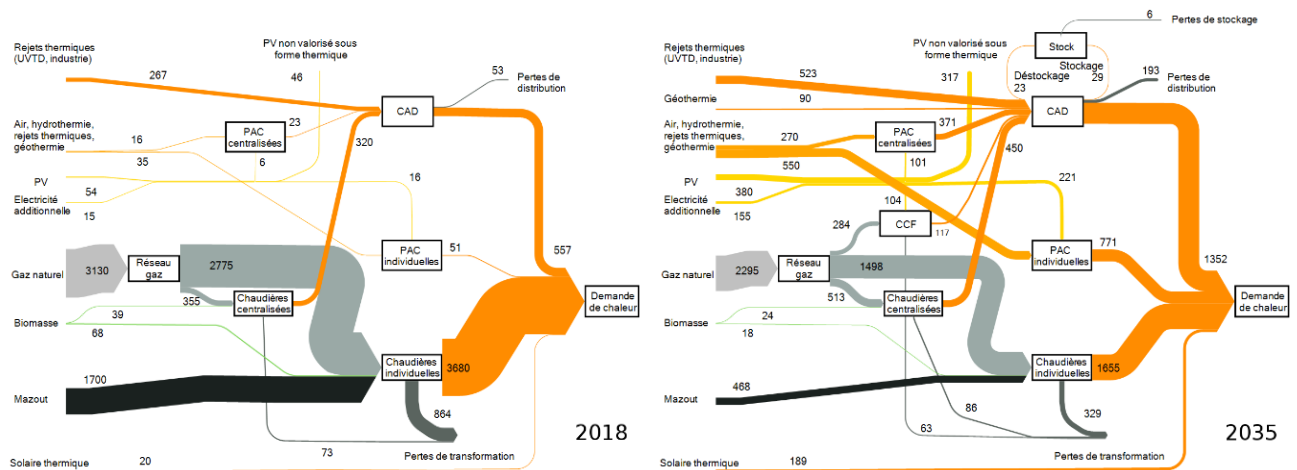


Figure 52: Current heat demand and thermal energy scenario for 2035 (values in GWh/yr.) [3].

In this context, subsurface formations will have a double importance in near future. They will be used: i) as a heat source injected directly or indirectly (temperature upgrade by heat pump) into the DH system; ii) as a storage medium for summer DH heat surplus [39].

In this context and in order to integrate geothermal energy massively into Geneva's heating system, reducing of current DH temperature levels remains the main constraint to overcome. Existing DH operates at a 120°C/70°C temperature regime (supply/return), which imposes a geothermal exploitation at a depth of 2'000 m or deeper (average geothermal gradient 33 K/km [34]) to ensure the direct use of underground heat in the DH. Obviously, lower depth geothermal units can also be used, in conjunction with heat pumps (HP), which however entails additional electricity consumption.

Apart from temperature compatibility between geothermal resources and DH, the use of geothermal heat is constrained by the DH demand, and in the case of UTES systems, also by the amount of excess heat available to charge the storage. For the latter, charging energy must be available at relatively low cost and DH must be able to accept the extra energy from the UTES. These aspects are very important to ensure the economic feasibility of the project and have to be analysed during the project phase, alike energy losses and storage efficiency.

6.3.2 Geological context and potential of medium-depth aquifers

The Geneva Basin is located between the Jura Mountains (NW) and the subalpine units (SE). Promising aquifers units (for heat production or storage) are present between 500 and 2'500 m depth in karstified and/or fractured Mesozoic carbonates units [40], but major uncertainties exist regarding the spatial repartition of the reservoirs and the related water-flow rates.

Historically, only little oil and gas exploration was conducted in the area, mostly based on 2D active seismic acquisitions and very few exploration wells. From a geothermal perspective, the available data resulted to be scattered and scarce. With the launch of the GEothermies program in 2014, and after a first phase of data reprocessing and reinterpretation, new data started to be collected. In 2018 a first geothermal exploration well was drilled at 744 m depth (Geo-01), targeting the Mesozoic carbonates reservoirs, and confirmed a good potential with an artesian flow of 55 l/s at 34°C and 8 bars wellhead pressure. However, in 2020, a second well targeting the same reservoir at larger depth 1'456 m (GEo-02), revealed a very low water-flow (~ 0.5 l/s) despite the encouraging reservoir temperature of 55°C and 12 bars of static wellhead pressure. This demonstrates the complexity of the subsurface conditions in Geneva and the challenge in identifying permeable fractured zones.

Futures operations are already planned: the acquisition of a 3D seismic survey (2021) and the drilling of two additional exploration wells between 1'500 and 2'000 m (GEo-03 and GEo-04, in 2022-2023) for testing different geological contexts and characterizing the geothermal potential at the basin's scale.

6.4 DH model and future evolution

6.4.1 Input-output model

As described before, the evaluation of the DH heat demand and supply is carried out by way of an input-output model inspired from EnergyPLAN [4] which is validated at cantonal level [29]. In 2019, the model was adapted and temperature constraints were implemented to guarantee a more precise source to sink matching, especially concerning low-temperature renewable resources and geothermal energy [28].

In the model, hourly profiles are used to ensure the matching between fluctuating renewable energy sources and weather-dependent heat demand. Space heating (SH) and domestic hot water production (DHW) dynamics are based on measured load curves of existing DH network, which are up/down scaled for taking into account the evolution of the heat demand related to improvements on the thermal performance of retrofitted buildings (SH reduction), climate change (SH reduction) and the increasing share of DHW on new buildings. Production profiles also come from *in situ* measurements, in particular those related to solar thermal and solar PV production, and are up/down scaled in relation with the installed capacity.

Balance between heat supply and demand takes into account the diverse source and sink dynamics (hourly time-step) and the corresponding temperature profiles; the efficiency and capacity of the production plants; transport heat losses; as well as the merit-order for the activation of the diverse resources and production plants.

6.4.2 Evolution of heat demand and temperature levels

The evolution of the DH demand is based on extension projects defined by the local energy supplier, Services Industriels de Genève (SIG), in concordance with the cantonal energy strategy. More than 60 km of new DH are planned and the delivered heat should increase from about 500 GWh/yr. in 2019 to more than 1'000 GWh/yr. by 2035 [28]. This evolution and the related hourly dynamics for three specific years are depicted in Figure 53.

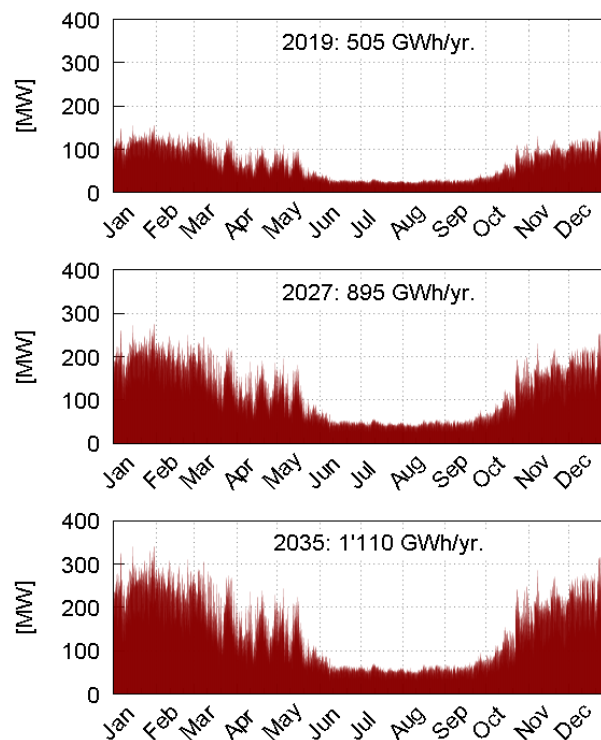


Figure 53: Prospective values for DH demand evolution, hourly time-step (Source: SIG).

In parallel to the heat demand, the DH operative temperature will also be adapted, so as to optimise the DH efficiency and facilitate the inclusion of renewable heat sources. Figure 54 shows the temperature profiles used to simulate the existing (2nd generation DH – 2GDH) and the projected grids (3rd generation DH – 3GDH). Current values [29] were used as reference to design the DH temperature dynamics. During the heating season, a linear relation between the supply temperature and the outdoor temperature is used, while the return temperature is set to a constant value during the whole year. Figure 54 also shows the predicted impact of optimisation programs on the 2GDH temperature levels, with a significant reduction on the return temperature.

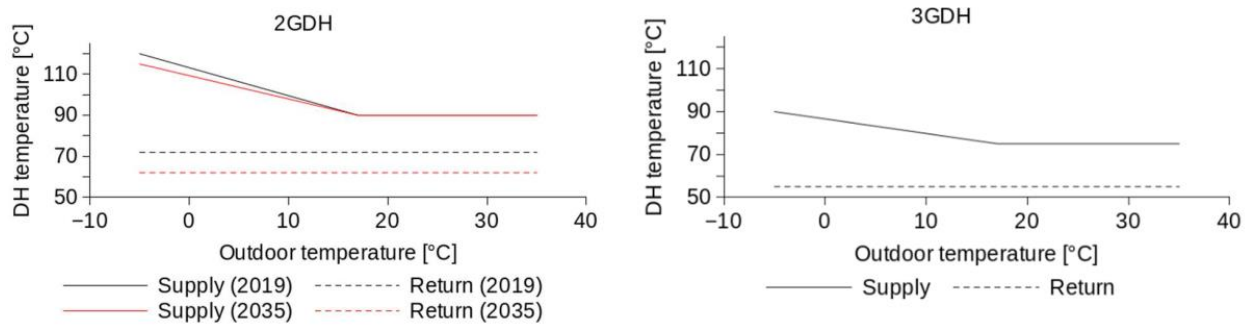


Figure 54: DH temperature levels for existing (2GDH) and planned (3GDH) thermal networks.

While the 3GDH and 2GDH will each work at their respective temperature level, interconnection between both of them will allow transfer of heat from one to another (by way of heat exchangers from 2GDH to 3GDH, or by way of HPs the other way around). However, within this study we are working with a simplified hypothesis of a common DH supply and return temperature, which is defined in hourly time-step by the mean temperature of the different DH branches (weighted by their respective energy demand).

6.4.3 Renewable production and merit-order

In order to guarantee the required minimum renewable share on the network (at least 80% by 2030), different local heat resources will be used. Low temperature resources (lake, sewage plant and medium-depth geothermal) will be exploited by centralized HPs, which will produce heat at 90°C. However, since the DH supply temperature might exceed the maximum HP production temperature during the heating season (Figure 54), gas boilers will be installed to ensure the complementary temperature lift. Available production capacity and its implementation evolution is shown in Figure 55. For more detailed values, refer to scenario “Geo” of reference [28].

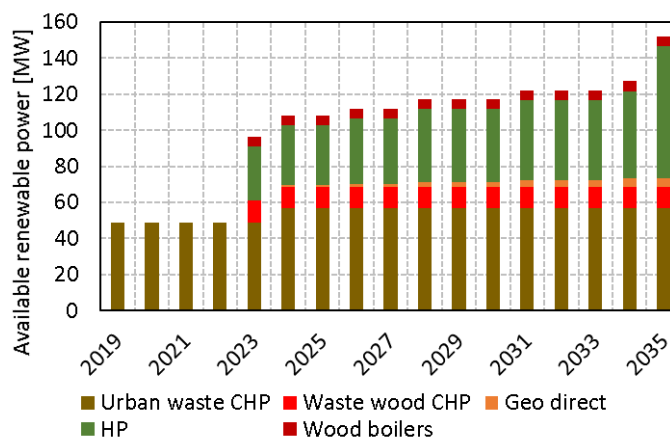


Figure 55: Available renewable power capacity and its time evolution. Project values from SIG.

As pointed out before (section 6.2.1), the merit-order for activation of the diverse DH resources and supply plants can be set by the software user. In this study, the merit-order was defined with the aim to increase waste heat recovery and to minimise fuel consumption. In this case, combined heat and power (CHP) plants

(urban waste and waste wood) are used to cover the base load demand, followed by geothermal units (direct use and assisted with HP) and low temperature resources (sewage and lake water, exploited by HPs). Wood and gas boilers are used to cover winter peak loads.

6.4.4 Evolution of DH energy mix

The evolution of the DH demand and the related energy mix is depicted in Figure 56. By 2035, summertime heat demand is met almost at 100% by the urban waste CHP plant, that, together with waste wood CHP plant, cover 45% of total annual DH demand. For the simulated scenario, the gas share (peak production + HP temperature lift) should be close to 25% of the annual demand, as demonstrated in [28]. In order to be in accordance with existing legislative constraints (section 6.3.1) and reduce fossil fuel utilisation, supplementary renewable capacity must be installed, which represents a good market opportunity for UTES systems.

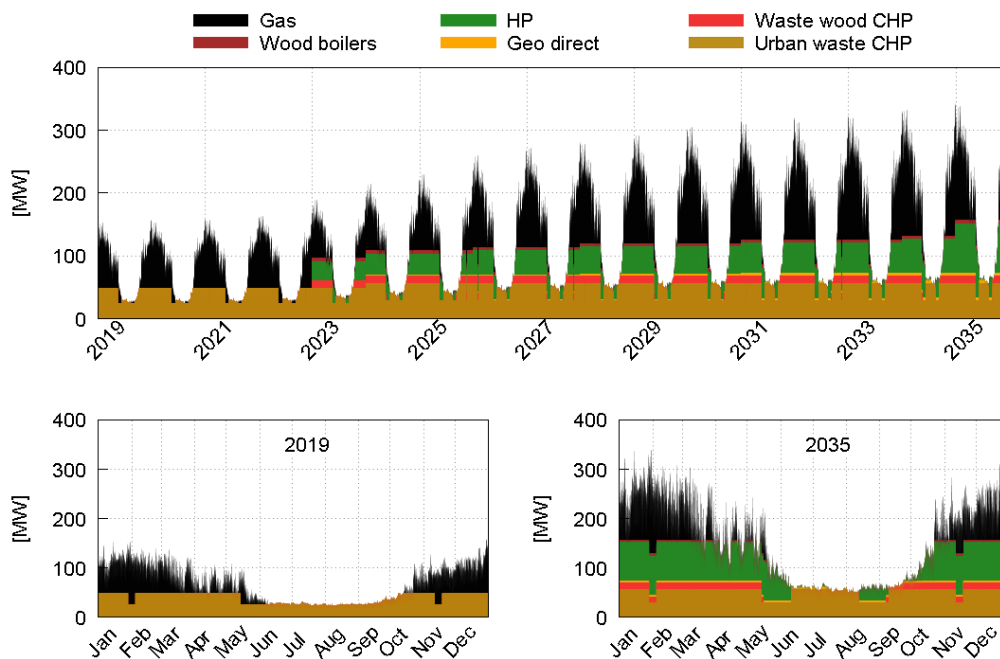


Figure 56: Time evolution (top image) and focus on two different years (bottom images) of DH demand dynamics and energy coverage (hourly time-step).

6.5 Thermal storage design and integration aspects

6.5.1 Storage design

UTES efficiencies are highly dependent on geological conditions, but also on charging / discharging profiles over the system lifetime [25]. In this section, we will address these considerations in regard to annual energy and maximum heat load.

a) Charging of UTES

In the Geneva case study, available energy for charging a UTES essentially comes from the urban waste CHP plant and from future geothermal units. The use of wood, which is a scarce resource and is already a stored form of energy, is limited to the heating season [28]. The evolution of the theoretical available energy to charge the UTES is shown in Figure 57, in hourly and weekly values. As can be seen, excess heat is mainly present during June – September, when heat demand is limited to DHW, with the exception of August, when the urban waste CHP plant is in maintenance. Furthermore, the available excess heat reduces over the years, due to DH extension and related increase of heat demand to cover DHW needs during summer (Figure 53). The evolution of the annual available excess heat is further shown in Figure 58, in

integrated values over the entire year as well as over the 3 summer months (June – August), which confirms that most of the heat available for storage is concentrated on the 3 summer months.

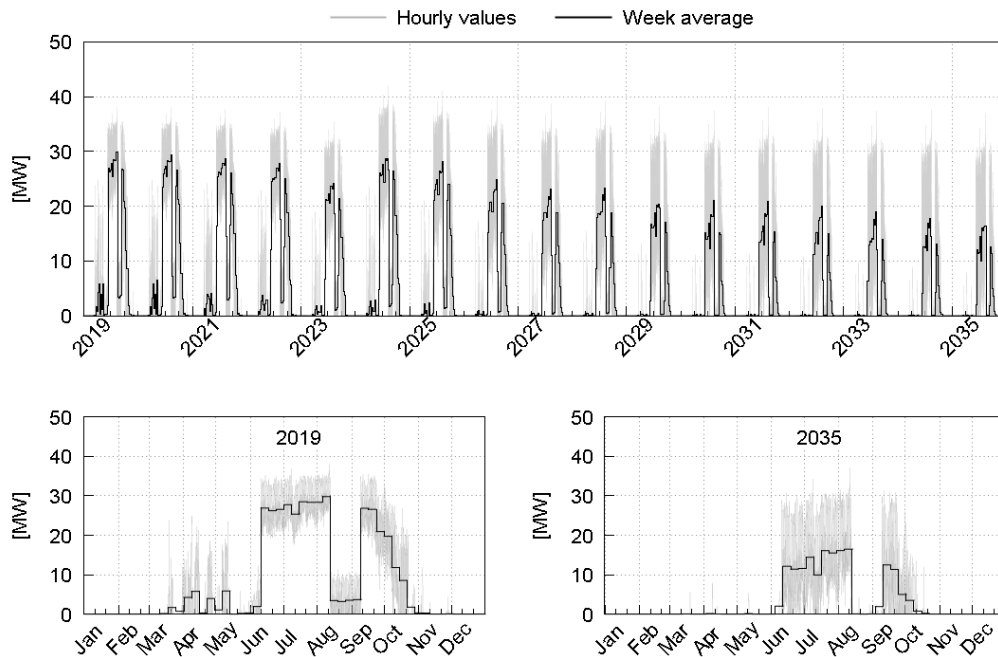


Figure 57: Available excess heat for charging of a UTES, in hourly and weekly values: evolution over the entire period (top) and focus on first and last years (bottom).

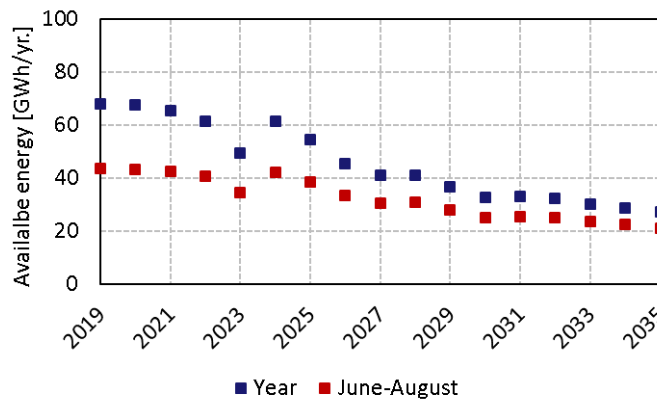


Figure 58: Evolution of annual available heat for charging of a UTES: integrated values over the entire year and over the 3 summer months (June – August).

As a complement to the available annual energy, the maximum heat load plays a fundamental role in the design of the UTES, as it is related with investments in heat transfer technologies (number of boreholes for BTES systems, flow-rate and number of wells for ATES systems). An option to reduce such investment costs is to integrate a buffer between the UTES and the DH. The buffer is designed to absorb high-frequency power fluctuation (short-term storage), while UTES is used as long-term storage for huge amounts of energy, at a more or less constant power [43]. As an example, in the Danish thermal district heating network *Braedstrup Fjernvarme* (total heat demand of 40 GWh/yr.), a 7'500 m³ hotwater tank buffer is used to enhance the technical and economic performance of the energy system (gas CHP plants, thermal solar panels, wind turbines and a BTES).

As can be seen in Figure 57, in the Geneva case study, a “one week buffer” would allow to reduce the maximum storage load significantly, with a maximum of 30 MW in the first years, respectively 20 MW in the

last years. Such a buffer would typically need a 300 MWh capacity (6'500 m³ water with ΔT of 40 K), with a maximum charging load from the DH designed at 20 MW.

On the side of the UTES, the relation between the maximum “injectable” heat load (MW) and the corresponding “injectable” annual heat (GWh) is presented in Figure 59, without and with an intermediate weekly buffer (top and bottom).

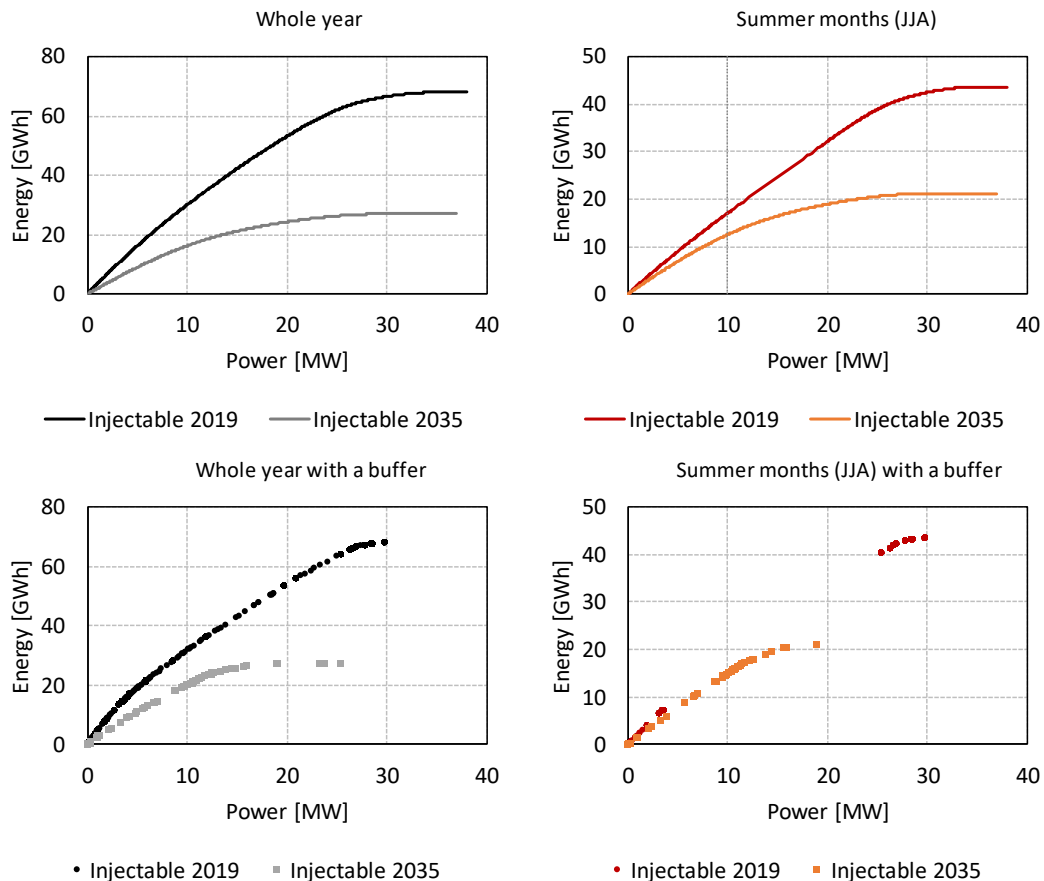


Figure 59: Annual “injectable” heat versus design heat transfer of UTES, without and with intermediate buffer (top and bottom), over the entire year or over the 3 summer months (left and right). Values based on hourly results.

Without intermediate buffer

In 2019, and without an intermediate buffer, injection of the total 70 GWh waste heat of the DH requires a heat transfer design capacity in the UTES of 38 MW (which is close to the maximum excess load on the DH - 42 MW in 2024, Figure 57). With the same transfer capacity, 65% of the “injectable” heat (45 GWh) is available during the 3 summer months (June-August). When reducing the heat transfer design capacity to 10 MW, only 35% of the available summer waste heat (17 GWh out of 45 GWh) can be transferred to the UTES.

In 2035, the summer waste heat on the DH reduces to around 20 GWh (out of 27 GWh), requiring 37 MW of transfer heat capacity. With a heat transfer design capacity reduced to 10 MW, the summer heat storage reduces to 13 GWh, corresponding to 75% of 2019 summer value.

In other words, while a 38 MW heat transfer design capacity would result in a full load equivalent of 1'200 h during the 2019 summer, this value would reduce to 550 h in 2035, potentially resulting in an important financial loss. On the other hand, a 10 MW heat transfer design capacity would result in an increased 1'710 h full load equivalent in 2019, respectively 1'260 h in 2035.

With intermediate buffer

As expected, an intermediate buffer between the DH and the UTES do not affect considerably the amount of available energy to charge the storage, but do have a big impact on maximum transfer power (Figure 59 - bottom).

In 2019, and after an intermediate buffer, the injection of the total amount of waste heat (70 GWh) would require a maximum heat transfer capacity of 30 MW (80% of maximum hourly value). For the same year and during the summertime, two distinct regimes appear. In this case, 30% of injectable power lies under 5 MW, with the remaining 70% been over 25 MW. Again, 17 GWh could be recovered during summertime for a heat transfer design capacity of 10 MW.

In 2035, it is possible to recover the total summer excess heat (20 GWh), with only two thirds of maximum hour load (25 MW). With a heat transfer design capacity reduced to 10 MW, up to 16 GWh can be injected into the storage, corresponding to 90% of 2019 summer value.

Finally, the design of the heat transfer capacity will depend on the different costs between power and energy facilities. In the case of BTES systems, the number of borehole have a high impact on the heat transfer capacity, while for PTES systems the volume of the pit conditions the maximum heat content rather than the heat transfer capacity. Concerning ATES, charging / discharging rates depend on hydro-geological conditions, which govern maximum water-flow rate (section 6.6).

b) Discharging of UTES

After the comparison of Figure 56 and Figure 57, it becomes evident that an UTES system could be used to increase the renewable share on the thermal grid at Geneva and reduce gas consumption, but what should be the new merit-order of the system?

To minimise rest time and consequently heat losses, storage discharge is planned to operate after CHP plants and direct geothermal units, yet before HP units. This will enable the good integration of the storage in the DH network without major impacts on CHP exploitation.

The evolution of the theoretical DH energy acceptance with the defined merit-order is shown Figure 60. As can be seen, heat acceptance is mainly present during heating season, with the exception of August, when the urban waste CHP plant is in maintenance and DHW demand cannot be covered by CHP units and direct geothermal plants. Furthermore, the heat acceptance increases over the years related to DH extension (Figure 53). The evolution of the annual heat acceptance is further shown in Figure 61, in integrated values over the entire year as well as over the 3 winter months (December – February), which confirms that at least 50% of DH acceptance is concentrated on the 3 winter months.

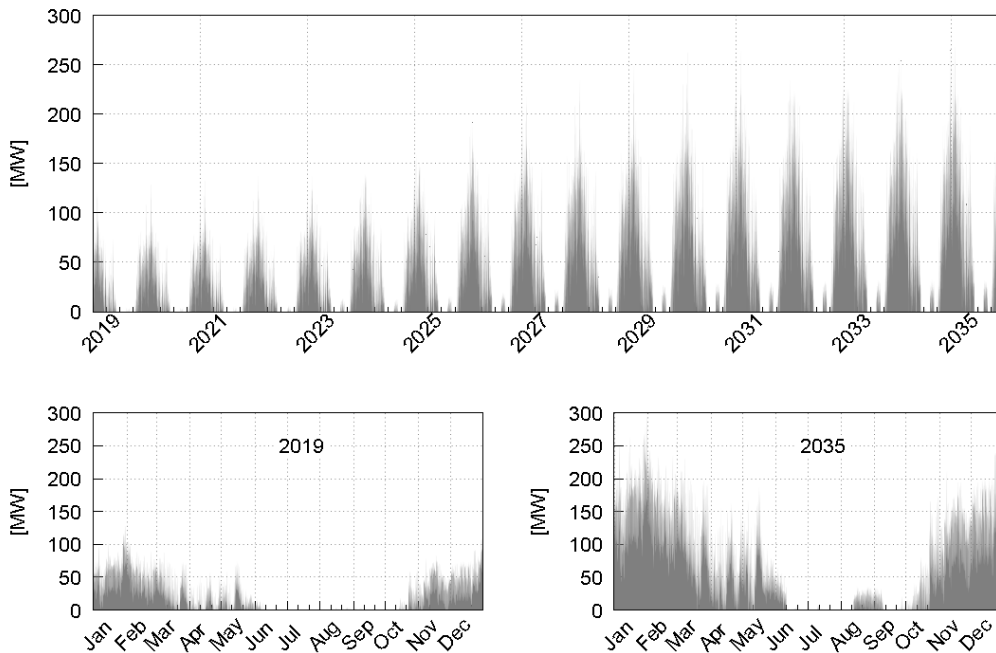


Figure 60: DH acceptance for charging of a UTES (hourly values): evolution over the entire period (top) and focus on first and last years (bottom). DH energy acceptance defined for the merit-order CHP-Geothermal-Storage-HP-Wood-Gas.

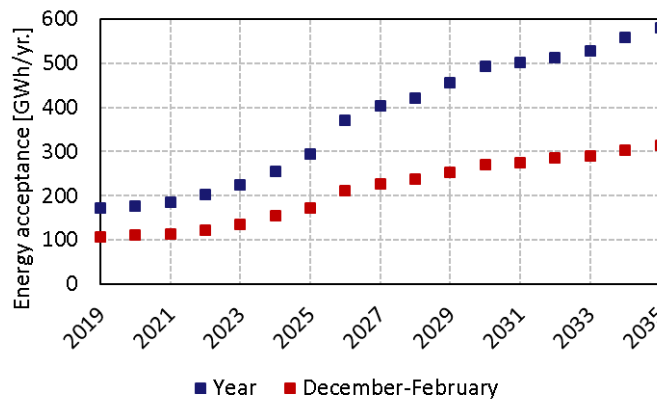


Figure 61: Evolution of annual DH energy acceptance: integrated values over the entire year and over the 3 winter months (December – February). DH energy acceptance defined for the merit-order CHP-Geothermal-Storage-HP-Wood-Gas.

Indeed, with the defined merit-order, there will be no energy restriction to discharge the storage; heat demand seen by the storage is at least twice higher than available “injectable” energy (Figure 58 *versus* Figure 61). In this case, the DH could accept up to 170 GWh/yr. and 130 MW the first year and almost 600 GWh/yr. (290 MW) by 2035, Figure 62.

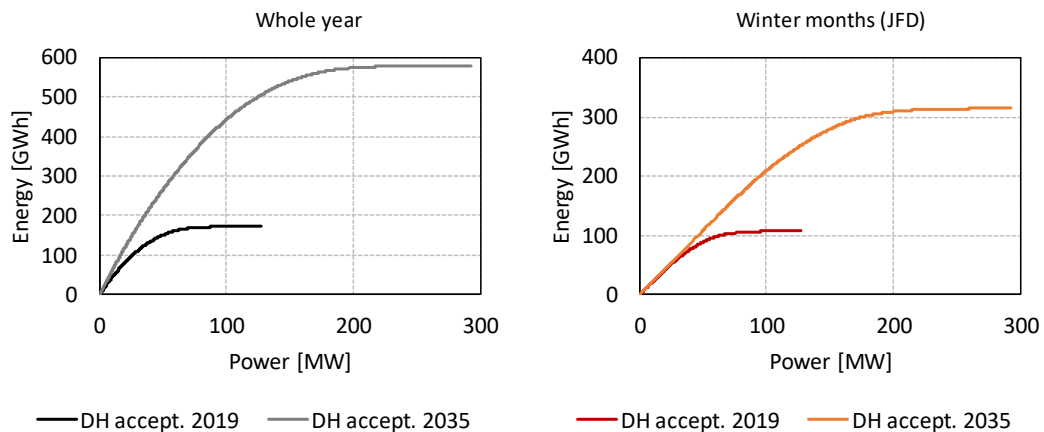


Figure 62: Annual DH energy acceptance versus design heat transfer over the entire year or over the 3 winter months (left and right). Values based on hourly results.

Again, power transfer limitations might constraint the amount of energy DH could accept from the storage. For example, with a power dimensioning of 10 MW, the maximum energy that DH could accept should range from 40 GWh/yr. to 60 GWh/yr. during the period 2019-2035. These values can be compared to the amount of energy that could be stored; as mentioned before, for a maximum power of 10 MW, the available “injectable” energy are lower than 20 GWh/yr. which reinforces the idea that there is a real market opportunity for an UTES in Geneva.

In conclusion, for the specific case of the evolving Geneva DH system, it would seem interesting to integrate a UTES system consisting of:

- A short-term storage (buffer system) designed to accept 300 MWh (one week load) with a 20 MW load capacity;
- A long-term UTES storage designed to accept between 50 to 150 GWh of heat, with a heat a transfer capacity in the range of 10 - 20 MW.

Such a design would enable to increase the renewable capacity in the DH network and limit oversized investments costs for future years.

6.5.2 System integration and discharging techniques

UTES energy discharge is highly dependent on temperature levels at the DH / storage interface. While the temperature profile of the UTES is a function of injected and extracted energy, it is very difficult to evaluate without specific simulations tools, in particularly for BTES and ATES systems, where the interaction between the heat-transfer fluid and the underground depends on multiple parameters.

Besides, energy and temperature response of the UTES is also a function of its integration in the DH system. To increase energy recovery [1], charging of the UTES is usually done in parallel to DH supply (T_s) and its energy evolution is limited by the temperature differential between the DH supply and the UTES (Figure 63). On the contrary, it is meaningful to discharge the UTES in series with the DH demand, and to inject the recovered heat into the return branch of the DH (T_r). In this way, discharging of the UTES is limited by the temperature differential between the UTES and the DH return, allowing for a larger energy recovery¹⁵ and enhancing storage efficiency. While usually not necessary with BTES, in the case of ATES and PTES, it is further necessary to invert the connection of the hot and cold side of storage to the DH heat exchanger (HEx), so as to properly use the temperature gradient of the storage for discharge.

¹⁵ The recovery factor is defined as the ratio between the extracted energy from the storage and the total injected energy into the storage.

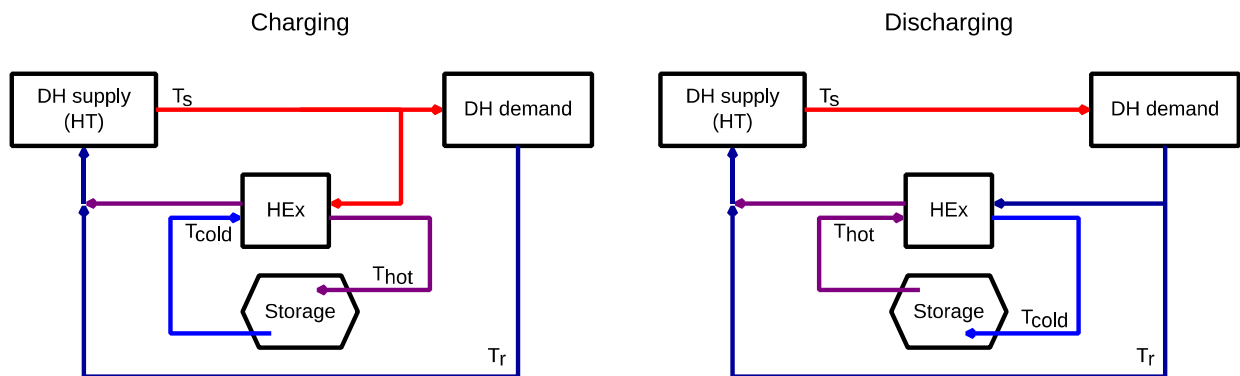


Figure 63: Integration of an UTES in the DH system, in charging and discharging modes.

Furthermore, depending on the UTES and DH return temperatures, several discharging techniques can be implemented:

- With a UTES temperature higher than the DH return temperature, direct discharge by way of a heat exchanger is possible (Figure 64). As depicted with the 2 cases of Figure 64, the higher the DH return temperature (T_r), the lower the temperature drop in the UTES and, as consequence, the lower the extracted energy. As a matter of fact, once the available UTES temperature reaches the DH return temperature, no additional heat can be directly extracted from the storage, even when its temperature is higher than the natural surrounding environment.
- With a UTES temperature lower than the DH return temperature, assisted discharge can be done by way of a heat pump (Figure 65).
- Finally, direct and assisted heat extraction can be combined to enhance heat extraction and to increase the production temperature on the DH return (Figure 66). In this mode, a first step of heat extraction is done by a heat-exchanger (direct mode), which is followed by a second step of heat extraction by a HP (assisted mode). Notice that more than one HP (connected in series) can be used to realize this temperature increase. Such a hydraulic configuration has been used for several years already in a geothermal DH in Switzerland, and has been studied in Finland [41, 42].

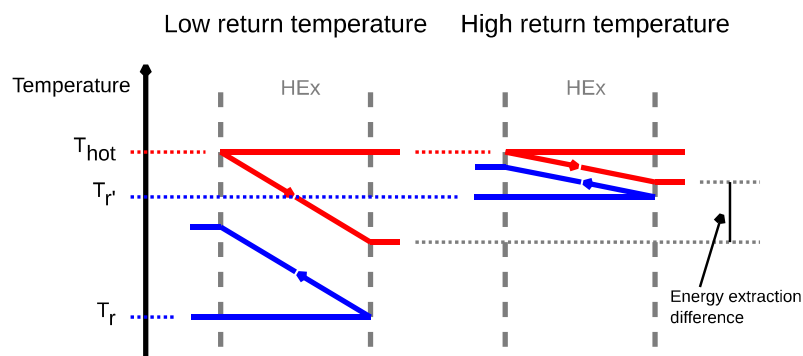


Figure 64: Direct discharge of a UTES, by way of a heat-exchanger (HEX). Case of a low DH return temperature (left) and of a high DH return temperature (right).

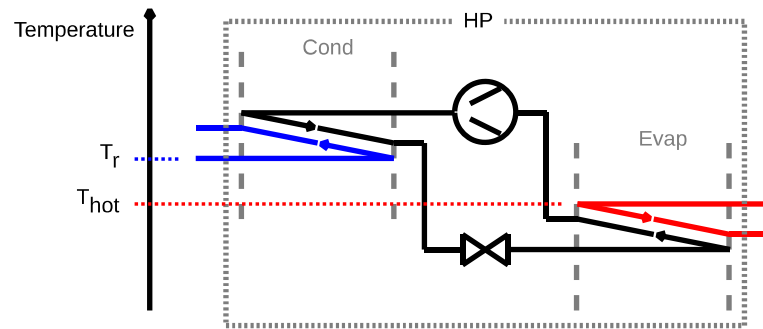


Figure 65: Assisted discharge of a UTES, by way of a heat pump (HP).

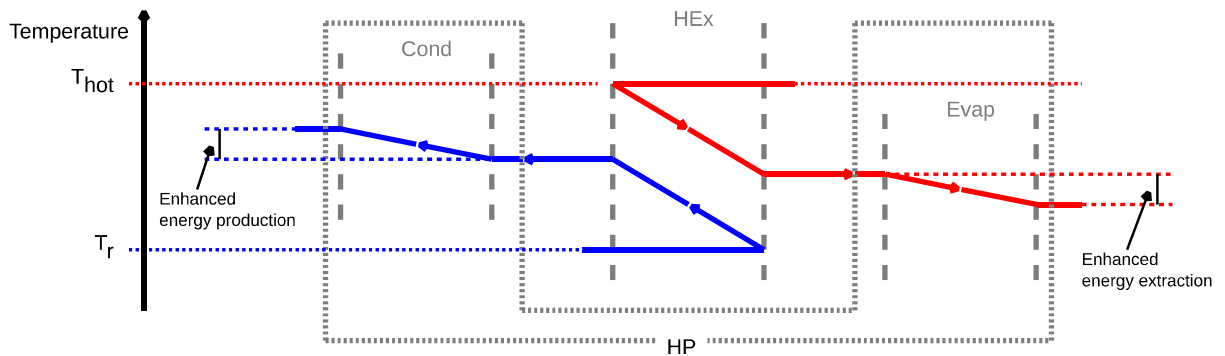


Figure 66: Direct + assisted discharge of a UTES, by way of a heat-exchanger (HEX) and a heat pump (HP).

6.6 ATES modelling

Aquifer response to charging and discharging is investigated with the Nexus-CSMP++ simulator [30] on an hourly time-step, over 15 years of operation. An isotropic and locally uniform porous rock is modelled to provide first results on fluid flow and heat transfer. Fluid flow through the aquifer is governed by mass and momentum conservative laws, where an accurate equation of state for water is integrated to simulate forced and natural convective processes. On the other hand, heat transfer (energy conservative law) is evaluated by the heat interaction between the aquifer fluid and the surrounding rock by advective and conductive process [31, 32].

Different hydro-geological configurations (aquifer thickness, permeability, porosity, depth and dip, artesian conditions and groundwater velocity) are tested, based on values from field analyses in the canton of Geneva [33, 34, 35, 36, 37, 38, 39, 40]. Latter conditions allow to determine the maximum operative flow-rate within the ATES, defined by a pressure on the well pipe which cannot exceed 80% of the hydro-fracture failure limit. The maximum hourly injectable / extractable energy rate is determined by the operative flow-rate and simulated temperatures of hot and cold wells.

In conjunction with the hydro-geological conditions, two integration modes of the ATES within the DH network are tested, namely direct or assisted heat extraction (without / with HP), and two possible well configurations (2 or 5 wells).

To estimate the thermal response of the ATES system, a simplified charging / discharging cycle is used: 4 months of charging (summer), 2 months of rest, 4 months of discharging (winter), and again 2 months of rest. Temperature constraints are imposed directly on the thermo-hydraulic module and are taken from typical DH temperature regimes in Switzerland [29]. They are set in a way to allow for simplified, yet realistic connection between the subsurface (ATES system) and the surface (DH network). In charging mode, the DH supply temperature (T_s) is set to 90°C (which, in the case of Geneva, corresponds to the summer supply temperature of the 2GDH, see Figure 54), corresponding to the maximum charging temperature (T_{hot}) into the hot well. In discharging mode, the DH return temperature (T_r) is set to 50°C (which, in the case of Geneva, corresponds to the winter return temperature of the 3GDH), corresponding to the minimum temperature at the hot well (T_{hot}) acceptable for discharging (cut-off temperature). As an alternative, assisted discharging is simulated by imposing a re-injection temperature of 20°C into the cold well (T_{cold}).

Unlike what is observed in the Geneva case study (section 6.5.1), the simulated ATES is exposed to “infinite” charging and discharging loads. However, associated to preceding constraints on maximum operative flow-rates (hydro-geological conditions) and on temperature levels at the DH / ATES interface, only limited energy is injected / extracted into / from the aquifer. These simplified assumptions enable to evaluate the ATES maximum potential, without taking into account limitations on the DH concerning available excess heat (charging mode) and energy acceptance (discharging mode), respectively.

Finally, a batch of more than 1'000 ATES scenarios is tested on a “what... if...” assessment. Each scenario is composed by a set of hydro-geological conditions and associated flow-rate, as well as a well configuration and heat extraction mode [32].

6.7 Simulation results for system integration

As pointed out above, within this study DH and ATES simulations were done independently from each other, and simulated ATES thermal response do not take into account charging / discharging dynamics and heat loads observed on DH simulation¹⁶. However, it is possible to assemble the results from both simulations to have a first preview on the overall system operation and efficiency.

As discussed previously, the integration of a hot water buffer tank should enhance the economic aspects of such a project. In the following analysis of the Geneva case study, we will hence consider a buffer which allows available excess heat to be averaged over a week (Figure 57).

¹⁶ Numerical simulations were done to evaluate ATES energy efficiency on its limits by exposing the system to infinity charging and discharging energies, constrained only by water-flow rates defined from hydro-fracture failure limit (section 6.6).

Let us consider an ATEs system in an aquifer of 50 m thickness, at a depth of 500 m, exploited by two wells (doublet configuration) situated 140 m apart. A 10% porosity and a permeability of 5.10^{-14} m^2 lead to a maximum operative water-flow of $72 \text{ m}^3/\text{h}$.

Comparison of the ATEs and DH simulation results yields following results (Figure 67 and Figure 68).

Direct discharge (without HP)

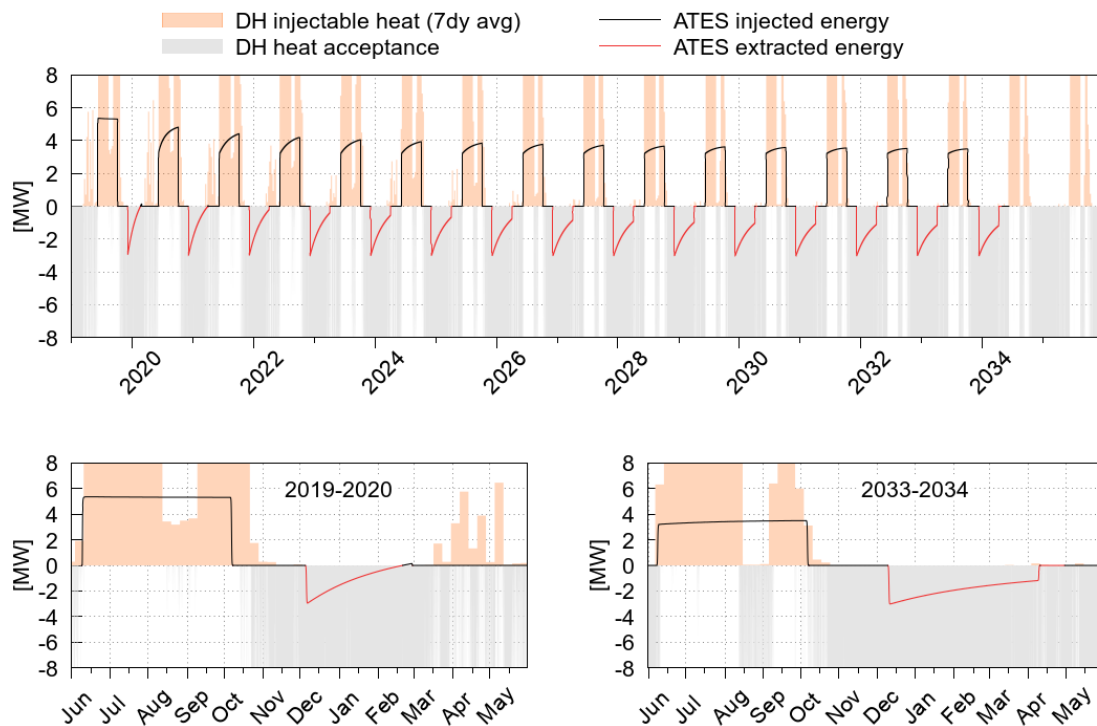


Figure 67: Charging / discharging dynamic of a direct heat extraction from an ATEs system (simulated data from [32]) compared to available injectable / acceptable load of the Geneva DH system. Evolution over the entire period (top) and focus on first and last years (bottom).

In the case of direct discharging into the DH (without HP) the re-injection temperature into the cold well is set at 50°C (as limited by the DH return temperature, see Figure 63).

We observe that most of the time the load injected into the ATEs is actually covered by the available “injectable” heat of the DH system (except once a year, during maintenance of the waste heat incineration plant in summer). Similarly, during discharge, the DH can always absorb the extracted load from the ATEs. This shows that such an ATEs, with a relatively small capacity, is well designed for integration in the DH system, and that in this case the separated simulation of both systems remains coherent.

At the beginning of each discharging cycle, the maximum extracted load turns out to be around 3 MW (with sharp drop leading to an average of 1.5 MW over the 4 month discharge period), for an annual extracted energy of 4.5 GWh/yr. (averaged over 15 years). The corresponding charging periods are characterized by a relatively constant load, around 5 MW, for an average annual injected energy of 11 GWh/yr. Overall, the ATEs efficiency hence amounts to $4.5/11 = 43\%$. Slightly better results during the last 5 years (more than 55%), once warming up of the ATEs from its initial temperature is completed.

Direct + assisted discharge (with HP)

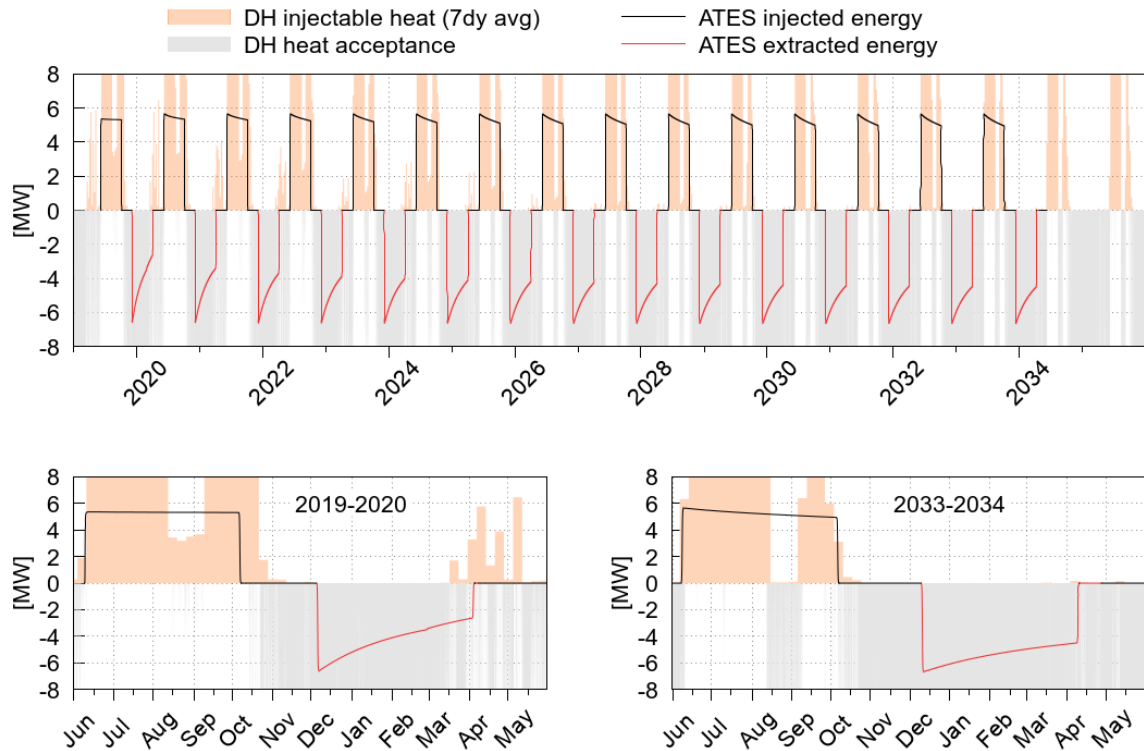


Figure 68: Charging / discharging dynamic of an assisted heat extraction form an ATES system (simulated data from [32]) compared to available injectable / acceptable load of the Geneva DH system. Evolution over the entire period (top) and focus on first and last years (bottom).

With an HP assisted discharge, more energy is extracted from the ATES and more energy can be injected during the charging periods. The underlying reason is the bigger temperature difference between hot and cold wells, since the temperature drop by the HP evaporator enables to re-inject water at 20°C (instead of 50°C). In this case, a cold bubble appears around the cold well and enhances the system efficiency. Latter reaches 95% in average over the 15 years period. However, it is important to notice that 23% of the extracted heat actually comes from electricity (constant SPF of 3, by hypothesis). In this case, the heat recovered from the ATES amounts to 15 GWh/yr., and represents 6% of the 2035 gas consumption on the DH system without ATES, which could help to reach the target of an 80% renewable energy mix on the DH system by 2030.

Finally, the annual heat flow diagram of both ATES configurations is presented in Figure 69.

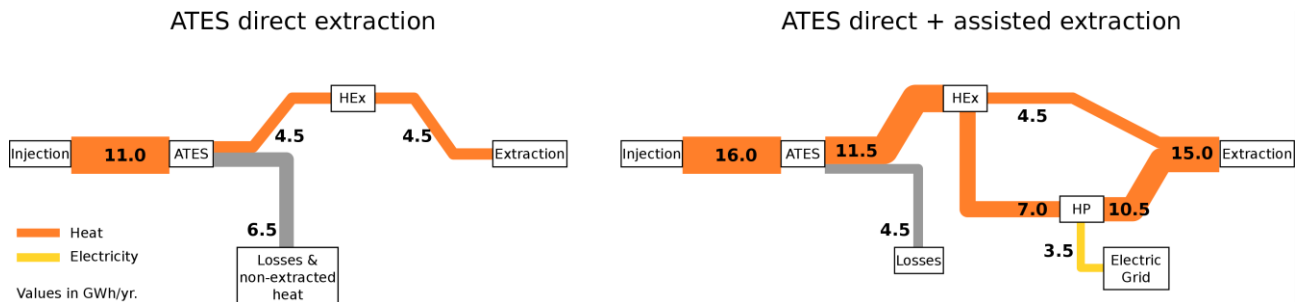


Figure 69: Heat flow diagram (average over 15 years) for an ATES system with direct or assisted (HP) discharge.

6.8 Limits and perspectives

Concerning simulation of the DH system, the main difficulty consists in defining realistic scenarios concerning evolution of the heat demand, in particular related to quality and rate of building retrofit, growth of building stock and efficiency of new buildings, as well as climate change. In addition, within this study some specific technical aspects were not addressed completely. For example, when simulating the DH, we considered a uniform temperature over the entire DH network. Since direct energy transfer can only occur from 2GDH to 3GDH grids, heat transfer in the opposite way would require the use of additional HPs, which would slightly change the DH production energy mix.

Concerning the ATES numerical simulations, mechanical constraints were simplified to prevent hydro-fracture failure and no chemical reaction module were added to the software. Mechanical constraints can limit the maximum water-flow in the system, while water chemistry might limit to a certain range the temperature of re-injected water. Both aspects should lead to somewhat lower values for charging and discharging energies. It could further be interesting to analyse how the energy efficiency of the ATES system would vary with a different set of charging temperatures and energy profiles.

The largest limitation of the present study is the separate simulation of the DH and ATES systems. An integrated simulation of the entire system would namely enable to test the reactivity of the ATES to the projected evolving profile of heat demand and supply on a DH system, like the one of our case study. However, for systems with small capacities (less than 10 MW in our case), simulation results with more complex / integrated numerical models should in principle not considerably differ from the results obtained here.

6.9 Conclusion

In this study, we shed light on the importance of analysing UTES systems with a holistic vision, since their integration within the DH network depends on a vast number of parameters. A long-term market strategy is important to guarantee that enough injectable heat is available throughout the lifespan of the project, and that the DH will be able to accept the extractable heat from the storage. Different merit-order strategies and system integration (hydraulic connections and heat extraction modes) also affect the energy efficiency of the UTES system.

Concerning technical aspects, the hydraulic connections and temperature levels at the UTES / DH interface must be taken into account very early in the project phase. In this regard, it is meaningful to discharge the UTES in series with the DH demand, and to inject the recovered heat into the return branch of the DH. In this way, discharging of the UTES is limited by the temperature differential between the UTES and the DH return (instead of supply), allowing for a larger energy recovery and enhanced storage efficiency. However, one must pay attention to the effective DH return temperature, since a high return temperature will limit the heat extraction and can have an important economic impact. For better exploitation of the UTES, an HP can be used to increase the heat discharge, as well as to increase the amount of heat accepted by the storage.

Finally, a buffer system seems to be a good option for BTES or ATES systems, where infrastructure costs are highly dependent on installed power. For this kind of system, buffer tanks can smooth the loading and unloading profiles and avoid high-frequency power fluctuations.

In the case of the of Geneva, integration of a small sized ATES (operative water-flow of 72 m³/h) with a buffer (20 MW and 300 MWh) could bring about an additional 6% fossil fuel saving and help reaching the target of an 80% renewable energy mix on the DH system by 2030.

7 Implementation of demand side management on a geothermal district heating system (Belgium)

7.1 Introduction

At the Belgian demo site in Mol, a demand side management system is implemented on an existing district heating network. This heating network started as a network of the first generation (1GDH) [44] with waste steam from a nearby electricity production plant. Gradually it was upgraded to a network of the second generation (2GDH) and still today, the network is evolving and expanding. In 2019 the geothermal power plant on the Balmatt site was commissioned and in the near future, the geothermal doublet will deliver baseload heating for the district heating network. In 2021 a new connection was made to a residential cluster nearby.

The integration of a geothermal heat source in an existing district heating network with many legacy systems poses certain challenges, for instance, significant peak heat loads occur and the return temperature of the network is relatively high and difficult to reduce. In order to maximize the share of renewable heat from the geothermal doublet, both problems have to be addressed. Peak heat loads and return temperature can be reduced on building level to a certain extent by optimizing the rule-based control system in each building connected to the network. However, in practice this is difficult to achieve since this approach is very time consuming and expensive (control specialist have to fine-tune the controllers). Moreover the result on network level is particularly insecure since each system works independently. Therefore an advanced demand side management platform was implemented, called Smart Heat Grid, hosted by the Swedish company Noda. On this platform, a self-learning controller for district heating networks is implemented, called The Storm controller.

7.2 Storm controller

The Storm controller is an advanced self-learning controller for district heating and cooling networks. The controller was codeveloped within the H2020 project Storm [45] by the Swedish company Noda and the Belgian company VITO. The purpose of the controller is to optimize the whole energy chain, from heat generation, distribution to the end consumer. The system is implemented on the existing Noda framework which is hosted on an cloud platform (Noda Smart Heat Grid). The Storm controller architecture consists out of four main modules:

- Forecaster: Forecasts the heat demand and thermal flexibility that can be activated
- Planner: Creates an optimal control plan, taking into account heat load forecasts and constraints
- Tracker: Sends control actions to the different controllable loads
- vDER: Executes control actions coming from the tracker

This architecture is summarized graphically in Figure 70. The Storm controller can be implemented in building- and HVAC control systems in different ways:

- Sensor override technology
- Via local gateway (open-source communication protocols)
- Digitally via data management platform (e.g. by using Building Management System (BMS) Application Programming Interface (API) service)
- A combination of the previously mentioned solutions

Additional sensors can be added easily (e.g. indoor temperature sensors etc.), depending on the requirements of the setup and the requirements.

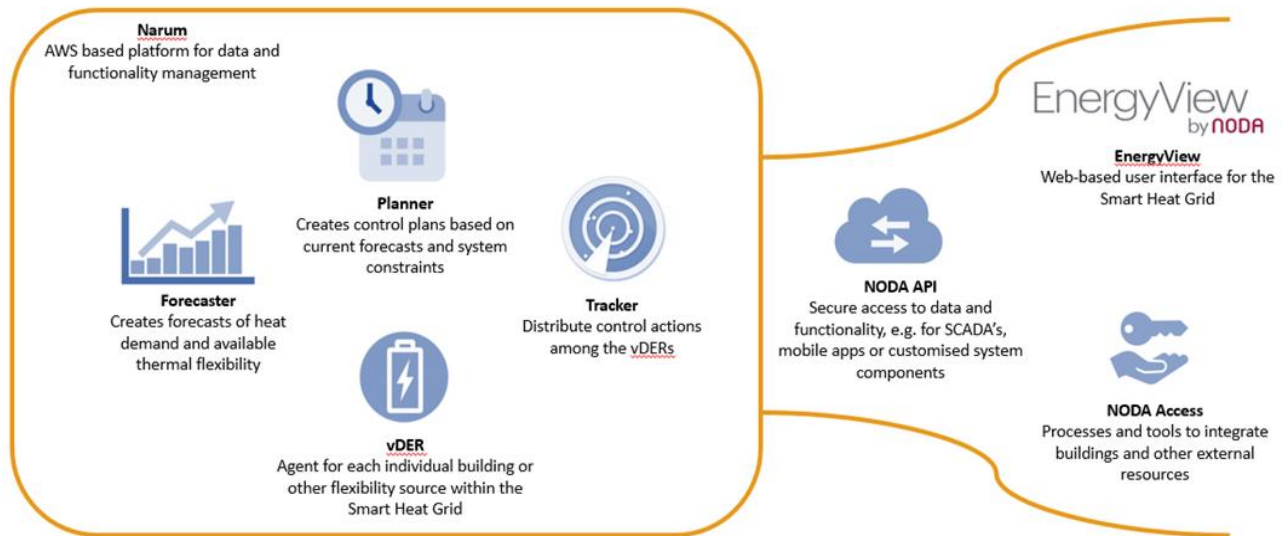


Figure 70: Overview of the Storm architecture with its main components [46].

7.3 Demo site overview and DSM setup

The district heating system in Mol is a high temperature network that provides heat to approximately 45 buildings (offices, laboratories, warehouses). In 2021, the network expanded further to the North in order to heat a newly renovated residential area nearby. Currently, the heat is provided by 3 gas-fired boilers with a total installed capacity of 22.5MW_{th}. By the summer of 2021 heat from the geothermal doublet will be used as primary heat source on the DHN. An overview of the network is given in Figure 71.

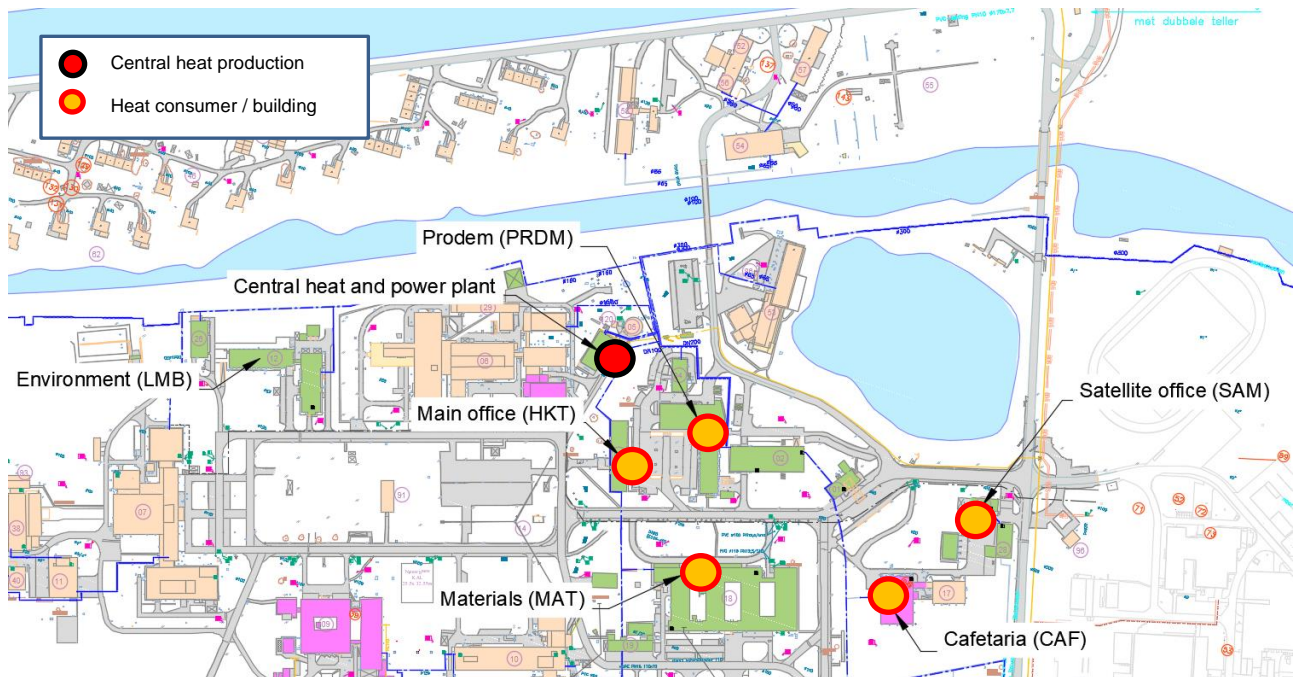


Figure 71: Map of the demosite with location of heat production units and heat consumers where the Storm controller is applied.

Table 24: Overview of the buildings where the Storm controller is implemented.

Building ID	SAM	CAF	HKT	PRDM	MAT
Building type	office	cafeteria	office	office lab	office lab
Building footprint	230 m ²	1'150 m ²	930 m ²	2'000 m ²	4'300 m ²
Number of floors	2	1	3	2	2
Indoor setpoint temperature	21 °C	21°C	21°C	21°C	21°C
Temperature regime heating	variable	variable	variable	variable	variable
Heat emitters	radiators	radiators AHU	radiators underfloor heating	radiators AHU	radiators AHU
Peak heat load (-10°C)	60 kW	300 kW	240 kW	500 kW	1'100 kW
Annual heat demand	48 MWh	493 MWh	180 MWh	1'180 MWh	1'320 MWh

Figure 73 gives a schematic overview of the DSM setup at the demo site. Each of the 5 buildings is equipped with a local controller with sensor override technology. Here the outdoor temperature sensor used by the local BMS is rerouted to the local controller. This controller allows to influence the outdoor temperature reading by the BMS and, depending on the settings of the heating curve, the supply temperature to the building's heating systems (radiator, floor heating, etc) can be changed consequently. This approach is demonstrated in Figure 72. By changing the supply temperature to the building's heat emitters, the heat load of the building can be influenced. By performing a series of tests, called response tests, the controllable load of a building can be characterized.

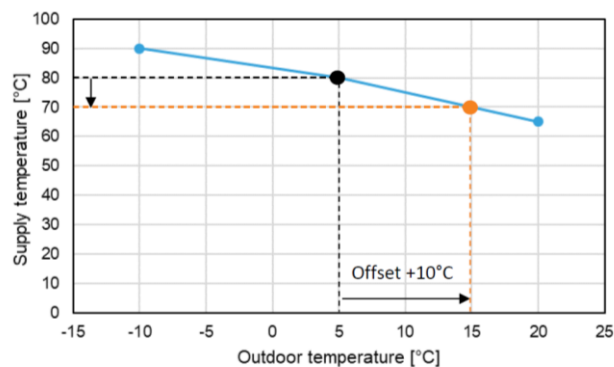


Figure 72: Outdoor temperature sensor override principle.

The Storm controller does not replace the building's HVAC control system, it adds an additional control layer to it. This means that, when the Storm controller is disabled or in standby mode, the building automatically returns to its original HVAC control strategy.

The supply temperature of the district heating network is also controlled by the Storm controller. Whereas a traditional district heating network is typically demand-driven and the supply temperature is set statically, dynamic control over both supply and demand offers several advantages:

- Increase heat production efficiency
- Decrease distribution losses
- Lower system temperatures
- Advanced network monitoring features

The Energy Management System (EMS) of the heating plant provides a API interface which can be used to exchange data. A synchronization script was written in Python to allow the exchange of data in both directions between the EMS API and the API service of the Smart Heat Grid platform. Within this script, certain error handling procedures were taken into account. For instance, a failover mode in case the communication is lost during a control action (the DHN supply temperature setpoint returns to its original value). In addition, the setpoint can only be changed within a pre-defined range, this range has to be set manually within the local controller for safety reasons.

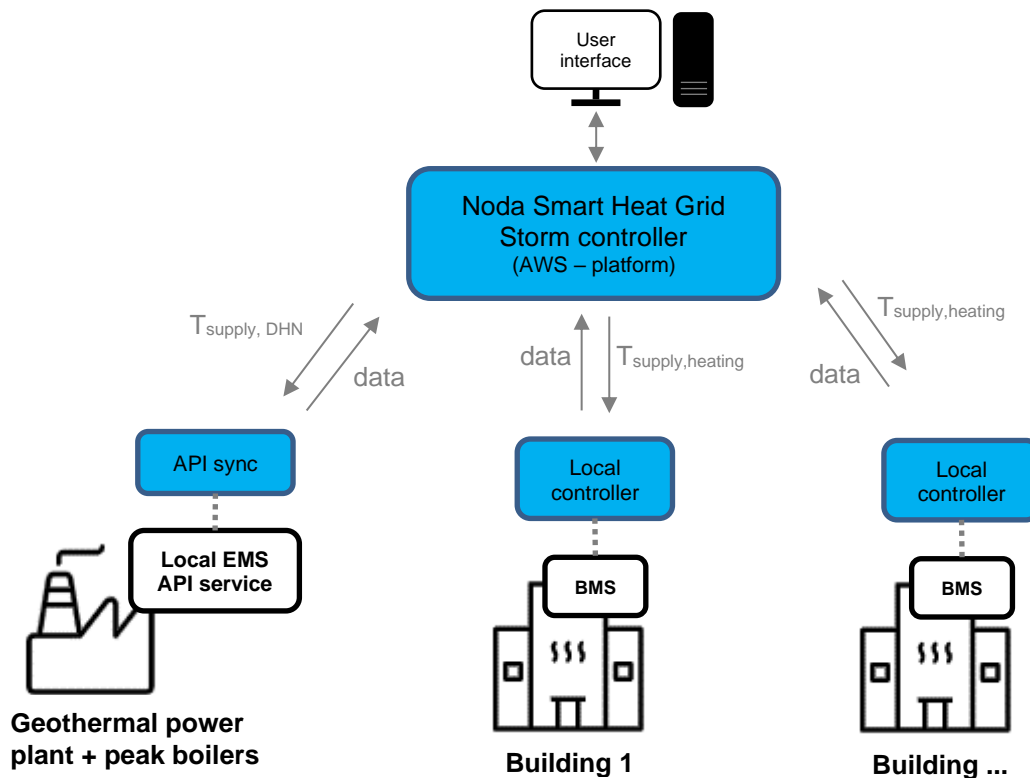


Figure 73: Principle diagram of DSM implementation at the Belgian demo site.

The setup can be scaled and replicated to other buildings. Table 25 provides an overview of relevant measurements for the Storm controller, gathered on building level (consumer side):

Table 25: Relevant measurements for the Storm controller.

Parameter	Description	Sample interval
Heat load	Building heating demand	5 min
Flow rate	Flow rate on primary side of building heat exchanger	5 min
$T_{\text{supply, DHN}}$	Supply temperature on primary side of building heat exchanger	5 min
$T_{\text{return, DHN}}$	Return temperature on primary side of building heat exchanger	5 min
$T_{\text{supply, heating, 1...n}}$	Supply temperature(s) to building heating system(s)	5 min
$T_{\text{return, heating, 1...n}}$	Return temperature(s) to building heating system(s)	5 min
$T_{\text{indoor, room 1...i}}$	Building indoor temperature(s)	10 min
T_{outdoor}	Outdoor temperature (measured locally)	10 min

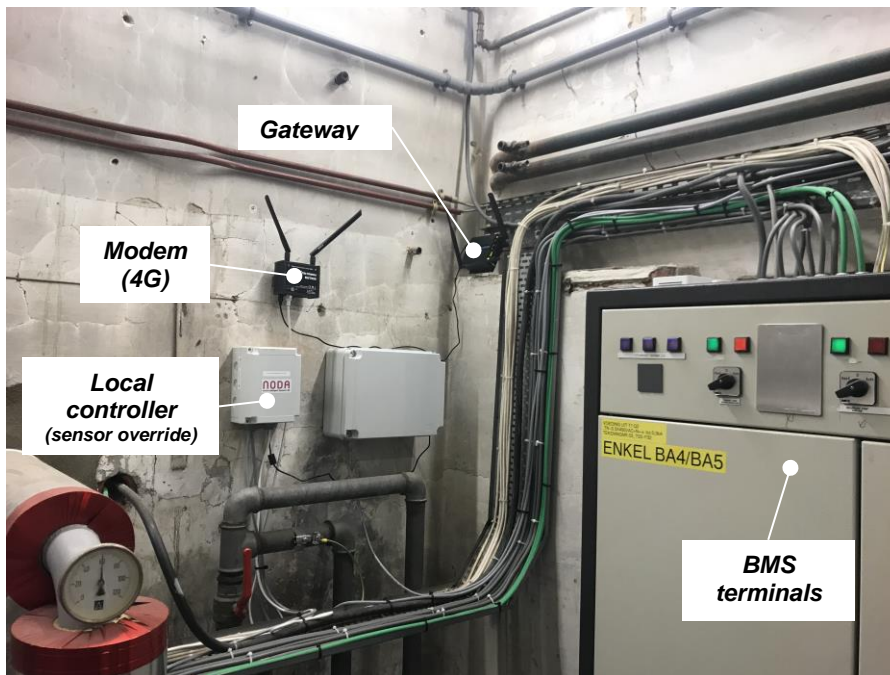


Figure 74: Picture of Storm controller hardware in one of the connected buildings.

7.4 System simulation - heat load forecasting

Heat load forecasting is a crucial component in demand side management applications for thermal energy systems and in optimization frameworks for district heating systems in general. Different methods for thermal load forecasting have been investigated in literature and put into practice. The methods applied for heat load forecasting can be categorized in two major classes, the forward method and data-driven approach [47]. While in the forward method the physical behaviour of the system is taken into account, the data-driven approach only uses measurement data of a system to build the thermal model. In the Forward methods, thermal system simulation software such as Modelica, EnergyPro or Trnsys is often used. In general the forward methods prove to be quite complex to use for heat load forecasting since many physical parameters, user behaviour and technical constraints have to be taken into account. While this approach could still be manageable for a single house or a small office building, it quickly becomes too complex, unreliable and time-consuming for larger and interconnected thermal systems such as heating networks. A dedicated physical model has to be created for each new system making the forward method also more difficult to scale. Therefore the Storm controller uses a data-driven approach, machine learning techniques to be more precise, for heat load forecasting.

In the Storm project different forecasting algorithms were evaluated and tested [48] [47]. In addition, an expert advice system which tracks the best forecasts of the following forecasting algorithms was evaluated. In the Belgian demo site, both the artificial neural network (multilayer perceptron) and decision trees (gradient boosting) are used for heat load forecasting. The Storm forecaster calculates a heat load forecast every day for the next day (96 quarters), using the following data as input:

- Historical heat load
- Outdoor temperature forecast
- Day of week
- Day of year
- Quarter of day

Before the heat load on network level could be forecasted, reliable measurement data was needed to train and validate the forecaster. Since there was no good data available (only a subset of heat meter data was recorded), a clamp-on ultrasonic flowmeter was installed and connected to the data platform.

After the implementation of this central heat meter on the output of the heat plant, the DHN heat load forecasting algorithm was activated on 13/03/2021. The DHN heat load profile and heat load forecast is

plotted in Figure 75 a from 13/03/2021 until 29/04/2021, a more detailed overview is given in Figure 75 b from 16/04 to 30/04. As can be derived from the graph, significant peak loads occur on the network with an amplitude of +/- 8,5MW. At the end of March, there were some short periods without heat demand as a result of relative high outdoor temperatures (more than 20°C).

Qualitatively, the forecasted heat load is in good agreement with the measured heat load, however, there are still some significant deviations, mainly during the peak loads. In general, over longer periods, the accuracy of the forecaster is expected to increase further. Results from previous tests with the Storm controller have indicated that the accuracy of heat load forecasting is less during summer months or periods with low heat demand [46].

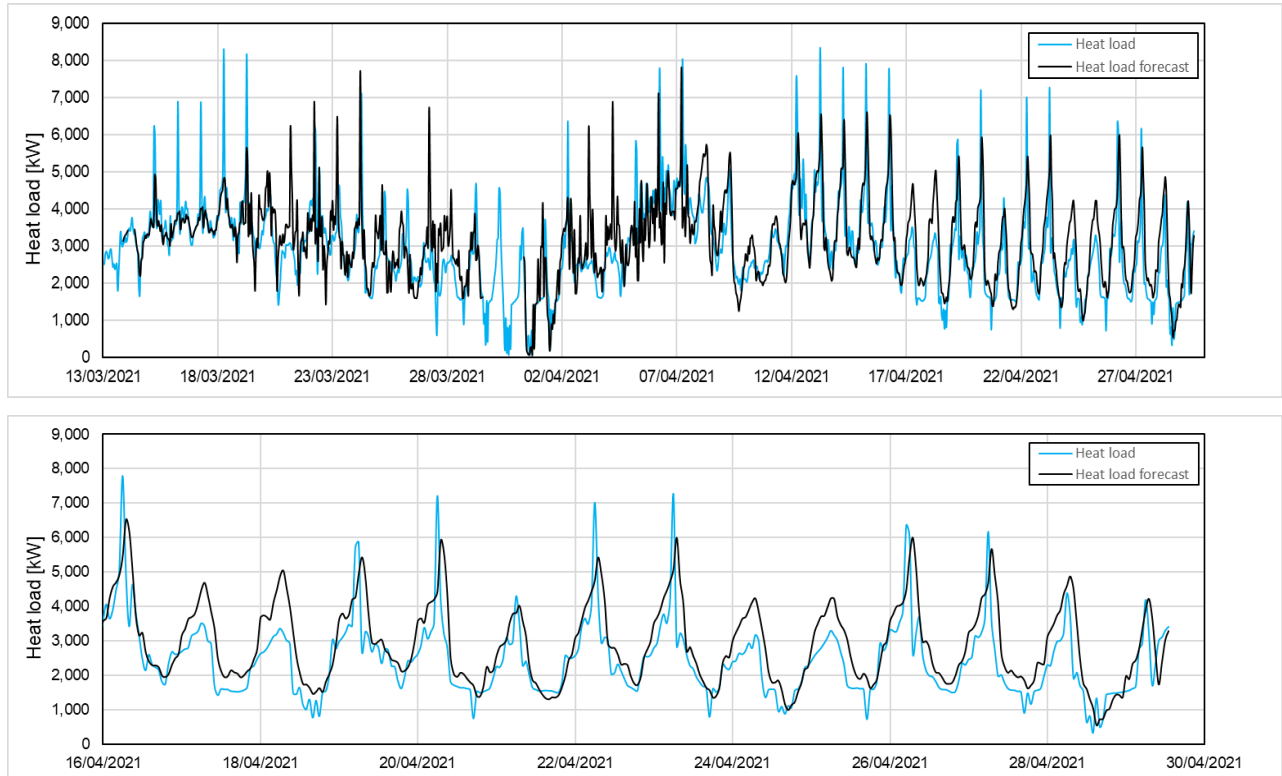


Figure 75: Heat load measurement and forecast on the thermal network.

In order to assess the accuracy of the forecast the Mean Absolute Error (MAE) and Mean Absolute Percentage Error (MAPE) were calculated.

Mean absolute error (MAE):

$$MAE = \frac{1}{n} \sum_{i=1}^n |f_i - y_i| = \frac{1}{n} \sum_{i=1}^n |e_i|$$

Mean absolute error percentage (MAE%):

$$MAE\% = 100 \frac{\sum_{i=1}^n |e_i|}{\sum_{i=1}^n |y_i|}$$

Mean absolute percentage error (MAPE):

$$MAPE = \frac{100}{n} \sum_{i=1}^n \left| \frac{f_i - y_i}{y_i} \right| = \frac{100}{n} \sum_{i=1}^n \left| \frac{e_i}{y_i} \right|$$

Where f_i is the forecasted heat load in timestep i and y_i is the measured heat load.

The MAE calculates the mean absolute error over the whole timeseries and it does not scale the error to the heat load. The MAPE calculates the average of the percentage errors and it is often used to measure the accuracy of heat load forecasts. Care has to be taken while interpreting the MAPE since high errors during periods with low demands significantly impact the MAPE. Therefore, also the relative MAE is calculated by dividing the MAE with the average heat load of the dataset. An overview of the accuracy of the heat load forecaster is given in Table 26.

Table 26: Overview of heat load forecasting errors.

Performance indicator	(March – April)
MAE	600 kW
MAE%	19.2%
MAPE	22.4%

The error on the heat load forecast is higher than what was reported during previous tests. This can be explained by the short training dataset (Jan-Feb 2021). In other words, there are very limited ‘reference circumstances’ (spring weather conditions) present in the training data. It is expected that the performance of the forecaster will increase as more measurement data becomes available. Normally, larger datasets of at least one year are used to evaluate forecaster accuracy. In addition, the accuracy of heat load forecasts during periods with low heat demand is typically less than during winter months where heat demand is higher.

The supply temperature of the network is also forecasted since this is used as an input for the Dynamic Supply Temperature (DST) algorithm. The measured and forecasted supply temperature are given in Figure 76.

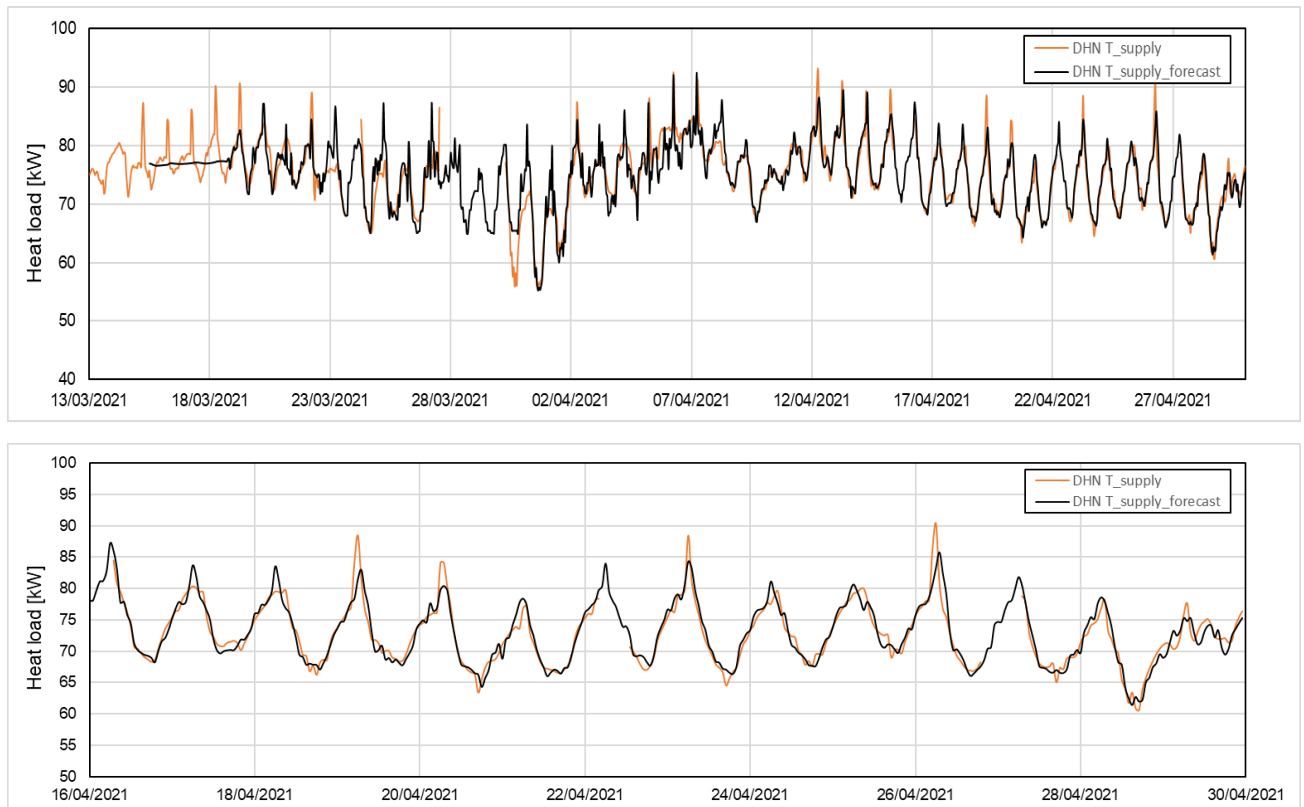


Figure 76: DHN supply temperature measurement and forecast.

Forecasting the supply temperature of a network is more straightforward than forecasting heat load since the supply temperature of the network is typically calculated based on the actual outdoor temperature and time related settings. It is a controlled variable and does not depend on the heat demand of the network. This is also visible in the accuracy of the forecast (see Table 27). The MAPE is 2.4% which indicates a good forecast.

Table 27: Supply temperature forecast accuracy.

Performance indicator	(March – April)
MAE	1.8°C
MAE%	2.3%
MAPE	2.4%

7.5 Control strategy

7.5.1 Default control strategy

The default control strategies of the HVAC systems applied in each of the demo buildings are quite similar, for instance, in each of the buildings the supply temperature to the buildings is controlled based on the actual outdoor temperature via a heating curve which is programmed in the local BMS (no additional functions are used such as averaging of outdoor temperature...) Furthermore, night setback is used in all of the buildings. Also in weekends, the heating is turned off completely. The buildings do not have a cooling system and domestic hot water is produced at a fixed temperature with a separate heat exchanger.

The clock settings in the BMS can also be derived from the heat plots of the building heat load data. Figure 77 shows the heat plot of one of the older, unrenovated office buildings over a period of approximately 100 days. From this plot the following settings can be derived:

- The heating system starts at 5:00AM¹⁷ on Mondays and 6:00AM on other weekdays (comfort setting)
- The heating system stops at 18:00PM and restarts at 00:00AM if minimum night set back temperature is not reached (in this case 15°C indoor temperature)
- There is practically no heat demand in the weekend, only on very cold days the heating system will start on Sunday.

¹⁷ UTC+1, time in graph is noted as UTC

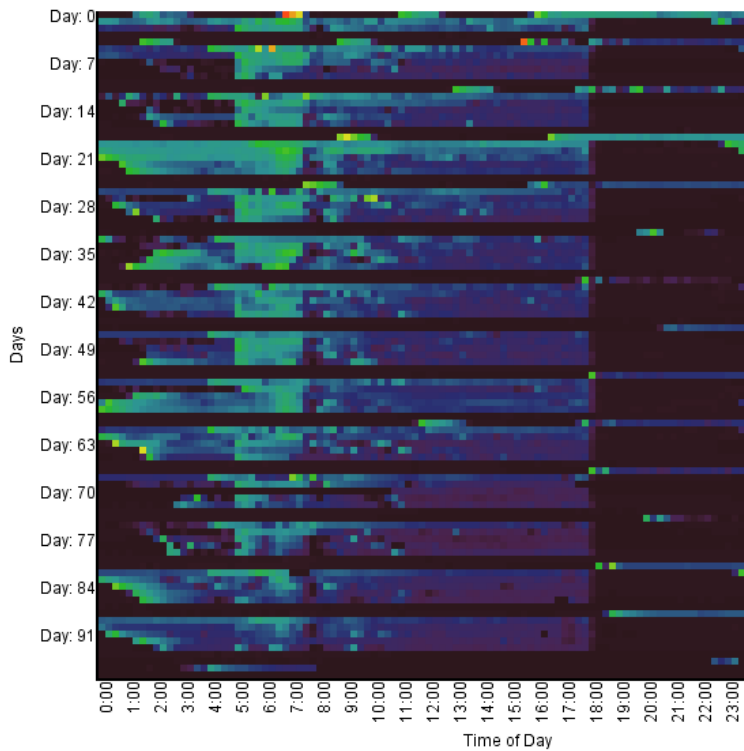


Figure 77: Heatplot of unrenovated office building (black (min): 0kW – red (max): 80kW).

A similar heat plot was made for another office building which is more recent and better insulated (Figure 78). The heat load of the building is mainly situated between 6:00AM and 7:00AM in the morning, when the building switches from night setback mode to comfort mode. During the rest of the day very little heat is necessary to keep the building up to temperature. Also here, the heating system switches off at 18:00PM.

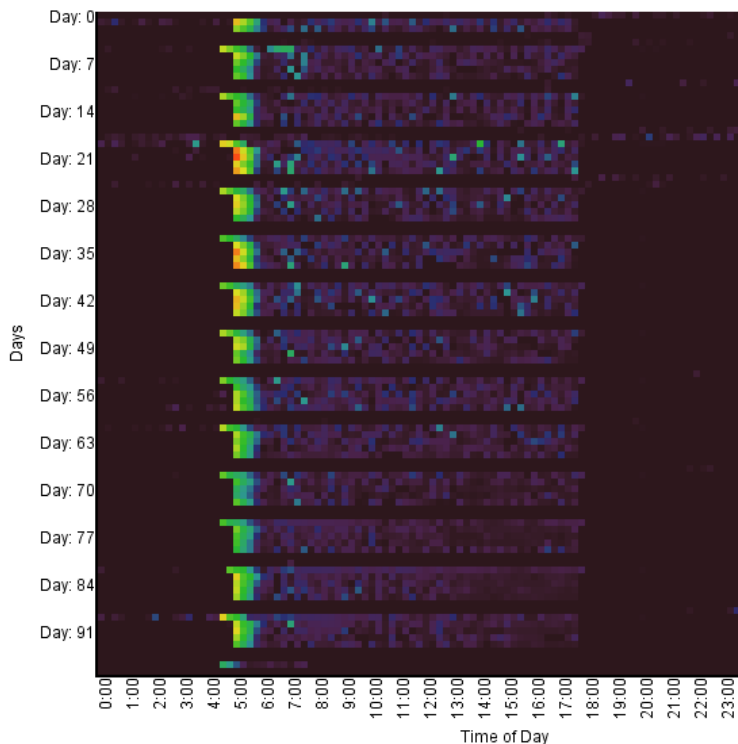


Figure 78: Heatplot of renovated office building (black (min): 0kW – red (max): 300kW).

The central heat production units follow the thermal demand on the network. The flowrate is controlled based on the differential pressure on the network (with outdoor temperature compensation). The supply temperature is based on the actual outdoor temperature (heating curve) with an additional boost function during the morning peaks (the supply temperature is increased temporarily within in a certain time interval). The maximum supply temperature on the district heating network is 95°C and the minimum supply temperature is limited to 55°C.

Since the buildings on the thermal network have similar time settings and use night setback, significant peak loads occur during the morning between 5:00AM and 7:00AM. This is not optimal since the geothermal doublet delivers heat with a constant output (approximately 3,5MW_{th} at reduced capacity). Gas-fired peak load boilers are therefore used to provide the majority of the heat during these morning peaks. In this perspective demand side management (building-level) and dynamic supply temperature optimization (network – level) can optimize both heat generation and distribution.

7.5.2 Peak shaving and dynamic supply temperature

The goal of the peak shaving algorithm is to keep the heat load on the network within the capacity of the base load unit (in this case geothermal heat) as closely as possible, thereby reducing the energy consumption of the non-renewable heat sources (gas-fired boilers).

An objective function is defined which is minimized by the planner, taking into account the price of each heating system:

$$Obj = \sum_t [\lambda_{geothermal} Q_t^{geothermal} + \lambda_{gas} Q_t^{gas}]$$

Where $\lambda_{geothermal}$, λ_{gas} are the marginal cost of production, $Q_t^{geothermal}$, Q_t^{gas} are the time dependent energy production for the geothermal and gas unit respectively.

This objective function is subject to different specific constraints related to:

- Overall energy balance: taking into account the output of each heat source and the demand on network level.
- Capacity bounds for heat units: defines the maximum output of the different heat sources
- Aggregated flexibility: aggregating the total flexibility of the different controllable loads
- Individual flexibility: constraint related to the flexibility of a single building
- Control signal bounds: limits the control signal in function of thermal mass and comfort in a building
- Degree-hour constraint: limits control action over longer periods

The planner creates an optimal control plan which is translated into concrete control actions. Next the tracker distributes the control signals (as outdoor temperature offset) to the local BMS inside each building. An example is given in Figure 79. The dashed lines represent the control actions which are distributed to the buildings (in this case two buildings called 'SAM' and 'HKT'). This control signal represents a temperature offset on the actual outdoor temperature at that specific building (displayed on the right axis). In this case a positive offset of 7-8°C is sent which results in a decrease of the supply temperature of the building's heating system which, in turn, will cause the heat demand to decrease.

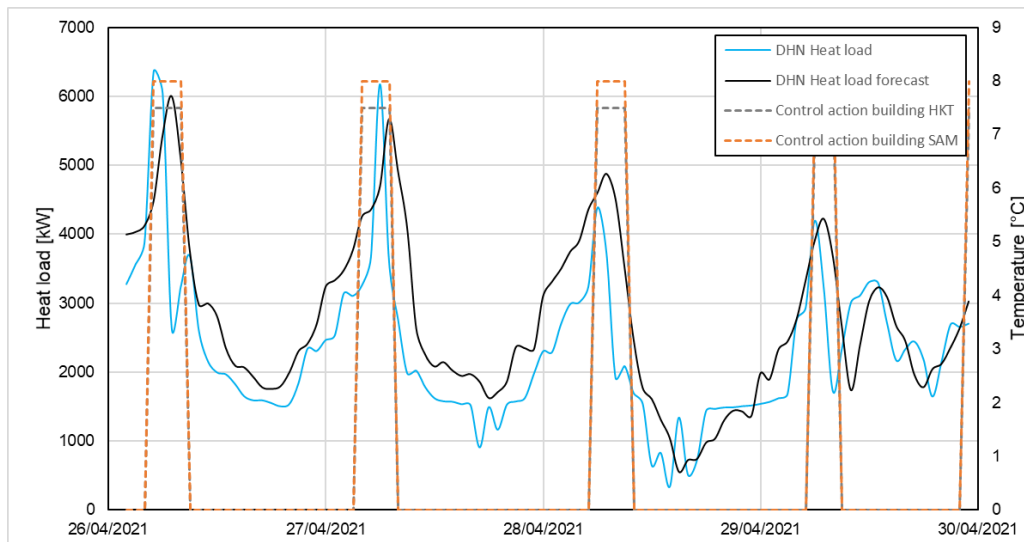


Figure 79: Control actions on building level.

In addition to the peak shaving algorithm, a dynamic supply temperature algorithm is implemented on network level. This DST algorithm is a set of different algorithms and functions that collectively make up the behaviour of the entire system. Two main processes are running simultaneously; the proactive modelling and the reactive boundary management. The proactive modelling is based on a Model Predictive Control (MPC) process where it tries to model the heat losses in the network and the heat propagation time delay in the network. The reactive boundary management on the other hand keeps track of the operational conditions (actual and prospective thermal flexibility of a building) at different locations in the network.

7.6 Conclusion

The Storm Controller was implemented on the geothermal district heating system in Mol, Belgium. While the controller was initially designed to unlock and activate thermal flexibility on building level, tests have indicated that also on the supply side important improvements can be made in relation to the general supply temperature of the network. The quality and reliability of smart control very much depends on the accuracy of forecasts e.g. on heat load and supply temperature, therefore different forecasting methods and algorithms were tested. The accuracy of the heat load forecast on network level is slightly lower than what was reported during previous tests. An important remark is that only very little training data was available. Moreover, at the end of the heating season where outdoor weather conditions tend to fluctuate heavily, heat load forecasting proves to be more difficult. After performing a series of response and stability tests, the DST algorithm is currently being tested on network level.

8 Concluding remarks

This report provides an overview of the system simulation frameworks used in HEATSTORE. Although each partner provides answers to specific research questions related to UTES, more general conclusions can be derived.

When looking into the design, integration and operation of UTES in heating systems, many aspects have to be considered. It is key to first understand the associated questions and problems involved before setting up a simulation framework that can be used to provide the necessary answers in order to come to an optimal solution. This is typically linked with the project phase or 'application level' as described in 2.3.2 and this can also be concluded from the different focus of each simulation framework discussed in this deliverable, for example:

- Evaluating the role of UTES in DH systems
- Simulating UTES dynamics over longer periods
- Dimensioning and configuring UTES, TES and other related components in the energy system
- Economic analysis to optimize the business case
- Deriving optimal system control parameters, settings and boundary conditions
- Forecasting system behaviour to optimize operations

Performing system simulations requires expertise in different fields which has to be brought together. For instance, geologists can model the subsurface dynamics in great detail while engineers focus more on how the heat can be used. Therefore, system simulations can become very complex and expensive due to the inherent complexity and level of detail of the models used. Simplified models can be used to make system simulations manageable (e.g. TNO used a simplified ATES model in the CHESS simulation environment to speed up the simulation time). Also, when performing system simulations on a higher level, e.g. related to strategic or planning aspects, simplified models can be used to give first insights and to save time.

In addition, each modelling software has its strengths and limitations when considering the whole energy system. It is often necessary to combine different models or software packages in order to construct an all-encompassing system model. This is not always straightforward and sometimes creativity is needed to set up the necessary interactions between different models:

- DK uses a combination of Trnsys and EnergyPRO to combine technically accurate models with economic analysis features
- IF and TNO both use their own modelling software for simulating ATES systems while a simplified and faster ATES model was used in the system modelling environment
- STORENGY and BRGM created their own models in Trnsys
- UNIGE adapted existing modelling software

Finally, the main task conclusions on energy system simulations are summarized:

- UTES has to be combined with short term storage both from a technical and economic point of view. PTES can be considered an exception since it can also be used for short term storage.
- Determining the optimal configuration of UTES and short term energy storage is often a trade-off between costs (both investment and operational) and other aspects (CO₂ - emissions, technical, legal).
- Long term effects (e.g. evolution of heat load, availability of surplus heat, DH developments) create uncertainties that can become more important than many other aspects considered in system simulations. This needs to be taken into account in the early phase of a UTES project. Energy system scenario analysis with simplified UTES models can be particularly helpful in the concept or planning phase
- District heating systems play a crucial role in the further uptake of UTES systems.
- Forecasting system behaviour (heat load, supply- and return temperatures) allows to further optimize an operational energy system, especially large scale infrastructure such as DH combined with UTES.

9 References

- [1] HEATSTORE, “Underground Thermal Energy Storage (UTES) – state-of-the-art, example cases and lessons learned. HEATSTORE project report,” A. J. Kallesøe and T. Vangkilde-Pedersen, Eds., GEOTHERMICA – ERA NET Cofund Geothermal, 2019, p. 130 + Appendix.
- [2] L. Quiquerez, B. M. Lachal, M. Monnard and J. Faessler, “The role of district heating in achieving sustainable cities: comparative analysis of different heat scenarios for Geneva,” in *15th International Symposium on District Heating and Cooling*, 2016.
- [3] F. De Oliveira Filho, L. Quiquerez, M. Ruegg, M. Monnard, B. Lachal and P. Hollmuller, “Évaluation quantitative de scénarios de développement du marché de la chaleur à Genève à l’horizon 2050 : du fossile aux renouvelables, pistes pour décarboner le système thermique,” Technical report, Université de Genève, 2020.
- [4] P. Østergaard, “Reviewing EnergyPLAN simulations and performance indicator applications in EnergyPLAN simulations,” *Applied Energy*, vol. 154, pp. 921-933, 2015.
- [5] K. L. Kipp, “HST3D; a Computer Code for Simulation of Heat and Solute Transport in Three-dimensional Ground-water Flow Systems,” U.S. Geological Survey, Denver, Colorado, 1987.
- [6] B. Drijver, G. Bakema and P. Oerlemans, “State of the art of HT-ATES in The Netherlands,” in *European Geothermal Congress 2019*, The Hague, The Netherlands, 2019.
- [7] B. Drijver, P. Oerlemans and W. Bos, “Full-Scale HT-ATES Tests Demonstrate that Current Guidelines Considerably Overestimate Sand Production Risks in Deeper Unconsolidated Aquifers,” in *1st Geoscience & Engineering in Energy Transition Conference, Nov 2020*, Strassbourg, 2020.
- [8] NLOG Dutch Oil and Gas Portal, “DoubletCalc2D Tool,” [Online]. Available: <https://www.nlog.nl/en/tools>. [Accessed 26 April 2021].
- [9] J. D. Ward, C. T. Simmons, P. J. Dillon and P. Pavelic, “Integrated assessment of lateral flow, density effects and dispersion in aquifer storage and recovery,” *Journal of Hydrology*, vol. 370, no. 1-4, pp. 83-99, 2009.
- [10] LOGSTOR, “Design - single pipes,” 05 2020. [Online]. Available: <https://www.logstor.com/catalogues-and-documentation>. [Accessed 26 5 2021].
- [11] O. Pruisen, V. Kamphuis, A. van der Togt and E. Werkman, “A Thermal grid coordinated by a multi agent energy management system,” in *4th IEEE/PES Innovative Smart Grid Technologies Europe*, 2013.
- [12] O. Pruisen, A. van der Togt and E. Werkman, “Energy Efficiency Comparison of a Centralized and a Multi-agent Market Based Heating System in a Field Test,” *Energy Procedia*, vol. 62, 2014.
- [13] TNO, “HeatMatcher - Innovation in control for heating and cooling systems and networks,” TNO, [Online]. Available: <https://www.tno.nl/en/focus-areas/ecn-part-of-tno/roadmaps/sustainable-energy/smart-energy-system-solutions/heatmatcher-innovation-in-control-for-heating-and-cooling-systems-and-networks/>. [Accessed 11 12 2019].
- [14] PlanEnergi, “SUNSTORE 3 – Slutrapport, Fase 1 - Projektering og udbud,” EUDP project number 63011-0178, 2011.
- [15] PlanEnergi, “SUNSTORE 3 - Phase 2 - Implementation,” EUDP project numbers 64009-0043 and 64010-0447, 2015.
- [16] G. Gauthier, “Modelling for design and optimization of performance and sustainability. Presentation of Danish PTES and BTES TRNSYS model studies.,” GEOTHERMICA – ERA NET Cofund Geothermal, 2021.
- [17] G. Gauthier, “Benchmarking and improving models of subsurface heat storage dynamics,” GEOTHERMICA – ERA NET, 2020.
- [18] T. Driesner, “Initial report on tools and workflows for simulating subsurface dynamics of different types of High Temperature Underground Thermal Energy Storage,” GEOTHERMICA –ERA NET, 2019.
- [19] H. Lund, S. Werner, R. Wiltshire, S. Svendsen, J. E. Thorsen, F. Hvelplund and B. V. Mathiesen, “4th Generation District Heating (4GDH): Integrating smart thermal grids into future sustainable energy systems,” *Energy*, vol. 68, pp. 1-11, 2014.

- [20] D. Connolly, H. Lund, B. Mathiesen, S. Werner, B. Möller, U. Persson, T. Boermans, D. Trier, P. Østergaard and S. Nielsen, "Heat Roadmap Europe: Combining district heating with heat savings to decarbonise the EU energy system," *Energy Policy*, vol. 65, pp. 475-489, 2014.
- [21] J. Chambers, K. Narula, M. Sulzer and M. K. Patel, "Mapping district heating potential under evolving thermal demand scenarios and technologies: A case study for Switzerland," *Energy*, vol. 176, pp. 682-692, 2019.
- [22] S. Djørup and N. Bertelsen, "An evaluation of the Hotmaps toolbox for national strategic heat planning," Technical report, Aalborg University, 2020.
- [23] M. J. S. Zuberi, "Improving energy efficiency in Swiss industrial sectors: status, emerging technologies and trends," PhD theses, Université de Genève, 2019.
- [24] J. Chambers, M. J. S. Zuberi, K. Narula and M. Patel, "Spatiotemporal analysis of industrial excess heat supply for district heat networks in Switzerland," *Energy*, vol. 192, p. 116705, 2020.
- [25] P. Fleuchaus, S. Schüppler, M. Bloemendal, L. Guglielmetti, O. Opel and P. Blum, "Risk analysis of High-Temperature Aquifer Thermal Energy Storage (HT-ATES)," *Renewable and Sustainable Energy Reviews*, vol. 133, no. 110153, 2020.
- [26] État de Genève, "Système d'information du territoire à Genève," 2021. [Online]. Available: <https://ge.ch/sitg>. [Accessed 15 Avril 2021].
- [27] S. Schneider, P. Hollmuller, P. Le Strat, J. Khoury, M. Patel and B. M. Lachal, "Spatial–Temporal Analysis of the Heat and Electricity Demand of the Swiss Building Stock," *Frontiers in Built Environment*, vol. 3, no. 53, 2017.
- [28] L. Quiquerez, F. De Oliveira Filho, S. Faÿ, P. Hollmuller and M. Meyer, "Scenarios for integration of medium-depth geothermal energy in an evolving district heating system: case study in Geneva (Switzerland)," in *World Geothermal Congress*, 2020.
- [29] L. Quiquerez, "Décarboner le système énergétique à l'aide des réseaux de chaleur: état des lieux et scénarios prospectifs pour le canton de Genève," PhD theses, Université de Genève, 2017.
- [30] HEATSTORE, "Interim report on UTES-type/site-specific simulators based on academic/research codes," S. Tómasdóttir and G. Gunnarsson, Eds., *GEO THERMICA – ERA NET Cofund Geothermal*, 2019, p. 55.
- [31] J. Mindel and T. Driesner, "HEATSTORE: Preliminary Design of a High Temperature Aquifer Thermal Energy Storage (HT-ATES) System in Geneva Based on TH Simulations," in *World Geothermal Congress*, 2020.
- [32] J. Mindel, L. Guglielmetti, F. De Oliveira Filho and T. Driesner, *Site-specific preliminary performance assessment of high temperature aquifer thermal energy storage systems based on thermo-hydraulic simulations*, In press, 2021.
- [33] M. Brentini, "Impact d'une donnée géologique hétérogène dans la gestion des géo-ressources: analyse intégrée et valorisation de la stratigraphie à travers le bassin genevois (Suisse, France).," PhD Theses, Université de Genève, 2018.
- [34] C. Chelle-Michou, D. Do Couto, A. Moscariello, P. Renard and E. Rusillon, "Geothermal state of the deep Western Alpine Molasse Basin, France-Switzerland," *Geothermics*, vol. 67, pp. 48-65, 2017.
- [35] N. Clerc and A. Moscariello, "A revised structural framework for the Geneva Basin and the neighboring France region as revealed from 2D seismic data: implications for geothermal exploration," in *Swiss Bulletin für Angewandte Geologie*, 2020.
- [36] L. Guglielmetti, F. Poletto, P. Corubolo, A. Bitri, C. Dezayes, B. M. Farina, F. Martin, F. Meneghini, A. Moscariello, C. Nawratil de Bono and A. Schleifer, "Results of a walk-above VSP survey acquired at the Thônex-01 geothermal well (Switzerland) to delineate fractured carbonate formations for geothermal development," *Geophysical Prospecting*, 2020.
- [37] Y. Makhloufi, E. Rusillon, M. Brentini, A. Moscariello, M. Meyer and E. Samankassou, "Dolomitization of the Upper Jurassic carbonate rocks in the Geneva Basin, Switzerland and France," *Swiss Journal of Geosciences*, 2018.
- [38] A. Moscariello, "The geomorphological landscapes in the Geneva Basin," R. E., Ed., Springer Nature, 2021, pp. 83-96.
- [39] A. Moscariello, L. Guglielmetti, S. Omodeo Sale, A. De Haller, O. Eruteya, H. Y. Lo, N. Clerc, Y. Makhloufi, D. Do Couto, G. Ferreira De Oliveira, L. Perozzi, F. De Oliveira Filho, P. Hollmuller, L. Quiquerez, C. F. Nawratil De Bono, F. Martin and M. Meyer, "Heat production and storage in Western

- Switzerland: advances and challenges of intense multidisciplinary geothermal exploration activities, an 8 years progress report," in *World Geothermal Congress*, 2020.
- [40] E. Rusillon, "Characterisation and rock typing of deep geothermal reservoirs in the Greater Geneva Basin (Switzerland & France)," PhD theses, Université de Genève, 2017.
- [41] J. Faessler and B. M. Lachal, "Géothermie moyenne enthalpie avec valorisation dans les réseaux thermiques : Retours d'expérience sur trois installations et Proposition d'une grille d'analyse," Technical report, Université de Genève, 2017.
- [42] O. Todorov, K. Alanne, M. Virtanen and R. Kosonen, "A method and analysis of aquifer thermal energy storage (ATES) system for district heating and cooling: A case study in Finland," *Sustainable Cities and Society*, vol. 53, p. 101977, 2020.
- [43] L. Mesquita, D. McClenahan, J. Thornton, J. Carriere and B. Wong, "Drake Landing Solar Community: 10 Years of Operation," ISES Solar World Congress, 2017.
- [44] H. L. e. al, "4th Generation District Heating (4GDH): Integrating smart thermal grids into future sustainable energy systems," *Energy*, vol. 68, pp. 1-11, 2014.
- [45] "H2020 project Storm," VITO, 2018-2021. [Online]. Available: www.storm-dhc.eu. [Accessed 7 5 2021].
- [46] T. Van Oevelen, C. Johansson, D. Vanhoudt and E. Smulders, "Report on the performance of the controller," H2020 Storm Project, 2019.
- [47] D. Geysen, O. De Somer, C. Johansson, J. Brage and D. Vanhoudt, "Operational thermal load forecasting in district heating networks using machine learning and expert advice," *Energy and Buildings*, vol. 162, pp. 144-153, 2018.
- [48] G. Suryanarayana, J. Lago, D. Geysen, P. Aleksiejuk and C. Johansson, "Thermal load forecasting in district heating networks using deep learning and advanced feature selection methods," *Energy*, vol. 157, pp. 141-149, 2018.
- [49] PJM, "Locational Marginal Pricing Fact Sheet," 23 February 2017. [Online]. Available: <https://www.pjm.com/~media/about-pjm/newsroom/fact-sheets/locational-marginal-pricing-fact-sheet.ashx>.
- [50] K. Kok and A. Subramanian, "Fast Locational Marginal Pricing for Congestion Management in a Distribution Network with Multiple Aggregators," in *CIGRE 2019*, Madrid, Spain, 2019.
- [51] K. Kok, "The PowerMatcher: Smart Coordination for the Smart Electricity Grid," VU Vrije Universiteit, Amsterdam, 2013.
- [52] FAN, "Energy Flexibility Interface," Flexible Power Alliance Network, [Online]. Available: <https://flexible-energy.eu/efi-energy-flexibility-interface/>. [Accessed 26 11 2019].
- [53] Wikipedia, "Separation of Concerns," Wikipedia, [Online]. Available: https://en.wikipedia.org/wiki/Separation_of_concerns. [Accessed 26 11 2019].
- [54] MatlabControl, "Matlab control - A Java API to interact with MATLAB," [Online]. Available: <https://github.com/diffplug/matconsolectl>. [Accessed 26 11 2019].
- [55] Merriam-Webster, "https://www.merriam-webster.com/dictionary/system," 2019. [Online]. [Accessed 11 5 2021].
- [56] Wikipedia, "Definition of system," 2019. [Online]. Available: https://en.wikipedia.org/wiki/System#cite_note-merriam-webster-system-1. [Accessed 21 5 2021].